Aus der Abteilung Genvektoren des Helmholtz Zentrums München
Leitung: Prof. Dr. Wolfgang Hammerschmidt

Characterization of dormant and chemotherapy-resistant ALL cells in PDX mouse models

Dissertation
zum Erwerb des Doktorgrades
der Naturwissenschaften
(Dr. rer. nat.)

an der Medizinischen Fakultät der
Ludwig-Maximilians-Universität München

vorgelegt von

Erbey Ziya Özdemir

aus Akyazi

2017

Gedruckt mit Genehmigung der Medizinischen Fakultät der
Ludwig-Maximilians-Universität München

Betreuer:	PD Dr. Aloys Schepers
Zweitgutachter:	Prof. Dr. Roland Kappler
Dekan:	Prof. Dr. med. dent. Reinhard Hickel
Tag der mündlichen Prüfung:	28.09.2017

Eidesstattliche Versicherung

Özdemir, Erbey Ziya

_____

Name, Vorname

Ich erkläre hiermit an Eides statt,
dass ich die vorliegende Dissertation mit dem Thema

Characterization of dormant and chemotherapy-resistant ALL cells in PDX mouse models

selbständig verfasst, mich außer der angegebenen keiner weiteren Hilfsmittel bedient und alle Erkenntnisse, die aus dem Schrifttum ganz oder annähernd übernommen sind, als solche kenntlich gemacht und nach ihrer Herkunft unter Bezeichnung der Fundstelle einzeln nachgewiesen habe.

Ich erkläre des Weiteren, dass die hier vorgelegte Dissertation nicht in gleicher oder in ähnlicher Form bei einer anderen Stelle zur Erlangung eines akademischen Grades eingereicht wurde.

_____ _____

Ort, Datum Unterschrift Doktorand

Parts of this work have been published in:

Sarah Ebinger*, **Erbey Ziya Özdemir***, Christoph Ziegenhain*, Sebastian Tiedt*, Catarina Castro Alves*, Michaela Grunert, Michael Dworzak, Christoph Lutz, Virginia A. Turati, Tariq Enver, Hans-Peter Horny, Karl Sotlar, Swati Parekh, Karsten Spiekermann, Wolfgang Hiddemann, Aloys Schepers, Bernhard Polzer, Stefan Kirsch, Martin Hoffmann, Bettina Knapp, Jan Hasenauer, Heike Pfeifer, Renate Panzer-Grümayer, Wolfgang Enard, Olivier Gires, Irmela Jeremias
"Characterization of Rare, Dormant, and Therapy-Resistant Cells in Acute Lymphoblastic Leukemia"
published in *Cancer Cell* (2016) 30(6):849-862
DOI: 10.1016/j.ccell.2016.11.002

*** Co-first author**

Table of contents

Abstract

The initial treatment of acute lymphoblastic leukemia (ALL) leads often to the decrease of symptoms in patients. However, potentially remaining leukemic cells after chemotherapy, defined as minimal residual disease (MRD), indicate a high risk for relapse. Patients with relapse are faced with poor outcome. Novel treatment strategies have to target MRD cells in order to minimize the relapse risk. Dormancy and chemotherapy resistance are associated with unfavorable and critical features in MRD. However, our knowledge of MRD cells is too limited to allow a specific and successful treatment of these cells in patients.

This present work is based on the individualized patient-derived xenograft (PDX) mouse model complemented with genetic engineering in PDX cells by expression of molecular markers and bioluminescence *in vivo* imaging. A novel preclinical model which uses prolonged chemotherapy treatment in mice to introduce MRD in PDX ALL, mimicking the situation in patients, was established. Histochemical studies of the murine bone marrow revealed that PDX MRD cells from this mouse model localized to the perivascular niche in the bone marrow; in contrast, in an additional, already established PDX mouse model of long-term dormancy, dormant PDX ALL cells were preferentially enriched in the endosteal niche where normal hematopoietic stem cells reside. Gene expression profiles (GEP) of rare, but highly enriched bulk and single PDX ALL cells demonstrated high similarities between the PDX MRD cells and dormant PDX cells of the two different mouse models; both populations showed major adverse characteristics typically associated with unfavorable prognosis in patients such as altered metabolism and signs of chemotherapy resistance. Most importantly, GEP of primary ALL cells obtained from children at MRD showed a high similarity to PDX MRD cells indicating that the new preclinical MRD model resembles the challenging clinical situation of MRD in patients with ALL.

The novel platform can now be used for developing innovative treatment strategies. Resistant ALL cells might be resolved from the bone marrow niche in order to sensitize them towards chemotherapy.

Zusammenfassung

Die Initialtherapie der akuten lymphatischen Leukämie (ALL) führt oft zu einer Minderung der Symptome bei betroffenen Patienten. Jedoch bergen persistierende Leukämiezellen nach der Chemotherapie, definiert als minimale residuale Resterkrankung (MRD), ein erhöhtes Risiko für ein Rezidiv und führen folglich zu einer schlechteren Prognose. Neuartige Behandlungsstrategien gegen die MRD Zellen müssen entwickelt werden, um die Rezidivrate in ALL zu senken. Dabei werden Zellruhe und Chemotherapie-Resistenz mit kritischen Eigenschaften der MRD assoziiert. Jedoch ist unser Wissen über die Zellen der MRD zu begrenzt, um diese gezielt und erfolgreich zu bekämpfen.

Diese vorliegende Arbeit basiert auf dem individualisierten Patienten-abgeleiteten Xenograft (PDX) Mausmodell. Ergänzt wurde dieses Modell durch Genmanipulationen an den PDX Zellen für die Expression von molekularen Markern und für die Biolumineszenz *in vivo* Imaging. Ein neues präklinisches Modell für die Simulation der MRD in der PDX ALL, welches auf eine langfristige Chemotherapie in Mäusen beruht und dabei die Situation des Patienten nachahmt, wurde etabliert. Histochemische Analysen von murinem Knochenmark ergaben, dass sich die PDX MRD Zellen aus diesem Mausmodell in der perivaskulären Nische des Knochenmarks lokalisieren. Im Gegensatz dazu, in einem zusätzlichem, bereits etabliertem PDX Mausmodell zur langfristigen Zellruhe, waren die ruhenden PDX ALL Zellen in der endostalen Nische angereichert, wo sich auch die hämatopoetischen Stammzellen befinden. Genexpressionsprofile (GEP) von seltenen, aber hochangereicherten Bulk- und Einzel-PDX ALL Zellen zeigten hohe Ähnlichkeiten zwischen den PDX MRD- und den ruhenden PDX Zellen aus den zwei verschiedenen Mausmodellen. Beide Populationen wiesen wesentliche Merkmale auf, die typischerweise mit ungünstigen Prognosen in Patienten assoziiert sind, wie z.B. veränderter Metabolismus und Anzeichen für Chemotherapie-Resistenz. Vor allem zeigten die GEP von primären ALL Zellen, isoliert aus Kindern in der MRD, eine hohe Ähnlichkeit zu PDX MRD Zellen. Dies lässt schlussfolgern, dass das neue präklinische MRD Modell die klinisch herausfordernde Situation der MRD in ALL Patienten wiedergibt.

Diese einzigartige neue Plattform eignet sich für die Entwicklung neuartiger Behandlungsstrategien. Resistente ALL Zellen sollten von der Knochenmarksnische zerstreut werden, um diese für Chemotherapie angreifbar zu machen

1 Introduction

1.1 Acute Lymphoblastic Leukemia

Acute lymphoblastic leukemia (ALL) is a malignant disorder of the lymphoblastic progenitor lineage. Instead of developing into mature lymphocytes, immature and non-functional blasts of B- or T-cells grow at high rates and accumulate in the bone marrow and infiltrate other organs via blood vessels. The accumulation of blasts leads to disturbed and suppressed hematopoiesis. Due to this dysfunction the symptoms are shown in anemia, increased risk of infections and bleedings, fever and the enlargement of spleen and liver (Esparza & Sakamoto. 2005).

ALL is the most common cancer in children and around 60% of all ALL cases occur at an age of 20 years and younger. Most of the affected children are between 2 and 5 years. The incidence is 3-4 cases per 100,000 children and 1 case per 100,000 adults each year. Among them B-ALL represent 80% of all ALL cases and is more frequently diagnosed in children as well as adults compared to T-ALL (Chiarini et al. 2016; Cobaleda & Sanchez-Garcia. 2009).

ALL is a heterogeneous disease with genetic alterations including hyperdiploidy, chromosomal translocations and deletions. Chromosomal translocations are the most frequent alteration in ALL. In more than 20% of all pediatric cases a TEL-AML1 (synonym: ETV6-RUNX1) translocation is detected, followed by MLL rearrangements (6%), TCF3-PBX1 (4%) and BCR-ABL (synonym: Philadelphia-chromosome; 2%)(Inaba et al. 2013). Many chromosomal rearrangements disrupt gene loci of important transcription factors regulating the hematopoiesis and lymphoid development (e.g. ETV6, RUNX1, TCF3, PBX1). The BCR-ABL translocation leads to a constitutive tyrosine kinase activity resulting in uncontrolled cell divisions, whereas MLL rearrangements disturb the histone methylations provoking altered gene expressions (Ferrando et al. 2003; Raitano et al. 1995). Most of the rearrangements are well characterized and are used to predict treatment efficiencies. For example, high hyperdiploidy and ETV6-RUNX1 translocations are associated with good prognosis in contrast to MLL rearrangements (Inaba et al. 2013; Pui et al. 2008).

1.1.1 Treatment

The high proliferation rate of many leukemic cells is taken advantage in the ALL therapy. Therefore, the treatment of ALL patients is based on chemotherapy (Inaba et al. 2013). Cytostatic drugs target unspecific all fast dividing malignant as well as healthy cells by

suppressing diverse proliferating processes, e.g. inhibition of the chromosome separation during cell division by application of Vincristine, which is a commonly used cytostatic drug in ALL treatment (Owellen et al. 1972). Thus, such a therapy is correlated with severe side effects due to elimination and damage of dividing healthy cells. Hair loss, mouth sores, vomiting and increased infection risk are some of the common side effects (Clevers. 2011; Zhou et al. 2009).

Most cytostatic drugs were developed before 1970 and are still very important in clinical treatment strategies. During the last decades the therapy protocols were optimized in dosage, frequency and the combination of chemotherapeutics leading to higher survival rates and better outcome (Inaba et al. 2013).

The average treatment duration in ALL is 2-3 years and is divided into three phases in which the cytostatic drugs, dosages and frequencies are changed. After diagnosis of ALL the induction therapy is immediately started. The aim of the first therapy phase is reaching remission by reducing the initial leukemic burden and restoring normal hematopoiesis. Remission is reached by easing the disease symptoms. After 4-6 weeks of induction therapy, the success rate is more than 90%, and the following consolidation therapy aims to eliminate residual leukemic cells in the next 20-30 weeks. Finally, by reducing the high dosage of cytostatic drugs, the maintenance therapy is carried out for 2-3 years in order to decrease the risk of leukemia regrowth, called relapse (Inaba et al. 2013; Pui et al. 2008).

The survival rate depends on the ALL classification considering the detected chromosomal translocations. Nevertheless, not more than 50% of adults and more than 80% of children have a long-term survival rate of more than 5 years after diagnosis (Bassan & Hoelzer. 2011).

The main reason for treatment failures is the occurrence of relapses. Patients with relapse have a dismal prognosis due to chemotherapy resistance of the re-growing leukemia. Two different models are described for the evolution of therapy-resistant clones causing ALL regrowth. Relapse arises either from an existing clone at diagnosis or from pre-leukemic ancestral clone, which gain a new chromosomal abnormality or gene mutation (Kunz et al. 2015; Mullighan et al. 2008). A recent study in B-ALL compared matched diagnosis and relapse samples and showed that 75% of the relapse clones were already found during initial diagnosis (Ma et al. 2015).

The standard ALL therapy with cytostatic drugs was optimized over the last decades and reached a level in which a significant increase of patients' outcome and survival rate is not possible by optimizing existing chemotherapy alone. Therefore, new treatment strategies are urgently needed (Cooper & Brown. 2015). More and more targeted therapy for ALL becomes

important to support the chemotherapy. Disease specific characteristics are attacked by targeted therapies. The challenge in developing these personalized therapies is the identification of proteins that are ideally expressed in malignant but not in healthy cells or display at least significant different expression levels. The advantages of this new approach are less toxicity on healthy cells and fewer side effects than cytostatic drugs alone (Portell & Advani. 2014).

The best described drug for targeted therapy in ALL is Imatinib. Imatinib binds specifically to the BCR-ABL1 fusion protein, which is presented exclusively in leukemic cells but not in healthy cells. This binding leads to the inhibition of the constitutively activated tyrosine kinase (Yanada et al. 2006). Thus, Imatinib has resulted in high improvement in the survival of BCR-ABL1 positive leukemia patients. In the last decades patients with BCR-ABL1 translocations had a poor prognosis. Less than 40% of these patients survived after chemotherapy. By inhibiting the constitutively activated BCR-ABL1 kinase with Imatinib, combined with chemotherapy, the survival rate increased up to 80% (Schultz et al. 2009).

In addition, many concepts of targeted therapies for ALL are in clinical studies, for example therapeutic antibodies as Blinatumomab and Inotuzumab ozogamicin (Portell & Advani. 2014). Blinatumomab is the first BITE (Bi-specific T-cell engagers)-antibody, which detects simultaneously two different antigens, the CD3 receptor of T-cells and the CD19 cell surface protein of B-cells. Both proteins are overexpressed in ALL compared to healthy lymphocytes. Specific binding of Blinatumomab marks ALL cells for an antibody-dependent cellular cytotoxicity reaction of the immune system, resulting in elimination of tumor cells via phagocytosis by natural killer cells, monocytes or macrophages (Brower. 2016; Mellor et al. 2013).

In contrast, the antibody inotuzumab ozogamicin is linked to a cytostatic drug and binds to the cell surface marker CD22, which is highly expressed in mature B-cells and blasts. The progenitor B-cells are not affected. Thus, the toxicity on the B-cell lineage is low. Furthermore, the high side effects of conventional chemotherapy are reduced by this antibody due to the targeted application of the cytostatic drug in specific areas (Kantarjian et al. 2012; Morley & Marks. 2016).

1.1.2 Minimal residual disease

Minimal residual disease (MRD) implies small numbers of remaining leukemic cells after reaching remission. During and after patients' treatment the therapeutic success is followed in the clinics as depicted in Figure 1. Chemotherapy reduces the leukemia burden within almost all patients (green circle) and remission is achieved in a short period of time. Nevertheless, treatment has to continue after remission to avoid relapse of the disease. A level of less than 1% of remaining ALL cells after therapy is defined as MRD (Buckley et al. 2013). Depending on patients' ALL, resistant leukemic cells can persist in different levels (red circle) and cause sooner or later relapses. Especially, MRD levels indicate the initial response to therapy and serve as prognostic marker for relapse risk. Patients with the lowest detectable MRD levels (e.g. 10^{-4}) have a better prognosis and lower risk of suffering relapse than patients with high levels of MRD cells (e.g. 10^{-2}) (Conter et al. 2010; van Dongen et al. 2015). Even in cases of a complete MRD response, which is characterized by non-detectable numbers of leukemic cells, patients can relapse. The monitoring of the MRD level is important for assessing the therapeutic success and for starting treatment upon regrowth of resistant cells (Borowitz et al. 2008; Stow et al. 2010; Vora et al. 2013).

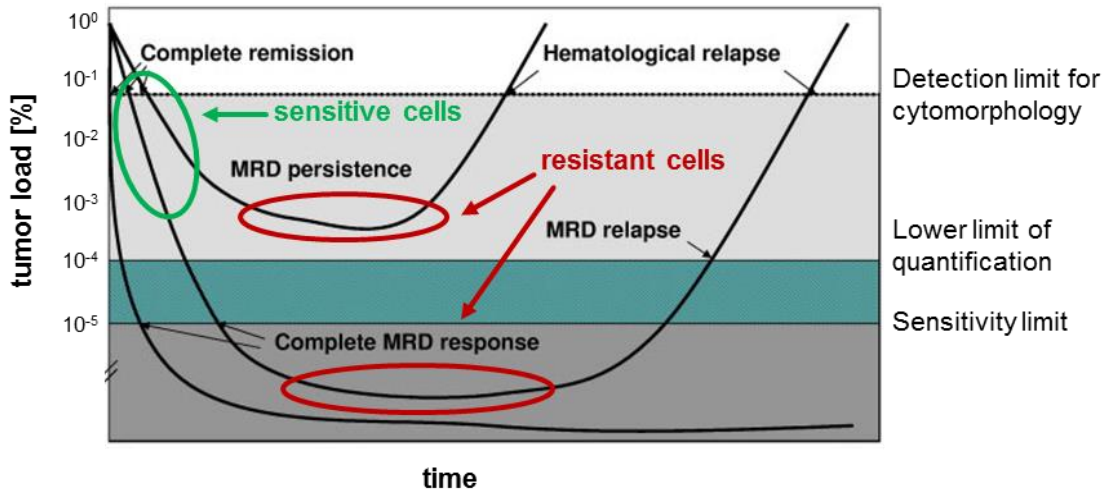

Figure 1: Monitoring of minimal residual disease in clinics.
Therapeutic effects in ALL treatment are monitored in clinics. Tumor load (proportion of leukemic cells among healthy cells) can be reduced by chemotherapy (green circle). Remaining leukemic cells are resistant to the current therapy (red circle). MRD level is reached in different levels depending on patients' ALL and serve as prognostic marker for relapse. Adapted from (Bruggemann et al. 2012).

Identification of residual leukemic cells among healthy cells in bone marrow aspirates is based on leukemia specific chromosomal translocations, gene mutations, immunoglobulin

receptor rearrangements or immunophenotypic abnormalities. Chromosomal translocations are highly specific for leukemia and are analyzed by polymerase chain reaction (PCR) as well as gene mutations and immunoglobulin receptor rearrangements (Greaves & Wiemels. 2003; van Dongen et al. 2015). The sensitivity can be up to 10^{-6} cells by analyzing translocations. The disadvantage of this method is that no information about the leukemia immunophenotype is gained (Bruggemann et al. 2010). This information might be useful for further therapy strategies. In contrast, fluorescence-activated cell sorting (FACS) analysis provides an immunophenotypical characterization of patients' leukemia with the detection limit of 10^{-5} cells (Bruggemann et al. 2010; Coustan-Smith et al. 2011). However, the challenge is to identify leukemia-associated immunophenotypes that are different from present normal bone marrow cells. Until now no common MRD signature exists due to the high variation of ALL (Basso et al. 2009; Coustan-Smith et al. 2011). Therefore, the leukemic antigen expression pattern of every patient has to be adjusted by using a leukemia-associated panel of at least 6 relevant markers, for example CD19, CD22, CD34, CD38, CD45 are the most common markers for identification of ALL cells in the bone marrow (Borowitz et al. 2008; Fiser et al. 2012). Nevertheless, false positivity still cannot be completely excluded because of similarities between leukemic lymphoblasts and normal lymphoid progenitor cells in the different phases of regeneration during and after treatment. (Basso et al. 2009; Coustan-Smith et al. 2011).

The challenge in the ALL therapy is not anymore the initial treatment to reach remission. The survival rate is more than 90% after the induction therapy (see 1.1.1). Remaining treatment-resistant MRD cells after chemotherapy are the main reason for regrowth of the leukemia. More ALL patients succumb of relapses than from the initial cancer. A better understanding of MRD cells would provide new insights for developing targeted therapies against MRD cells (Campana. 2010; Vora et al. 2013).

1.1.3 The role of the bone marrow

It is currently believed that the bone marrow environment plays a pivotal role in dormancy and chemotherapy resistance of leukemic cells (Pal et al. 2016). Colmone and colleagues presented the first important evidence for the interaction between bone marrow and leukemic cells. They demonstrated that leukemic cells are able to change the bone marrow microenvironment resulting in a dysfunction of hematopoietic progenitor cells (HPC) (Colmone et al. 2008).

Increasing understanding of the bone marrow structure and healthy hematopoiesis led to new insights of the leukemic niche. A niche is defined as a local microenvironment maintaining and regulating stem cells and progenitors (Morrison & Scadden. 2014). Two niches exist in the bone marrow: the endosteal- and perivascular niche (Chiarini et al. 2016; Ehninger & Trumpp. 2011; Lo Celso & Scadden. 2011). The endosteal niche (endosteum) is the region around the bone matrix with a distance of less than 100 µm to the closest bone matrix (Nombela-Arrieta et al. 2013). The perivascular niche is more central within the bone marrow consisting of sinusoids/endothelial cells, CXCL12-abundant reticular (CAR) cells and mesenchymal stem cells (MSC). These cell types are also found in the endosteal region, but with a lower frequency (Ehninger & Trumpp. 2011). Characteristic cells for the endosteal niche are osteoblasts and osteoclasts, which build a cell layer on the bone matrix. The function of all cell types are more or less known: Osteoblasts synthesize and osteoclasts resorb the bone matrix during bone formation, and CAR cells produce excessively the chemokine CXCL12 for homing and maintaining HSC in the bone marrow (Chiarini et al. 2016; Sugiyama et al. 2006). However, the knowledge about the interaction of these cell types within the microenvironment by secreted cytokines and cell surface ligands/receptors is still incomplete (Morrison & Scadden. 2014). Furthermore, a controversial issue exists about the localization of dormant HSC within the bone marrow. Many groups indicated that the endosteal niche maintains a small dormant HSC population in contrast to the perivascular niche harboring self-renewing HSC (Arai & Suda. 2007; Calvi et al. 2003; Haylock et al. 2007; Zhang et al. 2003). However, recent studies from laboratory of Prof. Morrison (UT Sothwestern Medical Center, Dallas) showed that the function of the endosteal niche is minimized to an indirect role in modulating HSC. The perivascular niche is settled by HSC and the endosteal niche by early lymphoid progenitors (Ding & Morrison. 2013). Furthermore, it was stated that dividing HSC are localized more likely in the endosteum than non-dividing HSC, which are restricted to perivascular subniches (Acar et al. 2015; Morrison & Scadden. 2014).

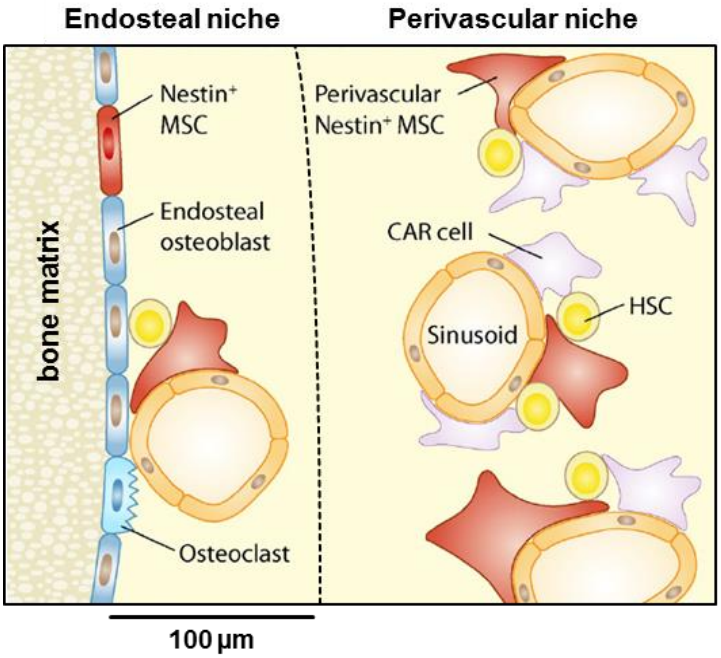

Figure 2: Bone marrow is divided into two major niches.
The bone marrow consists of the endosteal- and the perivascular niche for maintaining self-renewal and lineage differentiation of hematopoietic stem cells (HSC). The endosteal niche is close to the bone matrix and the perivascular niche is located more in the center of the bone marrow and is not influenced by osteoblasts and osteoclasts. The endosteal niche plays an important role for HSC dormancy, and the perivascular niche harbors dividing HSC. However this is controversially discussed. Adapted from (Ehninger & Trumpp. 2011).

In contrast to the controversially discussed role of the endosteal niche in the HSC maintenance, the role of the endosteum is clearer in the malignant hematopoiesis. Several studies demonstrated that the endosteal niche is associated with dormant and chemotherapy-resistant leukemic cells (Boyerinas et al. 2013; Chen et al. 2014; Ishikawa et al. 2007). Within the endosteal region leukemic cells interact with the cellular environment. Often some features of osteoblasts and osteoclasts are used or disturbed to gain an advantage in leukemia progression (Kode et al. 2014; Lawson et al. 2015; Schepers et al.). For example, Boyerinas and colleagues showed that blasts use osteopontin to localize themselves in the quiescent endosteal niche. Osteopontin, which is secreted by osteoblasts, acts as a chemokine and as an extracellular protein for bone remodeling. After homing in this niche, the leukemic cells start to produce and to secrete additional osteopontin into the local microenvironment in order to enhance the dormant effect (Boyerinas et al. 2013).

Next to the leukemia supporting endosteal niche, malignant cells are also able to evolve a protective niche by interacting with MSC during chemotherapeutical stress. The formation of a therapy-induced niche contributes to the chemotherapeutic resistance of leukemic cells (Duan et al. 2014).

Recently, new insights were obtained in understanding the interaction of leukemia with the microenvironment. The bone marrow supports the dormancy and chemotherapy resistance of leukemic cells (Pal et al. 2016). Novel ALL treatment strategies have to consider the bone marrow environment. By targeting the interaction of leukemia and bone marrow, drug resistant leukemic cells can be sensitized towards chemotherapy.

1.2 Challenging characteristics of tumor cells

In patients' remission, infinitesimal numbers of MRD cells can remain after conventional chemotherapy and indicate a risk for the reappearance of leukemia followed with bad prognosis. The final goal of all cancer therapies is to cure the patient by reaching a complete recovery without any risk of relapse. In clinics conventional chemotherapies usually do not overcome the challenging characteristics of relapse inducing cells. Unfavorable and challenging characteristics of these tumor cells are associated with quiescence, drug resistance and stemness (Kreso & Dick. 2014).

1.2.1 Dormancy

Therapeutic success is diminished by the existence of dormant cancer cells. Elimination of this inactive and non-dividing subpopulation is limited by the mode of action of conventional drugs. Most drugs in cancer therapy are cytostatic agents targeting different cellular processes for proliferation. Consequently, dividing cancer cells are killed, and dormant cells remain as the drugs are not affecting non-dividing dormant cells. These cells represent the residual disease and might be dormant over a long time period until starting to proliferate and resulting in relapse. Mechanisms of dormancy are still unclear in cancer cells (Essers & Trumpp. 2010; Greaves. 2013; Li et al. 2014). However, the microenvironment is very likely to have a crucial role at this critical feature. Novel treatment strategies aim to target dormant cancer cells or alter the microenvironment in order to re-activate the cell cycle and sensitize them towards chemotherapy (Saito et al. 2010).

1.2.2 Drug resistance

Chemotherapy resistance is another challenging and critical feature influencing patients' outcome. During drug treatment, some cancer cells escape from therapy and lead to a more aggressive and resistant disease. Here two different scenarios are conceivable to explain the drug resistance: either chemotherapy induces genetic alterations in cancer cells leading to a resistance or a chemotherapy-resistant subclone already existed within the initial tumor population. The molecular reasons for drug resistance are manifold and poorly understood so far. However, proteasome inhibition, altered membrane transport, altered target enzyme, decreased drug activation and increased drug degradation are one of many suggestions for causing intrinsic drug resistance (Luqmani. 2005; Paiva et al. 2016).

Extrinsic regulators were also implicated for drug resistance. The tumor microenvironment contributes to keep cancer cells in a dormant state (Boyerinas et al. 2013; Chen et al. 2014). This acquired dormancy leads to chemotherapy resistance due to downregulation of cell cycle processes (Li et al. 2014). Besides, the surrounding microenvironment might also inhibit the drug distribution resulting in protection of cancer cells (Meads et al. 2009).

In summary, new drugs with novel mode of actions are urgently needed to overcome resistances during chemotherapy.

1.2.3 Stemness

Therapy failures are also caused by the heterogeneity of the tumor. A tumor population consists of multi-clonal divergent fast-dividing and drug-sensitive cells. The cancer stem cell (CSC) model proposes that a tumor arises from a rare subgroup of dormant and drug resistant cells with self-renewal capacity. CSC constitute the malignant counterpart to stem cells, which are distinguished from CSC by the balance between proliferation and quiescence affected by the specific niche (Li & Neaves. 2006). Self-renewal of CSC is crucial for the maintenance and also for the relapse of the tumor. Asymmetric division of one CSC gives rise to two distinct daughter cells: one copy of the original stem cell and a second cell to differentiate into a non-stem tumor cell (Greaves. 2013; Magee et al. 2012; Shackleton. 2010). Furthermore, in one tumor several CSC clones might exist with diverse genotypes and phenotypes. By targeting and eliminating CSC, the source of tumor growth might be inhibited and the disease might become favorable and sensitive for treatments. Therefore, such treatment strategies try to target malignant cells with CSC characteristics (Clevers. 2011; Kreso & Dick. 2014).

The standard assay for identification and quantification of CSC in tumors is based on the xenograft tumor model. Cancer cells are transplanted into mice in dilution series allowing the calculation of CSC frequency from the number of engrafted cells. In general, CSC frequency is considered far below 0.1% of an unsorted cancer cell population (Iwasaki & Suda. 2009; Lapidot et al. 1994). However, the used CSC markers in all different types of tumors show controversial results. Consequently, these markers cannot be used for a precise detection of CSC in tumors (Clevers. 2011).

An exception of the hierarchical CSC model in tumors is ALL. An enormous cellular heterogeneity and clonal evolution is observed in ALL. Besides, all ALL cells have the capacity for self-renewal and therefore are attributed with CSC potential, termed as leukemia stem cells (LSC). The LSC frequency in ALL is very high compared to other types of cancer and leukemia. A stochastic model is even suggested to describe the LSC of ALL (Morisot et al. 2010; Vormoor. 2009). Consequently, no specific LSC markers have been defined so far for ALL (Kong et al. 2008).

Taken together, all challenging characteristics of dormancy, drug resistance and stemness have to be considered for developing new treatment strategies in order to improve patients' outcome especially after relapses.

1.3 Patient-derived xenograft mouse model of ALL

The patient-derived xenograft (PDX) ALL mouse model is based on primary patients' cells and is currently the best model for studying many diverse aspects of human leukemia (Poglio et al. 2016).

The PDX model was first described by John Dick and colleagues around 30 years ago (Kamel-Reid et al. 1989) and its importance increases continuously each year. This model is currently the gold standard model for analyzing the leukemia niche (Duan et al. 2014; Hawkins et al. 2016; Ninomiya et al. 2007), studying the clonal evolution of leukemic cells (Cheung et al. 2013; Clappier et al. 2011), performing preclinical treatment trials (Gao et al. 2015; Lee et al. 2007; Townsend et al. 2016) and advancing translational leukemia research (Fry & Aplan. 2015; Guezguez et al. 2013; Hidalgo et al. 2014).

For PDX-based studies in ALL, primary material is obtained from patients' bone marrow aspirates or peripheral blood. By injecting the primary ALL cells into immunocompromised

mice, human leukemia engrafts in the living organism and displays similar course of disease as in patients. Leukemic cells home and engraft first in the bone marrow before they expand and infiltrate other organs like spleen and liver. Leukemic PDX cells can be re-isolated from the bone marrow or spleen, and re-injected into the recipient mice for passaging (Gopalakrishnapillai et al. 2016).

An *in vivo* model is required for primary ALL cells as they are unfortunately reluctant to grow *in vitro*. Amplification of primary ALL cells requires passaging *in vivo*. In rare occasions, *in vitro* growing cell lines can be generated out of primary ALL cells. These cell lines acquire additional mutations and alterations which are not present in patients and introduce a major bias into all studies. In contrast, upon *in vivo* passaging PDX cells retain important characteristics of primary ALL cells, for example microenvironment interactions or molecular heterogeneity (Cassidy et al. 2015; Townsend et al. 2016).

The similarity between primary ALL and the PDX model was shown by comparing primary samples of diagnosis and relapse with their behavior as PDX. More aggressive types of leukemia and especially relapse samples engraft more efficient and faster in recipient mice than diagnosis samples. (Lock et al. 2002; Meyer et al. 2011). Furthermore, Clappier and colleagues demonstrated that the PDX cell population often arises from minor subclones existing in patients' diagnosis. These subclones are found predominantly in the corresponding relapse samples. Engrafted ALL cells resemble in the xenograft mouse model more aggressive relapse samples than diagnosis samples (Clappier et al. 2011).

Engrafted ALL samples have a high stemness frequency in the xenograft mouse model. Small numbers of ALL cells are injected into mice without enriching for any self-renewal marker like in other xenograft models. Thus, the efficiency of establishing new PDX ALL samples is very high compared to other cancer types or leukemia models (Morisot et al. 2010).

1.3.1 PDX mouse model for identification of dormant leukemic cells

The PDX mouse model of ALL was developed further in our lab by introducing lentiviral transduction for molecular manipulation in PDX cells (Terziyska et al. 2012; Vick et al. 2015). After a first passage of the primary sample in an immunocompromised mouse, lentiviral transduction is performed *ex vivo* to obtain PDX cells positive for reporter genes facilitating enrichment and detection of PDX cells (see Figure 3) (Terziyska et al. 2012; Vick et al. 2015).

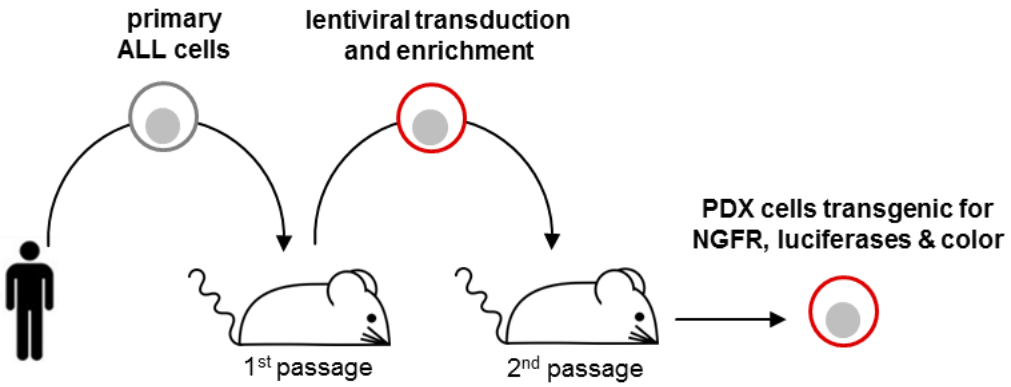

Figure 3: Scheme for production of transgenic PDX ALL cells.
Primary ALL samples from the clinics can be passaged in the immunocompromised NOD scid gamma (NSG) mice. After the first passage lentiviral transduction is performed to the isolated PDX cells from the enlarged spleens. PDX cells were transduced with the following transgenes: truncated NGFR for magnetic-activated cell sorting (MACS) targeting, mCherry for FACS detection and luciferase for bioluminescence *in vivo* imaging. Enriched transgenic PDX cells are reinjected. Adapted from (Ebinger, Özdemir et al. 2016).

In a parallel independent but collaborative PhD activity, Sarah Ebinger studied dormant ALL PDX cells. The identification and isolation of the dormant PDX cells were facilitated by the expressed transgenes luciferase, a red fluorochrome and the artificial surface antigen NGFR. (Ebinger, Özdemir et al. 2016). While transgenic luciferase was used for *in vivo* imaging and follow-up of the disease, the other two transgenes were used to isolate and enrich minor amounts of PDX ALL cells from murine bone marrow by a two-step procedure consisting of a magnetic-activated cell sorting (MACS) enrichment step using NGFR followed by a FACS enrichment using the fluorochrome. PDX cells were additionally labeled with the fluorescent cell staining dye, CFSE (Carboxyfluorescein succinimidyl ester) *ex vivo* (Weston & Parish. 1990). CFSE is an accepted marker for dormant cells. Each cell division diminishes the CFSE signal by 50%. Loss of the CFSE intensity is associated with continuous proliferation.
Triple transgenic, $CFSE^+$ PDX cells were injected into immunocompromised mice. After several weeks of cell injection the bone marrow was isolated and analyzed for the PDX cells. A small subpopulation of $CFSE^+$ PDX cells was identified after 3 weeks of injection. These cells did not lose the staining dye and are called label retaining cells (LRC; see Figure 4).
Two weeks after cell injection the identified LRC population constitute less than 0.1% of the PDX population in almost all analyzed ALL samples. These samples harbor various genetic alterations. While almost all PDX cells proliferate in mice and loose consequently the CFSE signal, the LRC show a dormant phenotype and retain the CFSE.

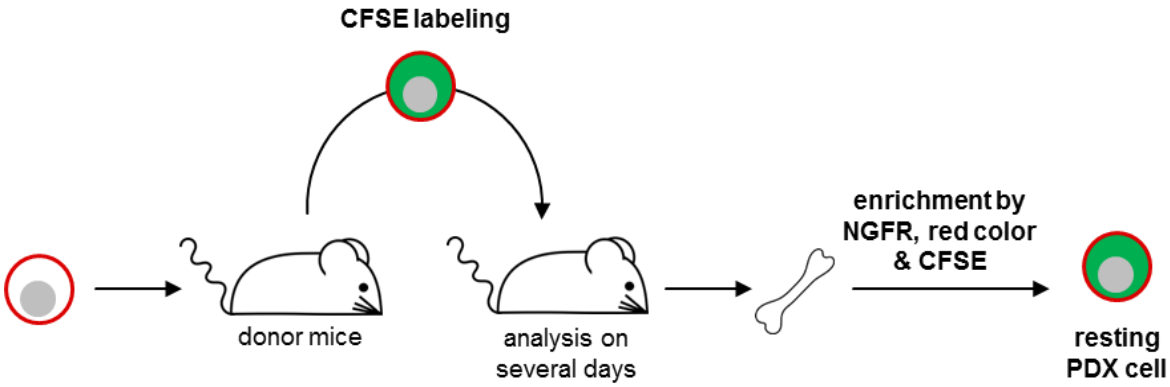

Figure 4: Scheme of the PDX LRC mouse model for identification of dormant leukemic cells *in vivo*.
Freshly isolated transgenic PDX cells from the spleen of the donor mice are labeled *ex vivo* with the proliferation marker CFSE. $CFSE^{+}$ PDX cells are injected into recipient mice. After several days the bone marrow is isolated. Resting PDX cells, which are characterized by their high CFSE signal, are called label retaining cells (LRC). The more days after injection the mice are sacrificed, the less LRC are isolated. The first time point, in which LRC are identified, is at day 10 after cell injection. LRC are defined as less than 2% of the entire PDX population and are isolated from the bone marrow and enriched by MACS and FACS via their transgenic PDX markers of NGFR, mCherry and the CFSE signal. Adapted from (Ebinger, Özdemir et al. 2016).

In functional studies, performed by Sarah Ebinger, LRC showed the critical cancer stem cells properties of dormancy, drug resistance and stemness. Before re-injecting the sorted LRC and the dividing PDX cells (non-LRC) into recipient mice, non-LRC were labeled again with CFSE as the marker was lost during the first passage. The same previous observed CFSE pattern was reproduced for both groups. Non-LRC converted into LRC and vice versa upon re-transplantation. Furthermore, in a limiting dilution transplantation assay (Schluter & Kaur. 2013) LRC were not enriched for stemness compared to the dividing non-LRC. Both populations were able to re-engraft with the same frequency and show a high plasticity in mice (Ebinger, Özdemir et al. 2016).

In *in vivo* treatment experiments LRC were drug resistant. In contrast, non-LRC showed a high sensitivity towards chemotherapy and was dramatically reduced. Sorted chemotherapy treated LRC inherited still leukemia-initiating potential in recipient mice, which resembled patients' relapse after treatment. By taking the LRC and non-LRC out of the bone marrow environment and treating them with chemotherapy *in vitro*, both groups exhibited same drug sensitivities suggesting the important connection between chemotherapy resistance, ALL plasticity and bone marrow environment (Ebinger, Özdemir et al. 2016).

In summary, functional studies showed that LRC obtain all critical features of challenging cells in patients' treatment. The LRC fate of dormancy, chemotherapy resistance and stemness are highly associated with the influence of the bone marrow environment.

This previously established PDX LRC mouse model was used in the following thesis for further characterization of LRC.

1.4 Aim of this work

Conventional therapy of ALL is based on the excessive application of chemotherapeutic drugs. The initial treatment is often successful and patients reach remission. However, certain ALL cells might survive in a disease status called minimal residual disease. MRD cells might progress into disease relapse with poor prognosis. Novel treatment options are required to eliminate tumor cells at MRD in order to prevent disease relapse; but developing such treatments requires appropriate preclinical models which were so far lacking.

The aim of the present study was to characterize ALL cells at MRD in order to lay the ground for developing novel therapies against these clinically challenging cells. As a first step, a preclinical PDX ALL model of MRD should be established in order to obtain reliable and numerous material for research. As a second step, the localization of PDX MRD cells in the murine bone marrow should be determined in direct comparison to dormant PDX ALL cells. In a third and last step, gene expression profiles should be obtained from PDX MRD cells and dormant PDX cells, and be compared to profiles from primary ALL cells from patients at MRD. Taken together, the present work aimed at a better understanding of MRD in ALL in order to enable developing novel therapies in the future.

2 Materials

2.1 Primary material

For gene expression profiles of patients' pediatric B-cell precursor acute lymphoblastic leukemia (BCP-ALL), thawed aspirates at the stage of diagnosis and minimal residual disease (MRD) were provided and sorted in TCL buffer (see 3.2.9) by the cooperation partner from Children's Cancer Research Institute and St. Anna Kinderspital (Department of Pediatrics, Medical University of Vienna, Austria) (see Table 1).

Table 1: Sorted primary ALL samples at the stage of diagnosis and MRD

sample	type of leukemia	age [years]	sex	multi-center study	BM blasts at MRD* [%]	Sort
1	BCP-ALL	4	F	BFM 2009	na	$CD19^+$, $CD10^+$, $CD20^-$
2	BCP-ALL	3	F	BFM 2009	na	$CD19^+$, $CD99^+$, $CD10^+$
3	BCP-ALL	5	M	BFM 2009	0.69	$CD19^+$, $CD10^+$, $CD123^+$
4	BCP-ALL	18	M	BFM 2009	1.10	$CD19^+$, $CD10^+$, $CD45^-$
5	BCP-ALL	3	F	BFM 2009	0.13	$CD19^+$, $CD10^+$,$CD20^-$

F = female; M = male; BFM = Berlin-Frankfurt-Münster; BM = bone marrow; na = not applicable; * MRD aspirates were taken at day 33 after onset of treatment;

2.2 Transgenic PDX cells

In this thesis two pediatric BCP-ALL samples, which were kindly provided from Dr. von Haunersches Kinderspital (LMU, Munich, Germany), were used consistently in the patient-derived xenograft (PDX) mouse models (see Table 2).

Table 2: Clinical data of patients' diagnostic ALL cells for xenotransplantation and sample characteristics

sample	type of leukemia	disease stage	age [years]	sex	cytogenetics	passaging time[§] [days]
ALL-199	BCP-ALL	2^{nd} relapse	8	F	somatic trisomy 21; leukemic homozygous 9p deletion	35
ALL-265	BCP-ALL	1^{st} relapse	5	F	hyperdiploidy with additional 6, 13, 14, 17, 18, 21, X chromosome	40

[§] passaging time in mice injected with at least 1 million cells until end stage of leukemia;

After transduction with the third-generation lentivirus vector system (Dull et al. 1998) by our institute members, both PDX samples, ALL-199 and ALL-265, expressed the following transgenes and were enriched to a 100% transgenic population (see Figure 5) (Ebinger, Özdemir et al. 2016): firefly luciferase for *in vivo* imaging (see 3.2.5), mCherry as a PDX marker and truncated NGFR without any intracellular part for magnetic-activated cell sorting (MACS) enrichment (see 3.2.8).

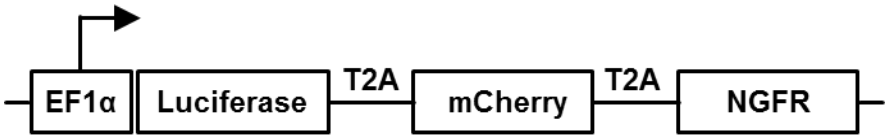

Figure 5: Lentiviral construct for equimolar expression of 3 transgenes in PDX cells.
Arrow indicates transcription start site; EF1α = elongation factor 1-alpha promoter; mCherry = red fluorescent protein from *Discosoma sp*.; NGFR = human low affinity nerve growth factor receptor lacking the intracellular signaling domain; T2A = self-cleaving peptide from Thosea asigna virus for linking the genes (Kim et al. 2011).

2.3 Antibodies

Table 3: Antibodies

name	host	application	supplier
anti-human-CD38-PE	mouse	FACS	BD Biosciences, Germany
anti-murine-CD45-APC (30-F11)	rat	FACS	Biolegend, USA
anti-human NGFR beads	-	MACS	Miltenyi, Germany
anti-FITC	rabbit	IHC	Thermo Fisher Scientific, USA
anti-mCherry	rabbit	IHC	Abcam, UK
anti-rabbit-Alexa594	goat	sec. ab	Invitrogen, USA

FACS = fluorescence-activated cell sorting; IHC = immunohistochemistry; sec. ab = secondary antibody;

2.4 Fluorophores

The lasers, filters and detectors of the BD FACS machines and the Leica TCS SP5 II confocal microscope (see 2.7) were adjusted to the following fluorophores with their specific spectrums.

Table 4: Fluorophores with maximum excitation and emission

name	excitation [nm]	emission[nm]
DAPI	358	461
CFSE	492	517
PE	496	578
mCherry	587	610
Alexa 594	590	617
APC	652	658

2.5 Buffer and medium

Table 5: Buffer and medium

name	composition
blocking buffer	PBS with 5% goat serum & 0.1% Tween-20
patient medium	RPMI-1640 supplemented with 20% FCS, 1% pen/strep, 1% gentamycin and 2 mM glutamine
PBS	140 mM NaCl, 2.7 mM KCl, 10 mM Na_2HPO_4, pH 7.2
PBE	PBS with 0.5% BSA & 5 mM EDTA
TCL-buffer	1x TCL buffer diluted with dd H_20 with 1% β-Mercaptoethanol

2.6 Chemicals, reagents & kits

Table 6: Chemicals, reagents & kits

name	supplier
Baytril 2.5%	Bayer, Germany
bovine serum albumin (BSA)	Sigma-Aldrich, Germany
CellTrace CFSE Kit	Life Technologies, USA
Cyclophosphamide	TEVA GmbH, Germany
DAPI	Sigma-Aldrich, Germany
D-Luciferin, sodium salt *UltraPure	Biomol, Germany
DMSO	Sigma-Aldrich, Germany
DNase	Sigma-Aldrich, Germany
EDTA	Sigma-Aldrich, Germany
ethanol ≥99,8%, p.a	Carl Roth, Germany
FACS Lysing solution	BD Biosciences, Germany
fetal bovine serum (FCS)	PAN Biotech, UK
Ficoll	GE Healthcare, UK
gentamycin	Lonza, Switzerland
glutamine	Gibco, USA
goat serum	Gibco, USA
heparin	Ratiopharm, Germany
isoflurane	CP pharma, Germany
isopropyl alcohol	Sigma-Aldrich, Germany
KCl	Sigma-Aldrich, Germany
Na_2HPO_4	Merck Millipore; Germany
NaCl	Sigma-Aldrich, Germany
O.C.T. compound	Sakura, USA
Osteosoft	Merck Millipore; Germany
penicillin-streptomycin 5000 U / ml	Gibco, USA
prolong gold antifade mounting	Life Technologies, USA

RPMI-1640	Gibco, USA
sucrose	Sigma-Aldrich, Germany
TCL buffer (2x)	Qiagen, Germany
trypan blue	Sigma-Aldrich, Germany
Tween-20	Sigma-Aldrich, Germany
Vincristine	cell pharm GmbH, Germany
zinc formalin	Sigma-Aldrich, Germany
β-Mercaptoethanol	Calbiochem

2.7 Equipment

Table 7: Equipment

Equipment	Manufacturer
Axiovert 200M microscope	Zeiss, Germany
Calibration Check pH-Meter HI 221	HANNA Instrument,Germany
BD FACSCalibur	BD Biosciences, Germany
BD LSRAriaIII	BD Biosciences, Germany
BD LSRFortessa	BD Biosciences, Germany
CryoJane tape transfer system	Leica, Germany
Cryostat CM1900UV	Leica, Germany
Fluidgm C1	Fluigm, USA
Heracell™ 150i CO2 Incubator	ThermoFisher Scientific, USA
IVIS Lumina II Imaging System	PerkinElmer, USA
Laminar Flow Hood	Heraeus, Germany
Leica TCS SP5 II confocal microscope	Leica, Germany
Microcentrifuge 5417C	Eppendorf, Germany
Rotanta 460R centrifuge	Hettich, Germany

2.8 Software

Endnote X7

FlowJo V10

Gimp 2

GraphPad Prism 6

ImageJ

javaGSEA Desktop application

Living Image software 4.4

Microsoft Office

R Studio

3 Methods

3.1 Ethical issues

3.1.1 Patient material

Written informed consent was obtained from all patients' parents/carers. For clinical routine analysis at the Dr. von Haunersches Kinderspital (LMU, Munich, Germany) and St. Anna Kinderspital (Medical University of Vienna, Vienna, Austria) fresh patient material was obtained from peripheral blood or bone marrow aspirates before treatment start. The remaining material was sent to our institute.

The study was performed in accordance with the ethical standards of the responsible committee on human experimentation (written approval by Ethikkommission des Klinikums der Ludwig-Maximilians-Universität München, Ethikkommission@med.unimuenchen.de, April 2008, number 068-08, and September 2010, number 222-10) and with the Helsinki Declaration of 1975, as revised in 2000.

3.1.2 Animal work

The maintenance of the NOD scid gamma (NSG; NOD.Cg-Prkdc^{scid} IL2rg^{tm1Wjl}/SzJ) mice from the Jackson Laboratory (Sweden) was done under specific pathogen-free conditions in the research animal facility of the Helmholtz Zentrum München. Free access to food and water, a 12 hour light-dark cycle and constant temperature were provided for the animals.

All animal trials were performed in accordance with the current ethical standards of the official committee on animal experimentation (written approval by Regierung von Oberbayern, poststelle@reg-ob.bayern.de, July 2010, number 55.2-1-54-2531-95-10; July 2010, number 55.2-1-54-2531.6-10-10; January 2016, number 55.2-1-54-2532-193-2015; May 2010, number 55.2-1-54-2532-193-2015 and August 2016, number 55.2-1-54-2532.0-56-2016). Animals were sacrificed before first clinical signs of illness became apparent.

3.2 Xenograft mouse model of acute lymphoblastic leukemia

The established acute lymphoblastic leukemia (ALL) xenograft mouse model in our institute is based on the immunocompromised NSG mice (Kamel-Reid et al. 1989; Lee et al. 2007; Liem et al. 2004; Terziyska et al. 2012).

3.2.1 PDX cell engraftment and expansion

For reliable engraftment and a shorter passaging time of the samples, 1-10 million fresh or freshly thawed ALL patient-derived xenograft (PDX) cells (in 100 µl sterile filtered PBS) were injected into 6-8 weeks old NSG mice via tail vein injection. Directly after cell injection, Baytril (2.5%, Bayer, Germany) was added to the drinking water of the mice in order to prevent infections.

Every two weeks a blood measurement was performed to detect the expansion of human PDX cells in peripheral blood (see 3.2.2). At a certain percentage of PDX cells in blood, which correlates with engrafting leukemia, mice were sacrificed and the PDX cells were isolated from the enlarged spleen (see 3.2.3) or the bone marrow (see 3.2.4). Definition of high PDX percentage in blood was depending on the sample. Mice with ALL-199 had to be sacrificed with around 30% of blasts in the blood, in contrast to the sample ALL-265, in which the limit was 80%. Re-passaging was always possible in both PDX samples (see 2.2). In addition to the blood measurement, *in vivo* imaging was performed to analyze the leukemia burden in mice. The advantage of this method was the high accuracy (see 3.2.5). For the verification of the samples, repetitive finger printing analysis, using mitochondrial DNA, was performed continuously in our institute (Hutter et al. 2004).

3.2.2 Blood measurement for monitoring the leukemia growth

Every second week leukemia growth was monitored by blood measurement for each PDX cell injected mouse. Blood (around 50 µl) from the tail vein was collected with a heparin coated glass capillary into a reaction tube with 5 µl heparin. The blood samples were incubated with 0.5 µl anti-human CD38 conjugated with phycoerythrin (PE) and 0.5 µl anti-mouse CD45 conjugated with allophycocyanin (APC) for 30 min at room temperature (RT). Subsequently, 1 ml FACS Lysing solution was added and incubated for 15 min at RT. Blood samples were washed twice with 3 ml FACS buffer. Each washing step included centrifugation at 300 g for

5 min at RT. Afterwards flow cytometric analysis was performed with a BD FACSCalibur (BD Biosciences, Germany) and the data were analyzed using the FlowJo software.

3.2.3 Isolation of PDX cells from spleen

High advanced leukemia in mice correlates with an enlarged spleen due to enrichment of ALL cells. After isolating the spleen, the organ was homogenized and a cell suspension in 30 ml PBS was prepared using a 70 µm strainer. Afterwards, 10 ml Ficoll was added to the cell suspension with a long needle and centrifuged with 400 g for 30 min at RT without rotor brake. The layer with mononuclear cells in the interphase of the Ficoll gradient centrifugation was harvested. Cells were washed twice with PBS (400 g, 5 min, RT) and resuspended in the required buffer.

3.2.4 Isolation of PDX cells from bone marrow

For isolation of PDX cells from bone marrow both femurs, both tibias, hip, backbone and sternum of each mouse were crushed by using mortar and pestle. The bone marrow was suspended with PBS and a cell suspension was prepared using a 70 µm cell strainer. After washing (2x, 400 g, 5 min, RT) the pellets were resuspended in the required buffer

3.2.5 Bioluminescence *in vivo* imaging for monitoring the leukemia burden

The transgenic PDX cells (see 2.2) expressed the recombinant codon-optimized form of the firefly luciferase (effluc). Therefore, it was possible to monitor the leukemia burden with bioluminescence *in vivo* imaging (Barrett et al. 2011; Bomken et al. 2013; Terziyska et al. 2012).

D-Luciferin, the substrate of the firefly luciferase to generate bioluminescence, was dissolved in sterile PBS to a final concentration of 30 mg/ml. After anesthetizing with isoflurane the mice were fastened in the imaging chamber of the IVIS Lumina II Imaging System (PerkinElmer, USA), and 150 mg/kg D-Luciferin was injected into the tail vein. The generated bioluminescence was measured immediately and pictures were taken for several seconds up to minutes, depending to leukemia burden. The following settings were used:
field of view = 12.5 cm; binning = 8, f/stop 1 and open filter.

The bioluminescence quantification was done with the software Living Image software 4.4 to get the leukemia burden in the unit lg photons s^{-1} (photons per second per cm^2 per steradian).

3.2.6 Quantification of PDX cell percentage in the bone marrow

Treatment start, stop and efficiency were determined by quantification of the relative amount of PDX cells in the bone marrow. The entire bone marrow was isolated, crushed and collected in 10 ml PBS (see 3.2.4). 1/20 of the bone marrow suspension was measured by the FACS Fortessa (BD Biosciences, USA) and finally analyzed using the software FlowJo. The number of mCherry-positive ($mCherry^+$) PDX cells was related to absolute event number without debris. The gating strategy is exemplary shown in Figure 6.

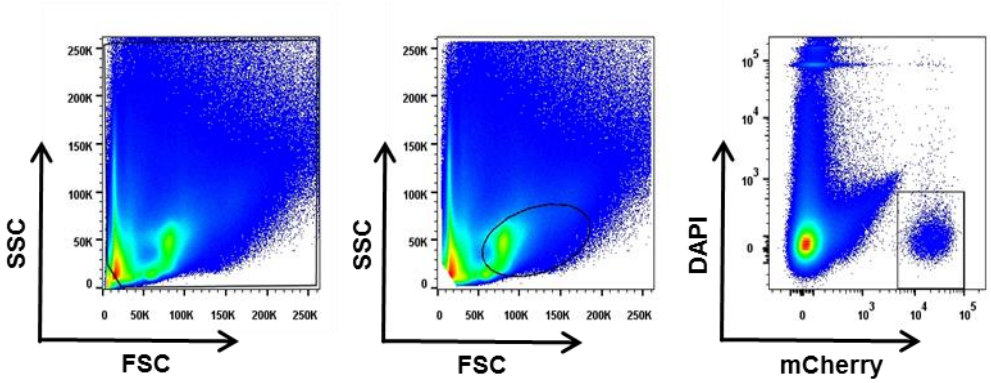

Figure 6: Gating strategy for determination of the relative PDX cell amount in the murine bone marrow. The first gating (left panel) included all events in the forward- and side scatter (FSC &SSC) apart from the debris, in the lower left part. Afterwards, the lymphocyte gate (middle panel) was set in the FSC and SSC. Finally, the $mCherry^+$ and $DAPI^-$ PDX population were gated. DAPI was added to the sample before FACS analysis. A negative DAPI signal correlates with a functional cell membrane and so for living cells.

3.2.7 *In vivo* treatment

In this study the commonly used cytostatic drugs of patients' ALL therapy, Vincristine (VCR; 0.25/0.5 mg/kg; i.v.) and Cyclophosphamide (Cyclo; 100 mg/kg; i.p.), were used to generate a drug treated/resistant PDX cell population in mice. After reaching high leukemia burden both PDX ALL samples (see 2.2) received the same drug concentrations once weekly for several weeks. Therapy start and efficiency was determined by bioluminescence *in vivo* imaging (see 3.2.5) and analysis of the PDX cell percentage in the bone marrow (see 3.2.4). In combination therapy VCR was injected two days before Cyclo because of the longer half-life of VCR (85

h) compared to Cyclo (7 h). Control animals received sterile PBS i.p. or i.v.. Drug solutions were prepared freshly with sterile PBS.

Human equivalent doses were calculated for mouse treatments to be close to the clinics (see Table 8). Following calculations were used (Nair & Jacob. 2016; Sharma & McNeill. 2009):

$$\text{human dose in } \frac{\text{mg}}{\text{kg}} = \frac{\text{human dose in } \frac{\text{mg}}{\text{m}^2}}{37}$$

$$\text{murine dose in } \frac{\text{mg}}{\text{kg}} = \text{human dose in } \frac{\text{mg}}{\text{kg}} \text{ x } 12.3$$

The conversion between human dose in mg/kg and mg/m² is done by the defined factor of 37. On the basis of the faster metabolism in mice, the human dose in mg/kg has to be multiplied with the factor of 12.3 to get the equivalent murine dose.

Table 8: Used drug concentrations in mice and patients

drug	mg/m² patient	mg/kg patient	mg/kg mouse (theory)	mg/kg mouse (used)
Vincristine	1.4	0.04	0.47	0.5
Cyclo-phosphamide	200	5.4	66.5	100

3.2.8 Enrichment of PDX cells by magnetic-activated cell sorting

Magnetic-activated cell sorting (MACS) was used for enrichment of small numbers of PDX cells from the murine bone marrow. Anti-human NGFR microbeads were used for targeting transgenic $NGFR^+$ PDX cells from the entire bone marrow. For this purpose 200 µl of beads were added to 10 ml PBE bone marrow suspension. After 45 min of incubation at 4°C under rotation, suspension was divided and loaded on two LS column (Miltenyi Biotech, Germany). Manufacturer's instructions were followed for the next washing steps and for the recovery of the PDX cells from the columns.

3.2.9 Sorting for dormant, drug treated and proliferating PDX cells

To obtain dormant, drug treated and proliferating PDX cell populations, cells isolated from the bone marrow (see 3.2.4) were enriched by MACS (see 3.2.8). Afterwards cell sorting with FACS Aria (BD Biosciences, Germany) was performed with similar gating strategies as in Figure 6 in the methods. The mCherry transgene in the PDX cells were used as an unique marker for PDX cell detection. Dormant PDX cells, which were defined as label retaining cells (LRC; see 1.3.1), were $CFSE^+$ (see 3.3.4) compared to the $CFSE^-$ proliferating cells. Therefore, an additional gate on $CFSE^+$ cells was used for sorting of LRC. All steps were performed at 4°C. The PDX cells were sorted either in FCS for freezing (see 3.3.2), in patient medium for single cell RNA-seq with at least 100 cells/µl or in TCL-buffer for bulk RNA-seq with the required concentration of 2,000 cells in 80 µl TCL- buffer.

3.3 *Ex vivo* methods for PDX cells

3.3.1 Cell counting

PDX cell numbers were counted with a Neubauer chamber. The cell solution was usually diluted 1:100 to count between 100 - 400 cells in all 4 squares of this chamber by using a light microscope. Only cells touching the lower and right borders of each square were included to the count.

To differentiate between living and dead cells, 0.4% trypan blue (w/v) were mixed 1:1 (v/v) with cell dilutions before counting. Under the microscope living cells appeared colorless while dead cells were stained blue.

Cell concentration was calculated as followed:

$$\text{cell concentration} = (\text{mean of counted cells}) \times (\text{dilution factor}) \times 10^4 \text{ cells/ml}$$

3.3.2 Freezing

$1x10^7$ PDX cells or 1/3 of the entire bone marrow were frozen in cryotubes with 1 ml fetal calf serum (FCS) containing 10% DMSO. For a sensitive freezing, each pellet was resuspended in 0.5 ml FCS after centrifugation (400 g, 5 min, RT). Afterwards 0.5 ml freezing medium (80% FCS with 20% DMSO) was added dropwise under shaking. Filled cryotubes were placed into a freezing container, loaded with isopropyl alcohol, for a cooling

rate of 1°C/min, and stored at -80°C for 24 h. For short term storage the cryotubes were kept at -80°C and for long-term storage in liquid nitrogen at -196°C.

3.3.3 Thawing

PDX cells were thawed by the standard protocol from our institute to obtain high viability. Frozen cells were defrosted immediately in a 37°C water bath. Under shaking 100 µl DNase (1 mg/ml) were added dropwise to the cell suspension. Cell suspensions were transferred to a 50 ml tube. Within two minutes first 1 ml FCS, then 10 ml PBS with 2% FCS were added and finally the suspension was filled up to 30 ml with PBS with 2% FCS. Afterwards the cells were centrifuged (400 g, 5 min, RT).

3.3.4 CFSE labeling

Freshly isolated PDX cells from the spleen of a donor mouse (see 3.2.3) were labeled *ex vivo* with CFSE for detection of dormant cells (LRC) in the next mouse passage. CFSE was a fluorescent cell staining dye, which was able to penetrate the cell membrane und bind covalently to intracellular molecules. With this covalent binding CFSE was retained in the cell.

$1x10^7$ PDX cells were suspended in 10 ml pre-warmed (37 °C) PBS with 0.1% BSA. CFSE was suspended in DMSO to a concentration of 5 mM and was added to the cell suspension with a final concentration of 10 µM. After 10 min incubation at 37°C, staining was stopped by adding five times staining volume of cold RPMI supplemented with 10% FCS, and incubated for 5 min on ice. Cells were then centrifuged (400 g, 5min, RT) and resuspended in sterile PBS for injection into recipient mice.

3.4 Immunostaining of femur cryosections

3.4.1 Femur preparation for cryosections

Femurs were treated as follow to allow storage and sectioning. All steps were performed at 4°C and between all steps femurs were washed with PBS. Freshly isolated femurs of one mouse were fixed in 10 ml zinc formalin fixative for 1 day, decalcified with Osteosoft (Merck; Germany) for 3 days and finally infiltrated with 30% sucrose PBS solution for 1 day before embedding in O.C.T. compound (Sakura; USA). Finally, femurs were stored at -80°C.

3.4.2 Femur cryosections

Cryosections of decalcified bones were obtained by using the cryostat CM1900UV (Leica; Germany) and CryoJane tape transfer system (Leica; Germany). Before sectioning, the samples were acclimatized for at least 30 min to the temperature of the cryostat, which was -19°C. The section thickness was 7 µm. Each section was captured on an adhesive tape window (Leica; Germany) and afterwards put on a CFSA4x slide (Leica; Germany). The binding between sections and tape window were broken by UV light from the CryoJane Tape transfer system (Leica, Germany) resulting in binding between section and slide. The slides could be stored for some days at -20°C.

3.4.3 Immunostaining

Slides with the cryosections were thawed to room temperature, hydrated with PBS for 10 min and blocked with the blocking buffer (PBS with 5% goat serum & 0.1% Tween-20) for 45 min. The blocking buffer was also used for antibody dilutions and for washing procedures (3x5 min) between all the steps.

The primary antibodies were applied on the sections for 1 day at 4°C in a hydration chamber. After washing secondary antibodies were applied for 45 min at room temperature. Sections were finally stained with 10 mg/ml DAPI for 15 min and slides were mounted with prolong gold antifade mountant (Invitrogen; USA). The stained sections were stored at 4°C.

Primary antibodies were rabbit-anti-FITC/CFSE (1:100; ThermoFisher; USA) and rabbit-anti-mCherry (1:100; Abcam; UK). Goat-anti-rabbit antibody conjugated with Alexa 594 (1:500; Invitrogen; USA) was used as secondary antibody.

3.4.4 Confocal microscopy

A Leica TCS SP5 II confocal microscope (Leica, Germany) was used to acquire 8-bit images of the stained cryosections using the hybrid detectors. With regard to the huge image size, half femur was scanned with the objective HCX PL APO LS 20x0.7 IMM UV (Leica; Germany) and the function of tile- & Z-Scan. Following settings were chosen to have a high scanning speed at the expense of a better resolution and increased noise:
format = 1024x1024 pixels; speed = 400 Hz; bidirectional scan = on; frame average = 0; sequential scan = off

3.4.5 Analysis of PDX localization within femur sections

The software ImageJ was used for the analysis of the images. A commonly threshold was set in the contrast settings to reduce the background noise of all images. Gamma correction was never used.
The endosteal region was defined by a distance as less than 100 µm from the bone matrix (Nombela-Arrieta et al. 2013). For determination of the absolute PDX cell numbers in each region, $mCherry^+$ cells were automatically counted (>10 pixel = one cell). The ImageJ function, watershed, was used to separate two overlapping cells.
The relative amount of PDX cells in the endosteal region was calculated as the absolute PDX cell number in the endosteum divided by the absolute PDX cell number in the entire bone marrow scan. Mean and standard error were calculated from at least 3 sections from 2 independent mice.
To visualize the LRC, which was defined as less than 2% of the PDX population at day 10 after cell injection (according to FACS data; Ebinger, Özdemir et al. 2016), CFSE signal intensity was adapted to the absolute numbers of $mCherry^+$ PDX cells from each consecutive section. This was done by adjusting CFSE intensity with the 8 bit threshold.

3.5 Analysis of RNA-seq data

Freshly isolated PDX cells (LRC, PDX MRD cells and their dividing/untreated controls) from the bone marrow (see 3.2.4) and frozen patients' aspirates (see 2.1) were sorted for RNA-seq (see 3.2.9) and were handed over to the working group of our cooperation partner Prof. Wolfgang Enard (Department Biologie II, LMU, Munich) for preparation of the cDNA library

and sending the samples for RNA-seq. In Table 9 all samples are listed which were sequenced in this study. Only matched LRC and non-LRC bulk samples were from the same mice.

Table 9: List of sequenced ALL samples

sample	bulk	single cell
ALL-199 LRC	4	-
ALL-265 LRC	1	15
ALL-199 non-LRC	4	-
ALL-265 non-LRC	1	35
ALL-199 MRD cells	14	90
ALL-265 MRD cells	4	-
ALL-199 ctrl cells	8	31
ALL-265 ctrl cells	4	-
patient MRD cells	3	-
patient diagnosis cells	5	-

LRC (label retaining cell) = dormant PDX cells; non-LRC = dividing PDX cells; MRD (minimal residual disease) cells = chemotherapy treated cells; ctrl (control) = untreated cells

Single cell cDNA and library preparation were done with Fluidgm C1 platform (Fluidgm, USA) and the bulk RNA-seq preparation was performed by the working group of Prof. Enard. The libraries were sent to the Laboratory for Functional Genome Analysis (Gene Center, LMU, Munich) for sequencing with Illumina HiSeq1500 (Illumina, USA). RNA-seq data were deposited in NCBIS`s Gene Expression Omnibus (GEO) database and is accessible through the GEO accession number: GSE83142. Raw count data from all sequencing reads were generated by the working group of Prof. Enard (Ebinger, Özdemir et al. 2016) and were used for the following analysis in cooperation.

3.5.1 Bioconductor R – DESeq2: from raw counts to fold changes

The R package DESeq2 was used to make a differential expression (DE) analysis (Love et al. 2014). For bulk RNA-seq only the cell data sets were taken which obtained at least $1x10^5$ reads, and for single cell RNA-seq only those with more than $1x10^6$ reads per each cell.
Log_2 fold changes were calculated by using the Wald test. Hierarchical clustering of samples was done with the complete linkage based on Euclidian distances of variance stabilizing data (VSD) from DE genes. Only the top 500 genes with lowest padj (FDR adjustment) were

plotted as heatmap. The reference expression value is the expression average of the control cells.

Principal Component Analysis (PCA) was performed using VSD of the 500 most variable genes to display the main sample variance.

To analyze combined data from all obtained single-cells, count data was normalized accounting for batch effects (Risso et al. 2014). For combined LRC signature (ALL-199 & ALL-265; top 250 genes with log2 fold change > 1; padj < 0.05) single cell datasets were included by summarized gene-wise median read count as one LRC and non-LRC replicate. For combined MRD DE genes of both PDX samples, the average of MRD 199 bulk count data was created to have identical numbers of MRD 265 bulk samples.

All used packages in R with the version numbers are listed in 6.3 in the appendix.

3.5.2 Gene Set Enrichment Analysis

Gene set enrichment analysis (GSEA) was performed using GSEA Desktop Application (Subramanian et al. 2005). For ranking all genes, a metric score was calculated and submitted to the Pre-RankedGSEA tool, like recommended from the authors:

$$\text{metric score} = \text{log2 fold change x } (-\log10(\text{padj}))$$

The statistical significance was determined by 1,000 gene set per mutations. The Molecular Signatures Database (MSigDB) (Liberzon et al. 2015) and the KEGG pathways (Kanehisa et al. 2012) were used for enrichment terms. Furthermore, published gene signatures from patient data were chosen for association with the PDX gene expression profiles. All gene signatures contain only upregulated genes.

3.6 Statistics

All the statistical analysis in this study was calculated with the GraphPad Prism 6 software. Two-tailed unpaired t-test was applied to evaluate differences. In case, the standard deviations differed significantly in the F-test, Welch´s correction was applied.

4 Results

The two features of dormancy and chemotherapy resistance are the major challenges in the conventional acute lymphoblastic leukemia (ALL) treatment. Therefore, the aim of this thesis was to characterize dormant and chemotherapy-resistant ALL cells in order to develop novel treatment strategies for improving patients' outcome. Towards this aim, my investigations made use of the patient-derived xenograft (PDX) mouse model, as primary dormant and chemotherapy-resistant leukemic cells are very low in numbers, difficult to identify in biopsies and cannot be cultivated *in vitro* (see 1.3).

4.1 Preclinical chemotherapy treatment trials in the PDX mouse model

The first step towards the aim of the thesis was to study chemotherapeutic effects and resistance against chemotherapy. Therefore, I established various PDX mouse models using different chemotherapy regimens *in vivo*.

4.1.1 Inducing minimal residual disease (MRD) after chemotherapy

ALL therapy is based on the excessive use of cytostatic drugs. During and after treatment chemotherapy resistance can be detected. Small numbers of leukemic cells remaining after therapy and within remission, without signs and symptoms of leukemia, are defined as minimal residual disease (MRD). The detection of less than 1% leukemic blasts in the bone marrow is termed MRD in the clinics. MRD is the main reason for patients' relapse and poor prognosis (see 1.1.2)(Borowitz et al. 2008; Buckley et al. 2013; Campana. 2010). Due to the minute numbers of patients' MRD cells in the entire bone marrow, no functional research is feasible. Thus, I aimed to establish a preclinical model for MRD using patients' leukemia cells growing in mice which, as far as to my knowledge, does not exist as such so far.

The ALL xenograft mouse model is based on the immunocompromised NOD scid gamma (NSG) mice (Kamel-Reid et al. 1989; Lee et al. 2007; Liem et al. 2004). NSG mice show reduced innate immunity by decreased activity of dendritic cells and macrophages. Furthermore, these mice have a disorder in the adaptive immune system by lacking mature T- and B-cells in addition to the null mutation in the interleukin 2 receptor gamma chain. These characteristics are necessary for the engraftment and growth of human primary material in

NSG mice (Ishikawa. 2013; Shultz et al. 2005). In this thesis the two PDX samples, ALL-199 and ALL-265, from two different ALL patients, were used continuously (see 2.2).

The transgenic PDX samples ALL-199 and ALL-265 were used for the establishment of a PDX MRD model (see 2.2). The aim was to mimic patients' MRD situation as close as possible. At diagnosis, patients usually show an advanced state of disease with high tumor burden in the bone marrow as clinical symptoms appear late. After initial chemotherapy this tumor load is decreased drastically. The defined MRD level of less than 1% blasts in the entire bone marrow is often reached (Buckley et al. 2013; Inaba et al. 2013). Thus I aimed at mimicking both, high leukemic burden as well as less than 1% MRD blasts after chemotherapy, in the PDX MRD mouse model.

Bioluminescence *in vivo* imaging for disease monitoring was used to define both disease stages in a non-invasive way. In contrast to other methods of disease monitoring like measurement of human blasts in mouse blood, imaging is sensitive enough to monitor the course of disease even at minor leukemia burden as in MRD (Terziyska et al. 2012; Vick et al. 2015).

To demonstrate the correlation of imaging signal and leukemic burden $1x10^6$ thawed or freshly isolated PDX cells from the spleen of a passaging mouse (ALL-199 and ALL-265) were injected in several recipient mice (see 3.2.3). The PDX cells were transduced with the firefly luciferase reporter gene. The injection of D-Luciferin, the substrate of firefly luciferase, induces an enzymatic reaction leading to bioluminescence, which is measured with IVIS Lumina II Imaging System (PerkinElmer, USA). With this technique leukemia burden was followed in living mice (see 3.2.5).

In both samples, low imaging signals of a maximum of $2x10^9$ photons per second per cm^2 per steradian (lg photons s^{-1}) correlated with less than 1% of PDX cells in the bone marrow. A high tumor load with more than 10% of blasts in the isolated bones resulted in high imaging signals with at least $1x10^{10}$ photons per second per cm^2 per steradian for ALL-265 and $5x10^{10}$ photons per second per cm^2 per steradian for ALL-199 (see Figure 7). *In vivo* imaging signals were reliable and correlated with high significance with the percentage of PDX cells in the bone marrow. Thus, bioluminescence *in vivo* imaging allows monitoring the entire tumor load spectrum required for establishing a PDX MRD model.

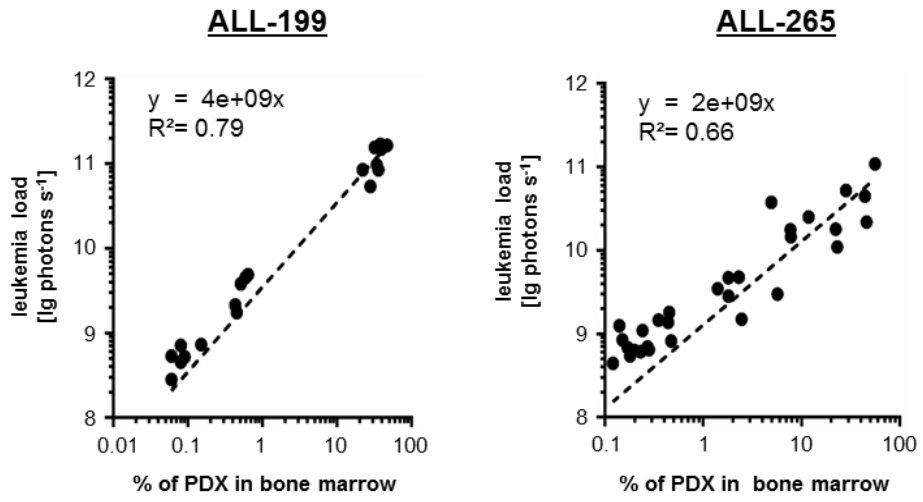

Figure 7: High correlation of *in vivo* imaging signal and PDX cell percentage in the bone marrow.
The PDX samples ALL-199 and ALL-265 were transgenic for the firefly luciferase. Before the bone marrow was isolated, the mice were imaged for *in vivo* bioluminescence. The percentage of PDX cells in the bone marrow, based on FACS data, shows a high correlation with the *in vivo* imaging results in both samples.

For the PDX MRD mouse model a reduction of high tumor load to MRD level was necessary and I aimed to reach this by using a polychemotherapy, which is defined as the use of at least two different cytostatic drugs (Lippert et al. 2014). Such treatment strategies are also pursued in patients. To establish polychemotherapy, suitable for mice and close to the situation in the clinics, pre-experiments were performed with 4 cytostatic drugs to test their tolerance in NSG mice and effects on leukemia growth. All drugs, which are commonly used in ALL patients' therapy, were administered once a week and the effects were determined by i*n vivo* imaging. The test series indicated that Vincristine (VCR) and Cyclophosphamide (Cyclo) were better tolerated by NSG mice and were more effective than Etoposide or Dexamethasone as shown by inhibition of tumor growth (see Appendix Figure 37). Treatment with the same drug concentration over several weeks without any significant weight loss (<10% after therapy start) of mice was defined as a good tolerated drug. Etoposide, which showed high leukemia burden reduction, was not considered for a long-term trial due to high toxicity (see Table 10).

Table 10: Summary of the tested cytostatic drugs according to tolerance in NSG mice and effects on leukemia growth inhibition over several weeks of treatment

drug	tolerance in NSG mice	effect in PDX ALL cells
Vincristine	high (<0.5 mg/kg)	high
Cyclophosphamide	high (<100 mg/kg)	low
Etoposide	low (30-50 mg/kg) low (< 10 mg/kg)	high low
Dexamethasone	low (2 mg/kg)	no effect

low tolerance = mice had to be sacrificed within 1 week due to high weight loss (>10 % of weight loss since therapy start);

To mimic patients' long-term treatment, one additional criterion was the moderate decrease of leukemia burden for several weeks. For this reason the concentrations of VCR and Cyclo were optimized with respect to a combined therapy over several weeks. The used concentrations matched also to patients' dose in the clinics (see Table 8 in Methods).

These experiments revealed that a treatment consisting of 0.25 mg/kg VCR (i.v. once per week) combined with 100 mg/kg Cyclo (i.p. once per week, two days after VCR) is well tolerated in NSG mice and effectively reduces tumor burden with a suitable kinetic. This chemotherapy scheme was used in all further experiments in both samples (see Figure 8).

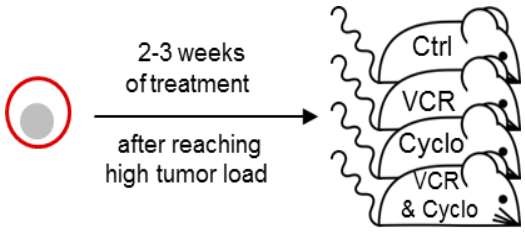

Figure 8: Scheme for generating PDX MRD cells *in vivo*.
$1x10^6$ freshly isolated or thawed transgenic PDX cells were injected into each mouse. PDX cells were positive for the following transgenes: mCherry, truncated NGFR and firefly luciferase. Leukemia engraftment and therapy effects were followed by *in vivo* imaging. After reaching high tumor load chemotherapy was initiated. VCR (0.25 mg/kg; i.v.) and Cyclo (100 mg/kg; i.p.) were injected weekly as single dose for a mono- or combination therapies. The untreated control group received PBS. After 2 or 3 weeks, depending on the sample, therapy was stopped and the mice were analyzed. Adapted from (Ebinger, Özdemir et al. 2016).

Next, we aimed to induce MRD with the established polychemotherapy protocol in order to isolate PDX MRD cells from the animals. Towards this aim, PDX cells were grown to an advanced disease stage as confirmed by *in vivo* imaging. Tumor burden of mice was analyzed at that time point and indicated approximately 40% blasts in the bone marrow. For treatment,

a single dose of each cytotoxic drug was injected weekly as mono- or combination therapies (see 3.2.7). Imaging was performed before each new treatment series. Figure 9A displays the raw *in vivo* imaging data as example for treatment effects in ALL-199. The untreated control group showed an increased imaging signal over 7 days after treatment start. This group had to be sacrificed between days 7 and 10 due to advanced leukemia, as indicated by the enlarged spleens at day 7. All treated groups indicated continuously decreasing signal intensities. The combination therapy showed higher reduction of leukemia cells compared to monotherapies. Figure 9B summarizes all imaging data over time of each sample and therapy group.

To determine tumor burden and to isolate PDX cells bone marrow of mice was analyzed after sacrificing. The untreated control group had to be taken down with approximately 60% of blasts after 1 week of therapy start for ALL-199 or after 2 weeks for ALL-265. Cyclo treatment (100 mg/kg) alone retarded the leukemia growth of ALL-199 and reduced the leukemia load to 10% of ALL-265 cells in the bone marrow after 2 weeks of treatment. In comparison, VCR treatment (0.25 mg/kg) reduced drastically the leukemia load to a level of approximately 1% blasts in both samples. ALL-199 (0.5% of blasts after two treatment rounds) was more sensitive to VCR than ALL-265 (1.8% of blasts after three treatment rounds; see Figure 9C).

MRD level of less than 1% blasts in the bone marrow was only obtained with combination therapy of VCR and Cyclo for both PDX samples. It was even possible to reduce the leukemia load to blast levels of around 0.1% after 2 or 3 weeks of treatment, depending on the PDX sample. Thus, ALL-199 and ALL-265 showed a similar treatment response in combination therapy, but differed in monotherapies (see Figure 9C).

In the following VCR and Cyclo treated PDX cells at MRD level are defined as PDX MRD cells. From each mouse with a level of 0.1% blasts, approximately 40,000 PDX MRD cells were isolated from the entire bone marrow.

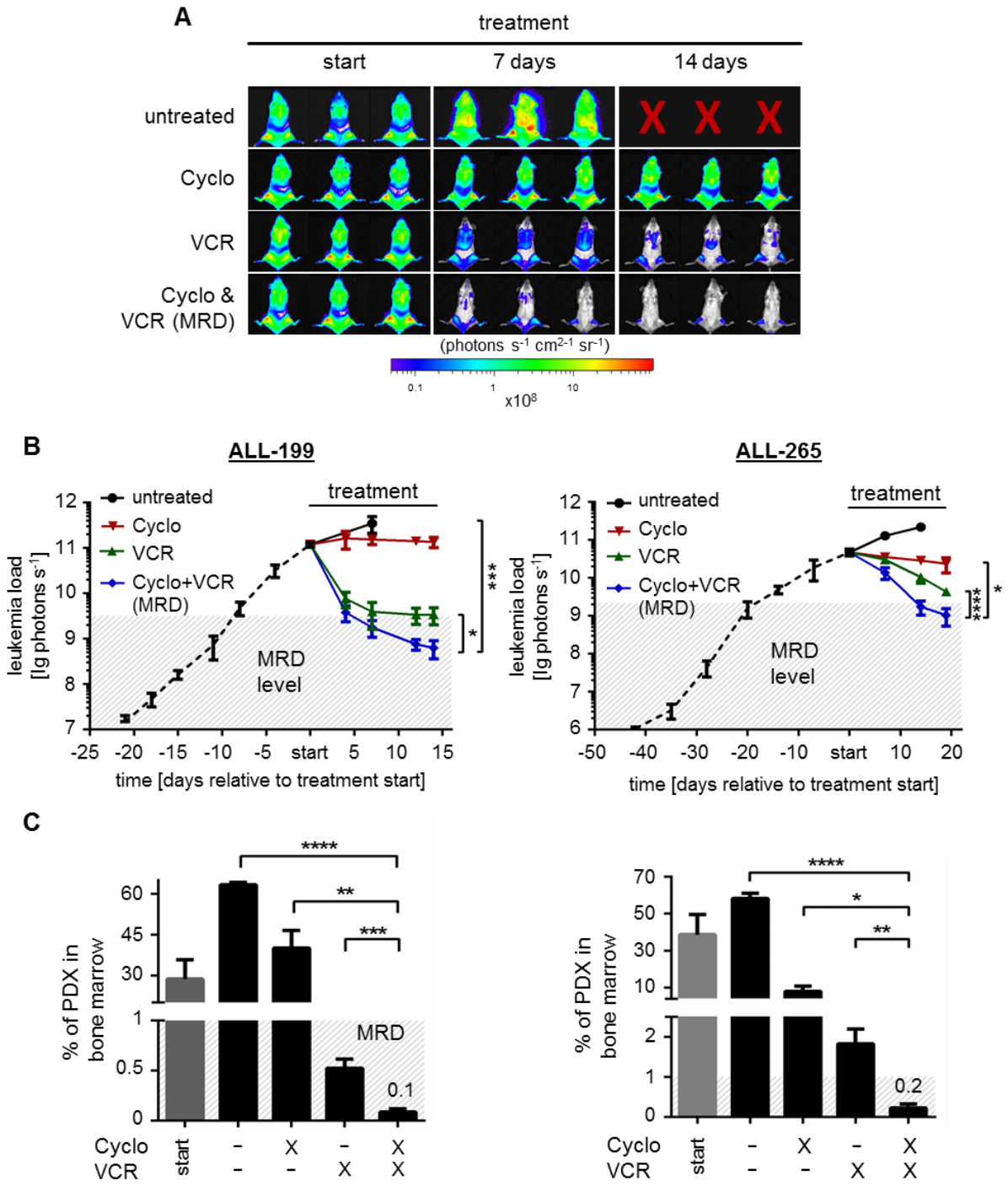

Figure 9: MRD level is achieved for both PDX samples with the combination therapy.

One representative experiment for each PDX sample is shown with at least 3 and maximum 8 mice per group. VCR (0.25 mg/kg; i.v.) and Cyclo (100 mg/kg; i.p.) were injected weekly as single dose for mono- or combination therapies. The untreated control group received PBS. MRD level was defined with less than 1% PDX cells in the bone marrow (grey background). (A) Raw *in vivo* imaging data of three representative mice per group of ALL-199 are shown. Units in rainbow color scales are photons per second per cm^2 per steradian (photons s^{-1} cm^{2-1} sr^{-1}). (B) The summarized *in vivo* imaging data over time shows the leukemia burden before and during treatment. (C) After sacrificing the mice, the percentages of PDX cells in the bone marrow were determined. The left panel summarizes the data for ALL-199 and the right panel the data for ALL-265. Statistical significances were calculated using two-tailed unpaired t-test (*p<0.05, **p<0.01, ***p<0.001, ****p<0.0001). Adapted from (Ebinger, Özdemir et al. 2016).

Taken together, a PDX MRD mouse model for two PDX samples was established mimicking the situation of patients with MRD. With VCR and Cyclo combination therapy, high leukemia load was reduced more than 100-fold to the MRD level of 0.1% PDX cells in the bone marrow.

4.1.2 Different effects in long-term VCR treatment in PDX samples

After establishment of the PDX MRD model, the effect of long-term VCR treatment was analyzed in both ALL samples according to development of chemotherapy resistance. The combination therapy with VCR and Cyclo was too stressful for mice after 3 weeks of treatment as the mice started to lose continuously weight. Therefore, monotherapy with VCR, which was more efficient than Cyclo, was used for long-term studies (see Figure 9).

After inducing leukemia with ALL-199 and ALL-265 and reaching high tumor load, treatment with VCR (0.5 mg/kg), one dose per week, was initiated. Compared to the established PDX MRD model the concentration of VCR was increased to the highest tolerable dose in monotherapy in order to raise the chemotherapeutic stress in the PDX cells (see Table 10). Both ALL samples showed a very different VCR sensitivity in long-term treatment (see Figure 10). After 4 weeks VCR treatment was stopped in ALL-199 due to a strong reduction of leukemic burden as determined by *in vivo* imaging. Suspending the VCR treatment in the ALL-199 sample led to the regrowth of the leukemia. In contrast, ALL-265 was resistant to VCR chemotherapy. Over a course of 10 weeks VCR treatment, the leukemia load decreased only slowly but never reached MRD level. The following low increase in *in vivo* imaging signal after this time point indicated an outgrowth of leukemia. After sacrificing the mice of the VCR ALL-265 group, the entire bone marrow contained 2.5% of PDX cells.

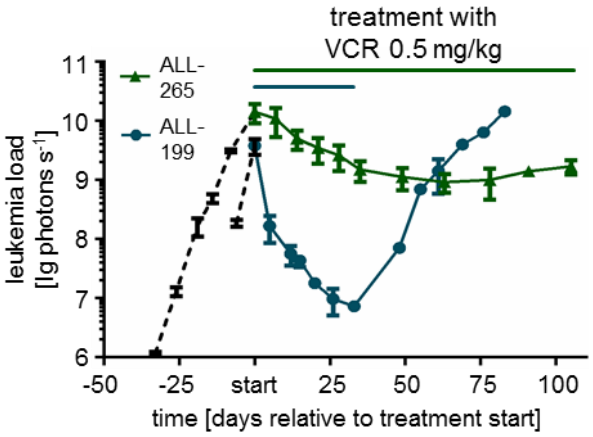

Figure 10: Long-term treatment with VCR shows different effects in PDX samples.
Both PDX ALL samples were treated weekly with a single dose of 0.5 mg/kg VCR (i.v.). ALL-199 was sensitive for VCR in contrast to ALL-265, in which a resistance to VCR was observed. Adapted from (Ebinger, Özdemir et al. 2016).

This experiment confirmed the observation that ALL-199 is more sensitive to VCR treatment than ALL-265 (see Figure 10). VCR reduced ALL-199 to very low cell numbers and easily reached MRD level. However, the remaining PDX ALL cells proliferated quickly after withdrawal of VCR. In contrast, a VCR-resistant population of ALL-265 arose after a long-term therapy.

4.1.3 PDX MRD cells reveal certain chemotherapy resistance

The next question was, whether the PDX MRD cells acquired functional changes by treatment influencing homing efficiency and chemotherapy sensitivity compared to untreated control cells.

To address this question, PDX MRD cells and untreated control cells were freshly isolated from the bone marrow of the first treatment round and PDX cells were enriched specifically using the mCherry transgene. All MRD cells of all mice in the MRD group (VCR & Cyclo; n = 6) were merged due to low cell numbers. The same was performed with the control group (n = 3). At the end the sorted cells were injected in 8 recipient mice per group with equal cell numbers of $4x10^4$ cells (see Figure 11).

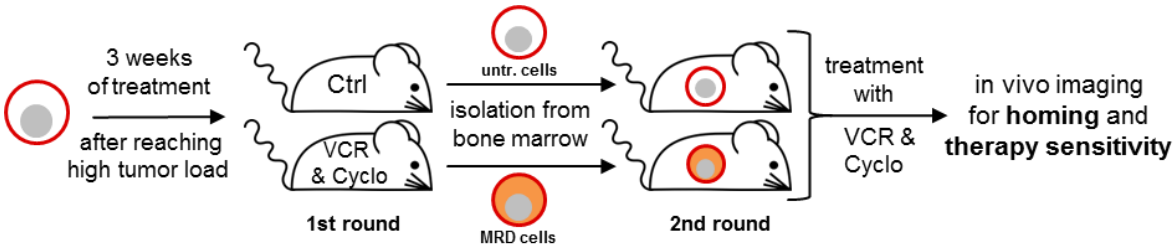

Figure 11: Scheme for re-passaging and retreatment of PDX MRD cells in ALL-265.
After first round of treatment with combination therapy with VCR (0.5 mg/kg; i.v.) and Cyclo (100 mg/kg; i.p.) for 3 weeks and reaching the MRD level, PDX cells were isolated from the bone marrow. Due to low MRD cell numbers, PDX cells of all 6 mice of the VCR & Cyclo group and PDX cells of the 3 mice of the untreated control group were combined in each case and $4x10^4$ of the sorted MRD or control cells were injected into each recipient mice per group (n=8) for the second treatment round. Upon engraftment cells were allowed to grow out to a high tumor load, potential differences in homing efficiency were determined and both groups were treated with the same combination therapy to investigate changes in treatment sensitivity.

In vivo imaging was performed to investigate potential differences in homing and engraftment between the untreated control cells and the PDX MRD cells from the first treatment round. No significant differences for homing and engraftment were observed between the two groups (see Figure 12A).

After reaching high tumor load, combination therapy with VCR and Cyclo was repeated for the MRD as well as the untreated control group from the first round. The treatment was initiated by reaching 50% PDX cells in the bone marrow (see Figure 12B). After 3-weeks of combination therapy, 0.1% of PDX cells in the bone marrow in the control group and 0.3% in the MRD group were reached. A 2.5-fold higher amount of PDX cells was isolated from the MRD group ($2.2x10^5$ cells) compared to the control group ($0.9x10^5$ PDX cells), which

received therapy for the first time (see Figure 12C). These significant differences were also observed in the *in vivo* imaging.

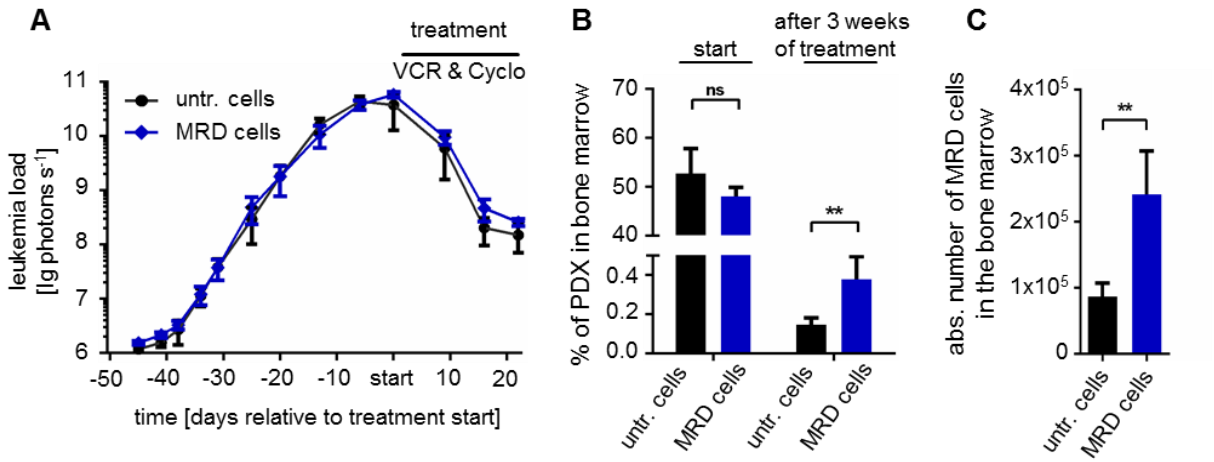

Figure 12: ALL-265 PDX MRD cells re-engraft in recipient mice and display higher chemotherapy resistance compared to the control group.

$4x10^4$ of ALL-265 untreated or PDX MRD cells were injected into each mouse for both groups (n=8). After reaching high leukemia load, the MRD group as well as the untreated control group was treated with the combination therapy of 0.5 mg/kg VCR (i.v.) and 100 mg/kg Cyclo (i.p.) as one passage before for the PDX MRD cells. (A) The summarized *in vivo* imaging data over time shows the leukemia burden before and during treatment. After sacrificing the mice, the percentage (B) and the absolute numbers (C) of PDX cells in the bone marrow were determined. Statistical significance was calculated using two-tailed unpaired t-test (ns = no significane, **p<0.01).

In summary, no differences in homing and engraftment were observed between the PDX MRD and control cells. Three weeks of combination therapy had no effect on PDX MRD cells for the outgrowth of leukemia in the next passage compared to the untreated control group.

However, the chemotherapy sensitivity was significantly different between the both groups. In the second treatment round, the MRD group was more resistant to combination therapy than the control group. The treatment in the first passage had an influence in the next therapy round. The PDX MRD cells acquired a certain drug resistance after the first combination therapy compared to the control group. In conclusion, an innovative mouse model of *in vivo* induced chemotherapy resistance was established.

Taken together, I developed the worldwide first preclinical PDX mouse model of MRD and a model of long-term treatment using VCR. I could show that PDX MRD cells develop certain chemotherapy resistance after treatment in mice.

4.2 Localization of dormant and chemotherapy-resistant PDX cells in the bone marrow

Dormancy and chemotherapy resistance in ALL is increasingly attributed to influence of the bone marrow environment (see 1.1.3) (Schepers et al. 2015). Furthermore, in our institute this concept was confirmed by the previously established label retaining cell (LRC) mouse model. In the LRC mouse model PDX cells were labeled with the fluorescent proliferation marker CFSE before cell injection into NSG mice. CFSE signal is halved by every cell doubling. A minute ALL subpopulation did not lose any CFSE signal over time. The retaining CFSE signal is associated with no cell division and consequently with dormancy. These dormant PDX cells (LRC) were chemotherapy-resistant *in vivo*, but chemotherapy sensitive *in vitro* like dividing PDX cells (non-LRC). Furthermore, a high plasticity within the both populations was observed. LRC and non-LRC were able to engraft in the next passage and showed the identical engraftment pattern of dormant and dividing cells (see 1.3.1; Ebinger, Özdemir et al. 2016).

These findings led to the hypothesis that the localization of LRC and PDX MRD cells in the bone marrow is crucial to gain the challenging features of dormancy and drug resistance. Therefore, my next aim was to identify the localization of dormant and chemotherapy-resistant leukemic PDX cells within the bone marrow.

4.2.1 After engraftment, the two PDX samples show different localization patterns

First, the bone marrow localization of PDX samples ALL-199 and ALL-265 was investigated directly after PDX cell injection and engraftment. The mCherry reporter gene, which is expressed in both PDX samples, allows their unambiguous identification and visualization in the femurs of transduced mice. The schematic outline of the protocol is shown in Figure 13.

To identify the localization of the PDX cells within the bone marrow, I newly established generating cryosections of femurs. Unfortunately, the fixation step of the femur preparation protocol destroyed the mCherry signal. For this reason, an antibody staining against mCherry had to be established for the detection of PDX cells. In contrast to the mCherry signal, the CFSE fluorescence signal of the PDX cells was still detectable after fixation. Therefore, $mCherry^+$ $CFSE^+$ PDX cells were used to establish the mCherry antibody staining while the CFSE signal was used as a positive control (see Figure 13). At day 3 after cell injection all PDX cells were still $CFSE^+$.

A high correlation between the CFSE and the mCherry antibody signal was observed in these femur sections. The mCherry signal was always detectable in $CFSE^+$ cells in the bone marrow (see Figure 38 in the appendix). The negative controls were femur sections without any PDX cell injection or with $mCherry^-$ PDX cells. These sections were completely negative for mCherry antibody staining.

After establishing the mCherry antibody staining for PDX cell detection in the bone marrow, an engraftment kinetic of leukemia growth was performed. Therefore, freshly isolated PDX cells from the spleen of a donor mouse were labeled with CFSE and $1x10^7$ $CFSE^+$ $mCherry^+$ PDX cells were injected into recipient mice. At days 3, 7, 10 and 14 after cell injection one mouse was sacrificed at each time point and the localization of the PDX cells was analyzed for both samples ALL-199 and ALL-265 (see Figure 13).

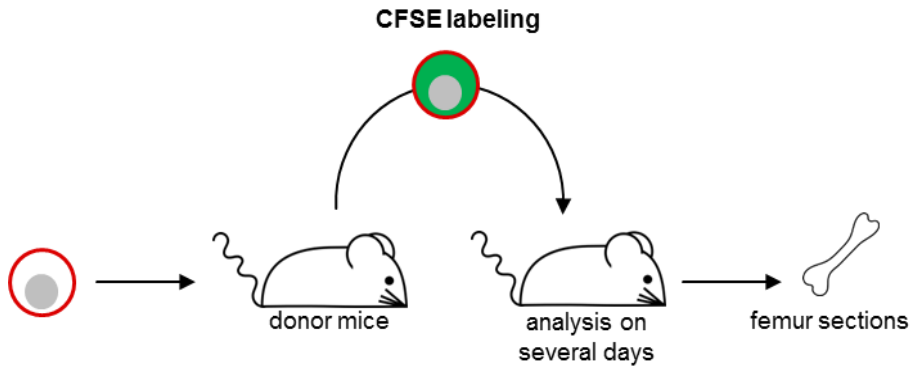

Figure 13: Scheme for the PDX cell localization in femur sections during engraftment.
$mCherry^+$ PDX cells were freshly isolated from the spleen of the donor mice and labeled with CFSE *ex vivo*. Recipient mice were injected with 10^7 $CFSE^+$ $mCherry^+$ PDX cells into the tail vein. After several days the femurs were taken for histological analysis. Adapted from (Ebinger, Özdemir et al. 2016).

The engraftment pattern was similar for all time points of each sample. PDX ALL-199 cells were randomly distributed in the bone marrow during engraftment (see Figure 14), whereas the sample ALL-265 engrafted close to the bone matrix (see Figure 15).

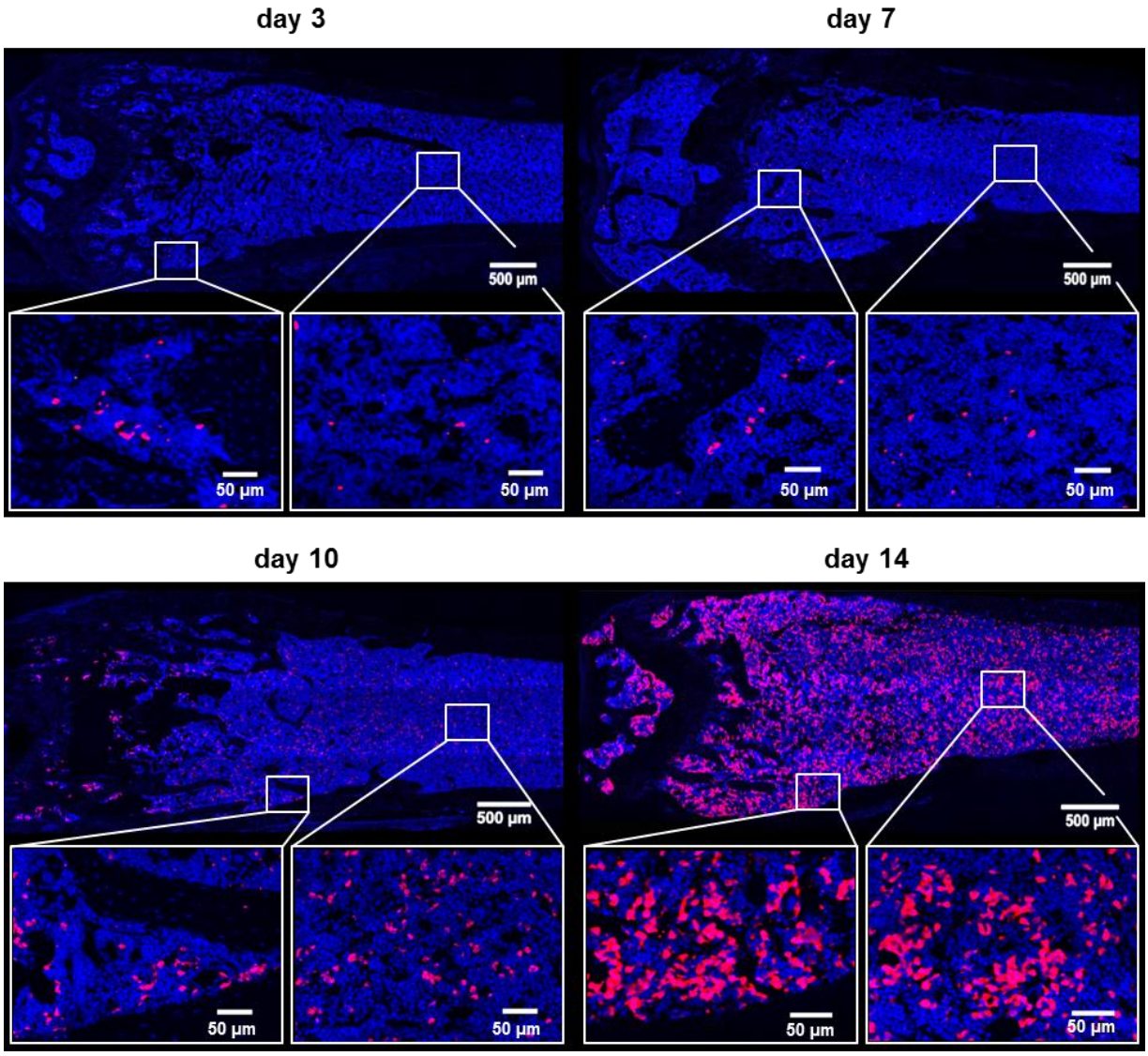

Figure 14: ALL-199 PDX cells engraft randomly in the femur.

ALL-199 PDX cells were positive for mCherry and were visualized by mCherry antibody staining shown in a kinetic at different days after cell injection. The nuclei were counterstained with DAPI. The left magnification box of each time point shows the area around the endosteum and the right magnification box of each time point shows perivascular regions. (red = mCherry; blue = DAPI)

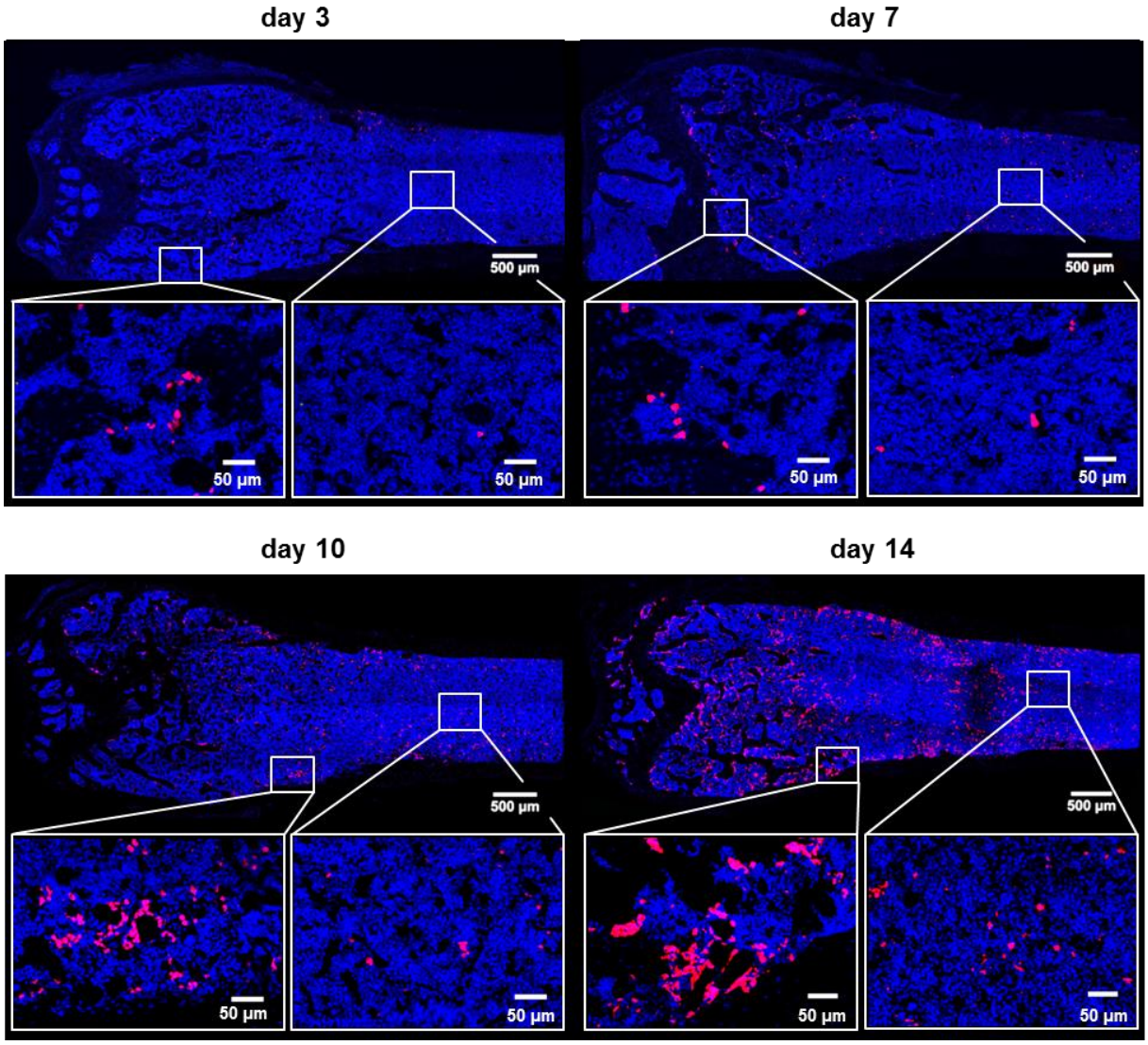

Figure 15: ALL-265 PDX cells engraft primarily in endosteal regions.
ALL-265 PDX cells were positive for mCherry and were visualized by mCherry antibody staining shown in a kinetic at different days after cell injection. The nuclei were counterstained with DAPI. The left magnification box of each time point shows the area around the endosteum and the right magnification box of each time point shows perivascular regions. (red = mCherry; blue = DAPI)

Femur sections were analyzed with the software ImageJ to quantify PDX cells localized in the endosteal region at day 3, 7 and 10 after cell injection. At day 14 after cell injection the PDX cell density was too high for precise quantification.

For the PDX cell localization of both samples similar kinetics were determined. At day 3 after cell injection the majority of the PDX cells were close to the endosteum. The region around the bone matrix is called endosteum or endosteal niche (see Figure 2 in the introduction). The endosteum is defined as the region with a distance of less than 100 µm from the bone matrix (Nombela-Arrieta et al. 2013). At day 3 after cell injection approximately 50% of ALL-199 PDX cells and approximately 70% of ALL-265 PDX cells localized in this region. Until day

10 the percentage of PDX cells in the endosteum decreased significantly (see Figure 16). However, ALL-265 engraftment remained more associated to the endosteal region than ALL-199 cells.

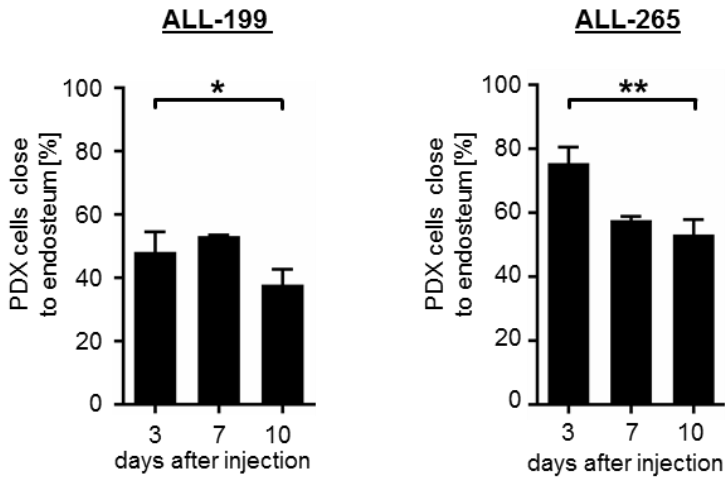

Figure 16: The PDX samples ALL-199 and ALL-265 show a similar distribution kinetic in the endosteum during engraftment.
Quantification of PDX cells in femur sections was performed using ImageJ. The endosteum is defined as the region with a distance of less than 100 µm from the bone matrix. At least 2-3 sections from both femurs of 2 mice per data point were analyzed. Statistical significance was calculated using two-tailed unpaired t-test (*p<0.5, **p<0.01). Adapted from (Ebinger, Özdemir et al. 2016).

The PDX samples showed a different engraftment pattern but a similar distribution kinetic over time in the endosteum. At day 3 after cell injection, most PDX cells were localized to the endosteum in both samples. In the following days the percentage of PDX cells in the endosteal region decreased constantly. However, ALL-265 cells were closely localized to the endosteal region at all-time points. In contrast, ALL-199 cells exhibited a more random engraftment pattern in the bone marrow.

4.2.2 Enhancing the CFSE signal by antibody staining

One hypothesis is that the dormant and drug resistant LRC and PDX MRD cells gain these features through a specific localization in the femur. Therefore, the next aim was to identify the localization of dormant PDX cells during engraftment in the LRC mouse model (see Figure 4 in the introduction). The fluorescent cell staining dye CFSE was used as proliferation marker for identification of dormant LRC ($CFSE^+$ PDX cells). With each cell division the CFSE intensity is reduced by half and consequently dividing PDX cells lose their CFSE

signal. Only non-dividing, dormant PDX cells keep the CFSE over time (Ebinger, Özdemir et al. 2016).

However, the CFSE signal at time points later than day 3 after cell injection was too weak for detection by confocal microscopy. Additionally, high autofluorescence signal in the spectrum of the CFSE signal (green light spectrum around λ=500 nm) made the detection of the CFSE signal complicated. This phenomenon was described in fixed bone marrow sections by Lo Celso and colleagues (Lo Celso et al. 2007). To increase the sensitivity of the experiment, a CFSE antibody staining had to be established allowing the detection of LRC within femur sections later than 3 days after cell injection.

The chemical structures of CFSE and FITC are very similar. Thus, a FITC-antibody (Thermo Fisher Scientific, USA) was tested for CFSE antibody staining (Willfuhr et al. 1989). Similar to the validation of the mCherry antibody staining, femur sections of day 3 after $CFSE^+$ PDX cell injection were used. The high CFSE signal at day 3 functioned as a positive control for the CFSE antibody staining. A secondary antibody, binding the primary FITC/CFSE antibody, was conjugated with the fluorophore Alexa 594 in order to separate the fluorescence spectra of the CFSE and the CFSE antibody signal.

The signal of the CFSE antibody staining correlated with the CFSE signal (see Figure 17). Femur section without any PDX cells or with $CFSE^-$ PDX cells used as negative controls, were indeed negative.

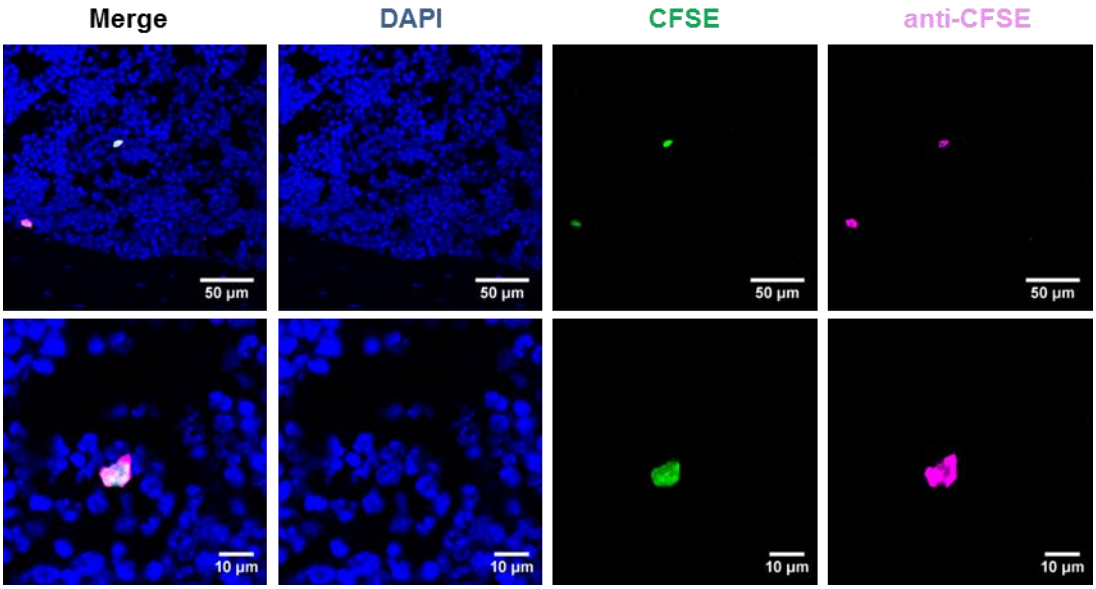

Figure 17: High correlation of the CFSE antibody signal with the CFSE signal.
Femur sections of day 3 after $CFSE^+$ PDX cell injection were stained with the CFSE antibody (purple). The CFSE signal (green) served as positive control for the staining. The nuclei were counterstained with DAPI (blue).

In femur sections of day 7 after cell injection the problem of low CFSE signal was obvious (see Figure 18). Without signal amplification of CFSE, LRC were not detectable in femur sections at later time points than 3 days after cell injection. Therefore, the CFSE antibody staining was necessary and I used the FITC/CFSE antibody to visualize low numbers of LRC in the femur with high specificity and sensitivity.

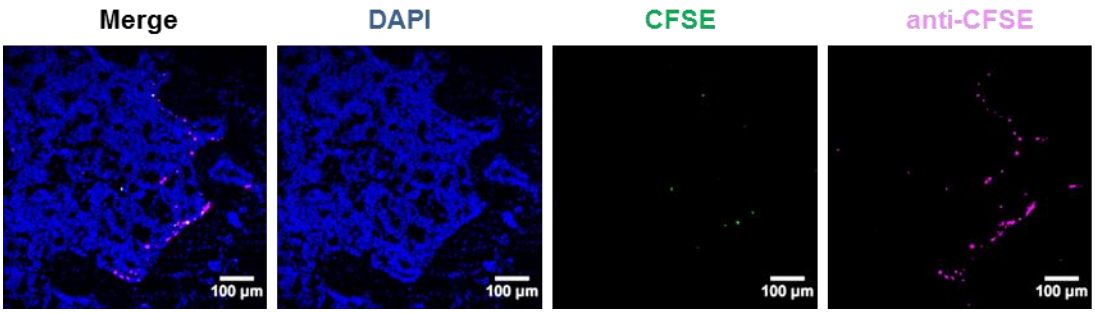

Figure 18: CFSE antibody staining is sensitive enough to detect CFSE$^+$ PDX cells in femur sections later than 3 days after cell injection.
Femur sections of day 7 after CFSE$^+$ PDX cell injection were stained with the CFSE antibody (purple) in order to amplify the CFSE signal (green) for further analysis.

4.2.3 LRC are localized in the endosteum

After establishment of the required CFSE antibody staining for signal amplification, the visualization of LRC was feasible in femur cryosections. Freshly isolated PDX cells from the spleen of a donor mouse were labeled with CFSE *ex vivo* and 10^7 CFSE$^+$ PDX cells were injected into each recipient mouse (see Figure 13). At day 10 after cell injection most PDX cells proliferate in the bone marrow as reasoned from the decreased CFSE labeling. At this time point LRC were identified by their high CFSE signal in FACS analysis, and defined as less than 2% of the entire PDX population or as approximately 0.01% of the entire cells in the bone marrow (see Table 11 in the appendix). A meaningful quantification at later time points was not possible due to continuously decreasing numbers of LRC in the bone marrow. Hence LRC localization was analyzed at day 10 after cell injection via CFSE stainings.
Furthermore, it was not possible to stain one section simultaneously for LRC (CFSE staining) and PDX cells (mCherry staining) as both antibodies had the same species type and required consequently the identical secondary antibody. Thus two consecutive sections were performed and stained either for PDX cells or for LRC.
The endosteal region of the bone marrow was described as the niche for dormancy as demonstrated for hematopoietic stem cells (HSC) (Haylock et al. 2007; Morrison &

Spradling. 2008). Therefore, the hypothesis was that LRC, showing a quiescent phenotype, were localized near to the endosteum.

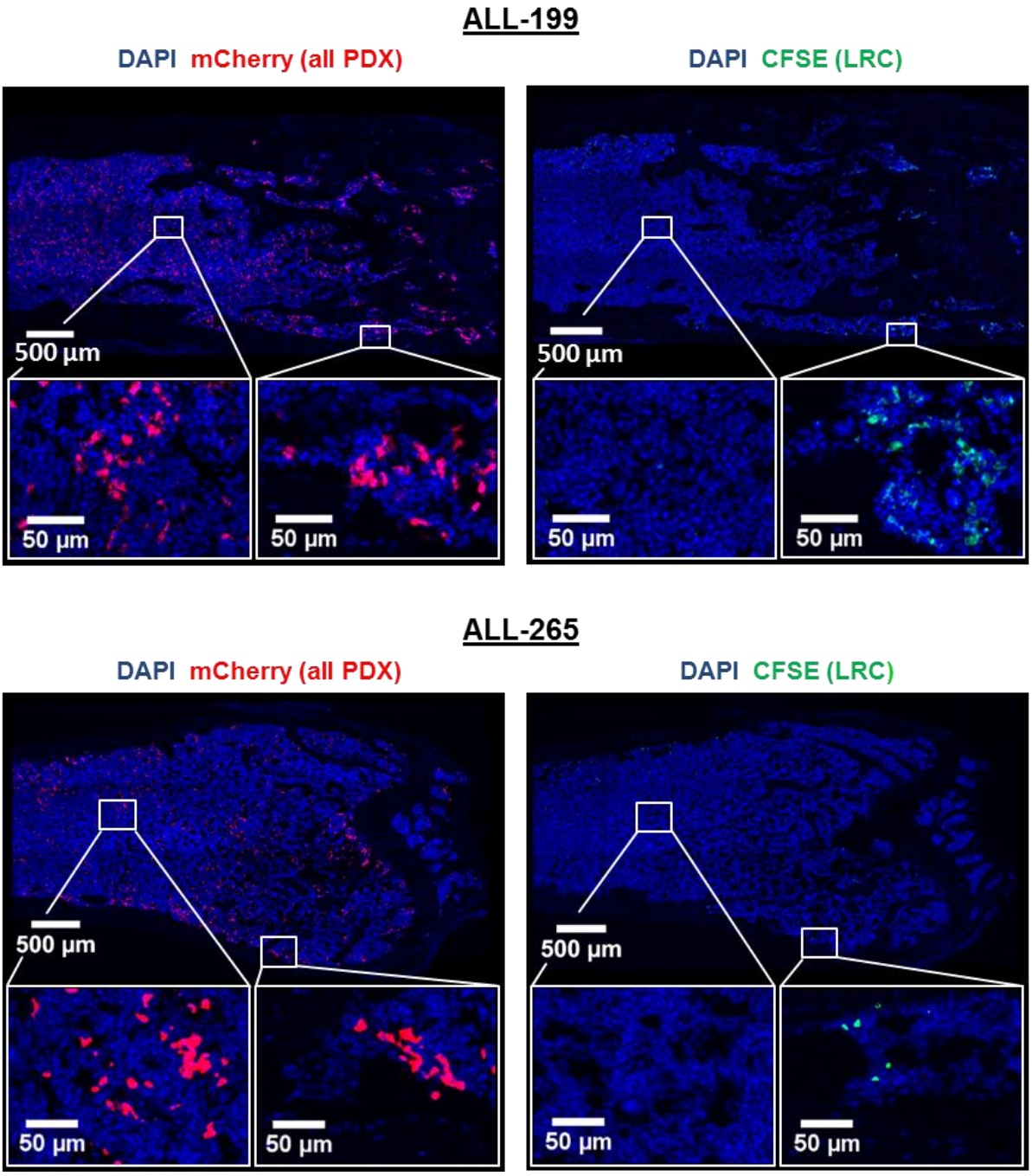

Figure 19: In both PDX samples, ALL-199 & ALL-265, LRC are concentrated to the endosteum compared to proliferating PDX cells.

Consecutive femur sections of day 10 after $CFSE^+$ PDX cell injection were stained with antibodies either for mCherry (PDX cell marker, red) or CFSE (LRC marker, green). The endosteum is defined as the region with a distance of less than 100 µm from the bone matrix. The left magnification box of each femur scan shows perivascular regions and the right magnification box of each femur scan shows the area around the endosteum. The nuclei were counterstained with DAPI (blue). Adapted from (Ebinger, Özdemir et al. 2016).

In both PDX samples LRC localized close to the endosteum, whereas PDX cells were detected in the entire bone marrow (see Figure 19). However, the ALL-265 PDX cells were preferably localized in the endosteal region, as already shown in Figure 15. Besides, ALL-199 exhibited a higher percentage of LRC at day 10 after cell injection than ALL-265 (see Figure 19). This observation was also demonstrated by FACS analysis. In ALL-199 ten times more LRC are present than in ALL-265 at day 10 after cell injection (see Table 11 in the appendix; Ebinger, Özdemir et al. 2016).

All consecutive sections stained for mCherry and CFSE were analyzed with the software ImageJ to quantify the amount of cells localized in the endosteum. Approximately 30% of ALL-199 PDX cells and 50% of ALL-265 PDX cells were located close to the endosteal region as already shown in Figure 16. Both PDX samples showed a complete different tendency to the endosteum during engraftment. However, 70% of LRC of both samples were localized to the endosteum (see Figure 20).

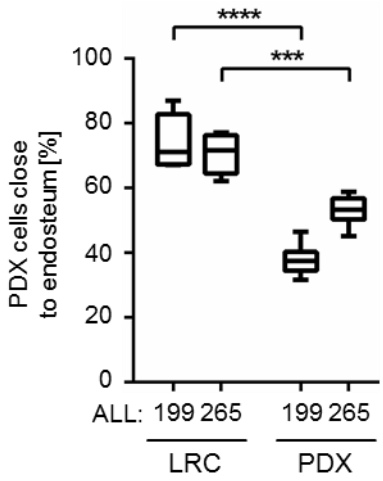

Figure 20: In both PDX samples significantly more LRC are localized in the endosteum compared to the entire PDX cell population.

Quantification of all consecutive femur sections, stained either for mCherry (PDX cells) or CFSE (LRC), at day 10 after cell injection was performed with ImageJ. At least 3 sections from both femurs in 2 mice were analyzed. Endosteal region was defined as less than 100 µm to the bone matrix. Statistical significance was calculated using two-tailed unpaired t-test (***$p<0.001$, ****$p<0.0001$). Adapted from (Ebinger, Özdemir et al. 2016).

Taken together, the hypothesis, that LRC are preferably localized in the endosteum, was confirmed. In ALL-199 as well as in ALL-265 the critical subpopulation of dormant PDX cells (LRC) preferably localized close to the endosteum. Although the rate of engrafted PDX cells differed significantly within both samples, LRC localization to the endosteal region was similar for ALL-199 and ALL-265 at day 10 after cell injection.

4.2.4 PDX MRD cells are localized randomly in the bone marrow

Next to dormancy, chemotherapy resistance is the second challenging feature of patients' MRD in clinics. The importance of the bone marrow environment of chemotherapy-resistant leukemic cells was shown in various studies (see 1.1.3). Leukemic cells interact with the bone marrow microenvironment in order to survive chemotherapy (Boyerinas et al. 2013; Duan et al. 2014). To the best of our knowledge the localization of MRD cells of B-ALL was not investigated so far. Consequently, I next analyzed the localization of chemotherapy-resistant PDX MRD cells in the bone marrow.

The endosteal region provided a niche for dormant PDX ALL cells during engraftment (see 4.2.3 and Figure 19). However, cytostatic drugs can lead to an altered microenvironment in the bone marrow and the chemotherapy induced environmental changes are misunderstood (Wang et al. 2006).

To obtain femurs of chemotherapy treated blasts at MRD level, mice were treated with a combination therapy of VCR and Cyclo after reaching high tumor load. The therapy was administered for 2-3 weeks depending on the PDX sample as previously described in the PDX MRD model (see 4.1.1). At MRD level of around 0.1% blasts in the bone marrow, mice were sacrificed and femurs were prepared for bone marrow sectioning (see Figure 21). PDX MRD cells were positive for the transgenic mCherry and therefore suitable for mCherry antibody staining.

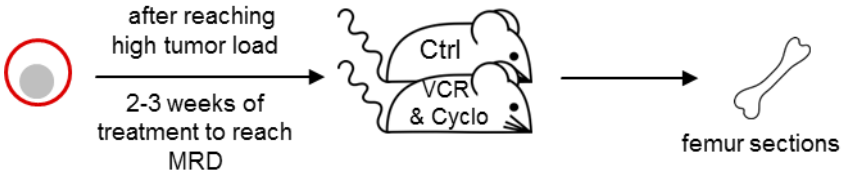

Figure 21: Scheme for generating PDX MRD cells for localization studies in femur sections.
$1x10^6$ freshly isolated or thawed transgenic PDX cells were injected into each mouse. PDX cells were positive for the following transgenes: mCherry, truncated NGFR and firefly luciferase. Leukemia engraftment and therapy effects were followed by *in vivo* imaging. After reaching high tumor load chemotherapy was initiated. VCR (0.25 mg/kg; i.v.) and Cyclo (100 mg/kg; i.p.) were injected weekly as combination therapy. The untreated control group received PBS. At MRD level of about 0.1% blasts in the bone marrow after 2-3 weeks of treatment, mice were sacrificed and the femurs were analyzed by staining for transgenic mCherry which is exclusively expressed by PDX cells.

After a long-term combination therapy with VCR and Cyclo the remaining PDX MRD cells of both samples, ALL-199 and ALL-265, were distributed randomly in the femoral bone marrow. No distinct morphological areas for PDX MRD cell accumulation were observed (see Figure 22).

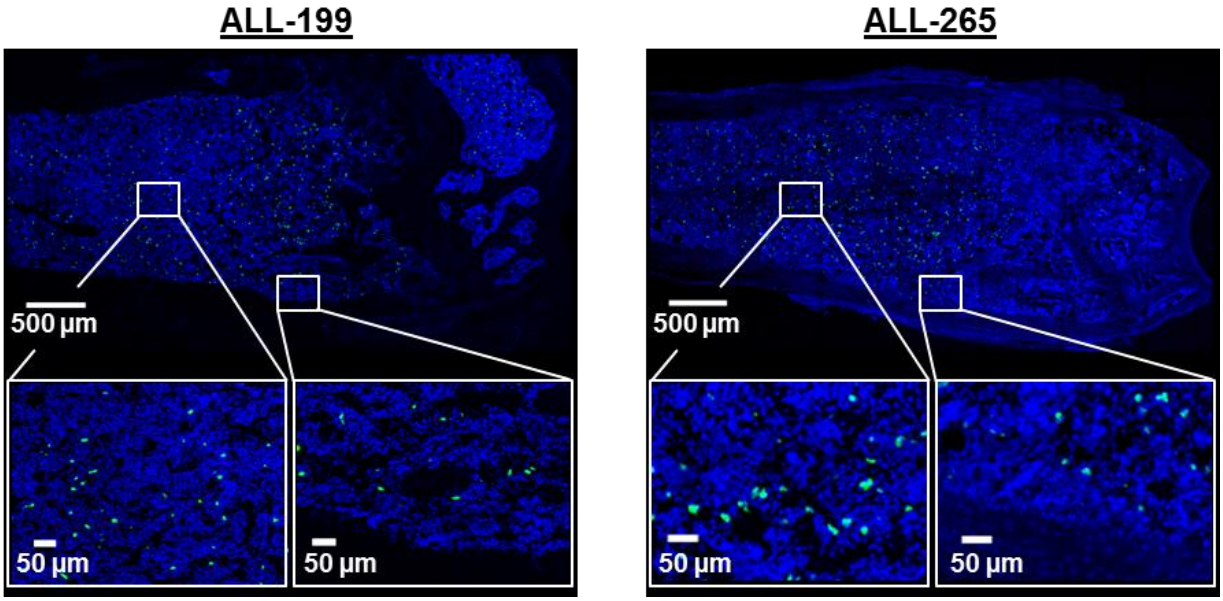

Figure 22: ALL-199 and ALL-265 PDX MRD cells are randomly distributed in the femur after combination therapy.
PDX MRD cells (less than 0.1% blasts in bone marrow after VCR and Cyclo treatment) were positive for mCherry and were detected by specific antibody staining (green = mCherry signal). The left magnification box of each PDX sample shows perivascular regions and the right magnification box of each PDX sample shows the area around the endosteum. The nuclei were counterstained with DAPI (blue).

ImageJ was used for the analysis of the bone marrow scans and revealed that only 30% of the PDX MRD cells were localized close to the endosteum after the combination therapy with VCR and Cyclo. This PDX MRD population showed a sample independent distribution similar to the LRC. In ALL-199 no difference in localization pattern of engrafted PDX cells and PDX MRD cells was observed. In contrast, engrafted PDX ALL-265 cells localized closer to the endosteum than the chemotherapy treated MRD cells (see Figure 23).

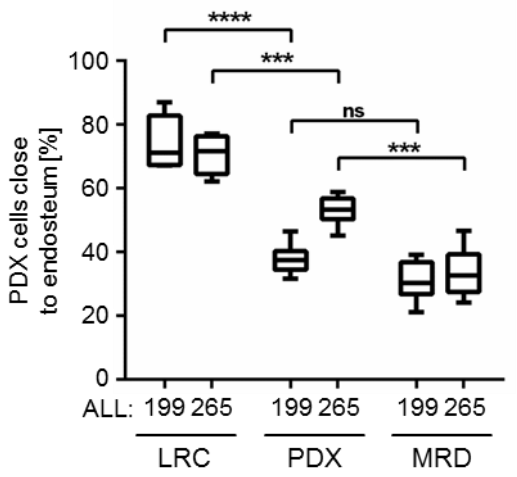

Figure 23: Less PDX MRD cells are localized in the endosteum than LRC or engrafted PDX cells after combination chemotherapy.

Quantification of femur sections, stained for mCherry at MRD level of less than 0.1% blasts in the bone marrow, was performed with ImageJ. At least 2 sections from both femurs in 4 mice were analyzed. Endosteal region was defined as less than 100 µm to the bone matrix. For a better overview the quantification of engrafting PDX cells and LRC at day 10 after cell injection was added (see Figure 20). Statistical significance was calculated using two-tailed unpaired t-test (ns = no significance, ***p<0.001, ****p<0.0001).

In summary, the PDX samples ALL-199 and ALL-265 exhibited a complete different engraftment pattern in the bone marrow. Both PDX samples own a different affinity to the endosteum during leukemia growth. ALL-199 PDX cells engrafted randomly in the bone marrow and ALL-265 PDX cells exhibited an engraftment concentrated to the endosteum.
However, the challenging (sub)-populations like LRC and PDX MRD cells showed similar localization patterns. The LRC accumulate to a higher degree in the endosteum compared to engrafted PDX cells. The PDX MRD cells are less concentrated to this area and are even randomly distributed within the bone marrow.

4.3 Gene expression profiles of dormant and chemotherapy-resistant PDX samples

The LRC and PDX MRD cells are characterized by the clinically challenging features of dormancy and chemotherapy resistance. Both populations depict a high plasticity in functional studies. They have the capacity to engraft in the next passage but are not enriched in stemness according to self-renewal frequency as compared to control cells (1.3.1 and 4.1.3). During one passage in mice the dormant LRC and chemotherapy treated PDX MRD cells differ highly from the proliferating untreated control cells.
It is very likely that dormant and proliferating PDX cells differ in their gene expression patterns. One method to determine the differences in gene expression is RNA-seq. The greatest advantage of RNA-seq compared to microarray is the accurate detection of differently expressed genes (especially with low expression levels) due to the sequencing at nucleotide level. In contrast, microarrays have a high false-positive rate because of unspecific nucleotide binding to the oligos on the microarray chip (Wang et al. 2014; Zhao et al. 2014).

Gene expressions of LRC, PDX MRD cells and the proliferating untreated control cells were determined by RNA-seq. Therefore, the mRNA of these PDX cells were isolated as bulk or single cell, and were sequenced with Illumina HiSeq1500 (Illumina, USA). Gene expression profiles (GEP) of LRC and PDX MRD cells were obtained by direct comparison of the gene expressions between these challenging PDX cells and their proliferating untreated controls. A detailed analysis of the RNA-seq data was performed with the GEP in order to improve our understanding according the challenging features of dormancy and chemotherapy resistance.

RNA-seq of the PDX cells was performed by our cooperation partner Prof. Wolfgang Enard and colleagues (Department Biologie II, LMU, Munich). After alignment of sequencing reads the obtained raw counts were forwarded to me for further bioinformatic analysis under supervision of our cooperation partner (see 3.5).

4.3.1 Gene expression profiles of LRC

First, GEP of LRC were obtained and analyzed in order to gain new insights into the observed reversible dormancy in the LRC mouse model. ALL-199 and ALL-265 PDX cells were isolated freshly from the spleen of the donor mice and labeled *ex vivo* with CFSE before injection into recipient mice. LRC and non-LRC were obtained from isolated bone marrow of the recipient mice approximately 14 days after PDX cell injection (see Figure 24). At this time point less than 0.05% of the PDX population consisted of LRC in both samples (see Table 11 in the appendix). In addition to the mCherry reporter gene, the PDX cells were also transduced for the truncated cell surface protein NGFR. Both transgenes in the PDX cells were used for the enrichment of the PDX population from the murine bone marrow. By using the NGFR transgene for magnetic-activated cell sorting (MACS) enrichment and the mCherry transgene for fluorescence-activated cell scanning (FACS) enrichment, a fast and effective sorting of LRC, $CFSE^+$ PDX cells, and non-LRC, $CFSE^-$ PDX cells, was feasible (see 3.2.9; Ebinger, Özdemir et al. 2016). At least approximately 2,000 LRC were harvested from the entire bone marrow from both samples (see Table 11 in the appendix). This amount is sufficient to perform RNA-seq.

The freshly isolated and enriched PDX cells were sorted directly either into lysis buffer for bulk RNA-seq or into patient medium for single cell RNA-seq (see 3.2.9). The laboratory of our cooperation partner Prof. Enard prepared the RNA libraries and all steps necessary for RNA-seq.

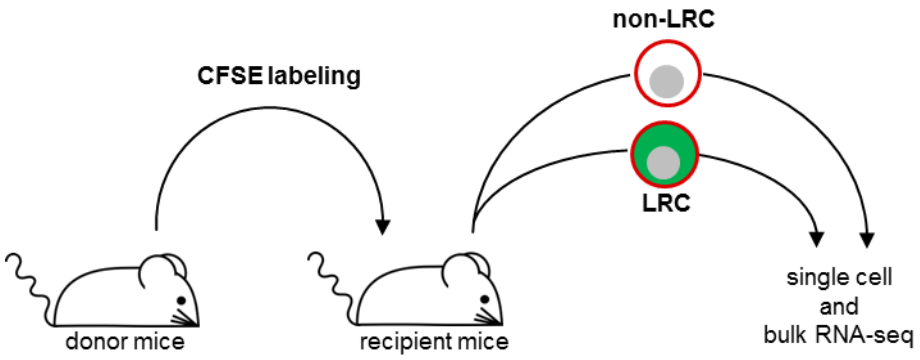

Figure 24: Scheme for preparation of LRC and non-LRC for single cell and bulk RNA-seq.
Freshly isolated PDX cells from the spleen of a donor mouse were labeled with CFSE *ex vivo*. Approximately $1x10^7$ $CFSE^+$ PDX cells were injected into the recipient mice. 14 days after cell injection the bone marrow was isolated. The PDX cells were enriched by using the NGFR and mCherry transgenes for MACS and FACS enrichment, and sorted for LRC and non-LRC either 1,000 cells in 10 µl patient medium for single cell RNA-seq or 2,000 cells in 80 µl in TCL-buffer for bulk RNA-seq. Adapted from (Ebinger, Özdemir et al. 2016).

4.3.1.1 GEP of LRC are clearly distinguished from non-LRC

The analyzed RNA-seq raw counts were depicted as a heatmap with hierarchical clustering and as a principal component analysis (PCA). This was performed in R using the DeSeq2 package (see 3.5.1). The differences between the GEP of LRC and non-LRC were highlighted by these two different visualization tools.

In a heatmap the most differentially regulated and significant genes are plotted for each sample. The disparate color patterns visualize the differences in the GEP of the compared populations. In contrast, PCA is a statistical procedure to sum up variables from each sample by reducing the dimension. The main purpose of the PCA is the analysis of data to identify patterns of different GEP (Raychaudhuri et al. 2000).

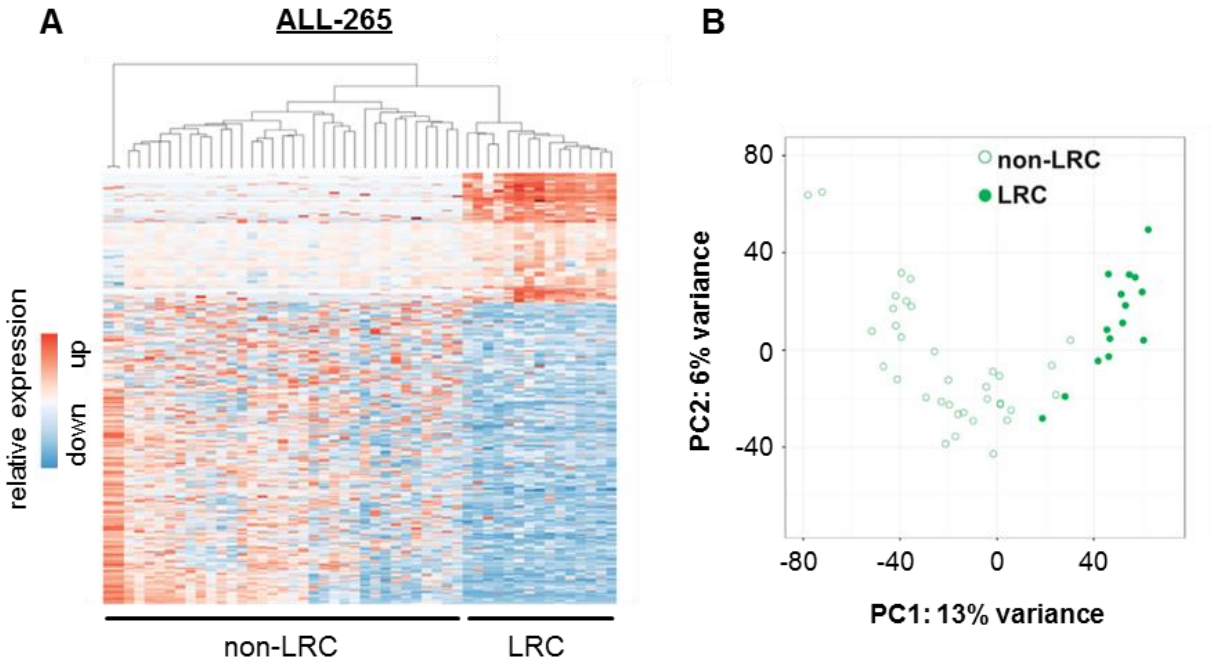

Figure 25: GEP of ALL-265 LRC and non-LRC are distinct in single cell RNA-seq.
For each LRC and non-LRC sample, PDX cells of one mouse was sorted for single cell RNA-seq. (A) Hierarchical clustering and gene expression heatmap across the 500 most differentially expressed genes (padj < 0.01) in 15 LRC and 35 non-LRC single cells were performed. Values are plotted relative to the average of non-LRC. (B) Principal component analysis (PCA) of the 500 most variable genes in all 50 single cells is shown. Each dot indicates a single cell. Adapted from (Ebinger, Özdemir et al. 2016).

Single cell RNA-seq was performed for the LRC sample ALL-265. GEP for 15 single cell LRC and 35 single cell non-LRC were obtained. In the heatmap the 500 most differentially expressed genes of the single cell LRC and non-LRC were depicted. LRC gene expression was more homogenous between the single cells of the LRC group compared to the gene expressions of the non-LRC group indicating a higher heterogeneity in the non-LRC

population (see Figure 25A). Furthermore, GEP of LRC and non-LRC in the single cell analysis were clearly distinct in the PCA. The non-LRC population was located on the left side of the PCA, whereas the LRC population was across, demonstrating a different GEP pattern between both cell populations (see Figure 25B). Some LRC were more similar in their GEP to the non-LRC population than to the LRC population and vice versa. This observation in the PCA confirmed the high plasticity, which was already described in the LRC mouse model (see 1.3.1).

Bulk RNA-seq was performed for ALL-199 LRC and non-LRC. The advantage of bulk RNA-seq was the higher sequencing depth allowing the detection of genes expressed at low levels (Bacher & Kendziorski. 2016). However, no statements about the homogeneity or heterogeneity of a population were obtained. The heatmap and the PCA in Figure 26 demonstrated the differences in the GEP of ALL-199 LRC and non-LRC.

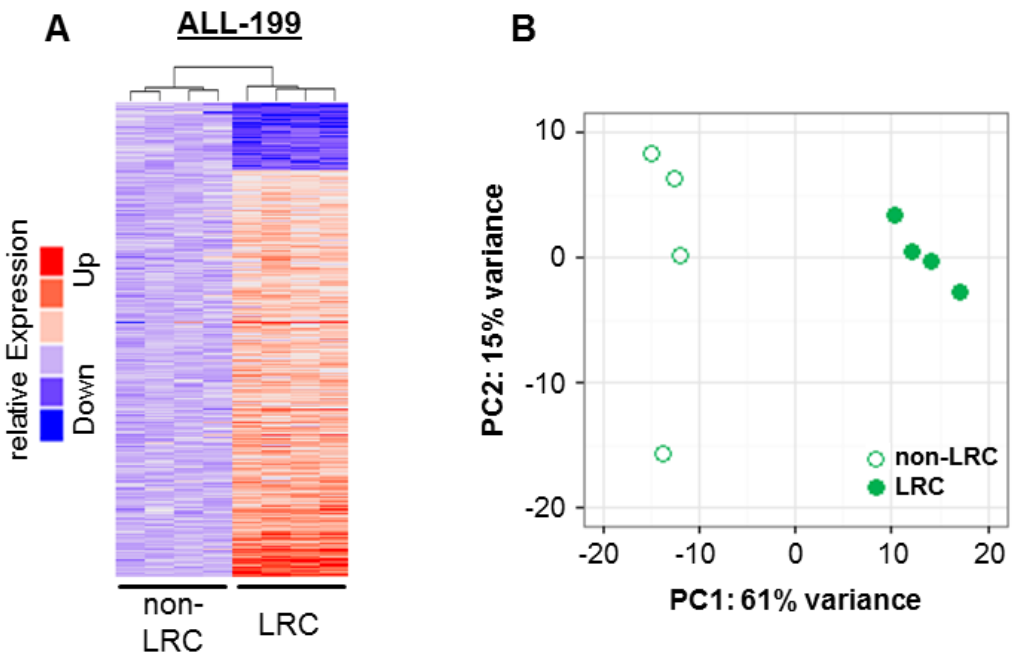

Figure 26: GEP of ALL-199 LRC and non-LRC are distinct as determined by bulk RNA-seq.
(A) Hierarchical clustering across the 500 most differentially expressed genes (padj < 0.01) in 4 biological replicates was performed and depicted as heatmap. Values were plotted relative to the average of non-LRC. (B) PCA of the 500 most variable genes in all 8 bulk samples is shown. Each dot indicates a bulk sample.

The LRC and non-LRC from both samples were distinct in the GEP. It was possible to detect gene expression differences in these two phenotypically different samples despite the high plasticity in this model.

All LRC and non-LRC sequencing data including ALL-199 and ALL-265 were summarized in one common GEP for further analysis and characterization of LRC (see 3.5.1). A combined LRC signature was defined. This LRC signature contained all significantly upregulated genes compared to non-LRC (around 250 genes with fold change > 1 and padj < 0.05; see Figure 39 and Table 12 in the appendix).

4.3.1.2 KEGG terms belonging to cell surface interactions are upregulated in LRC

Characterization of LRC based on their GEP was performed using gene set enrichment analysis (GESA). GSEA is a statistical bioinformatic tool to identify enrichment of specific gene sets in a GEP. Over-represented gene sets result in a positive normalized enrichment score (NES) and vice versa. The more genes from a gene set are regulated in the same direction, the more significant and higher the NES is (Subramanian et al. 2005).

For the first round of enrichment analysis, the KEGG (Kyoto Encyclopedia of Genes and Genomes) pathway terms were used as gene sets for GSEA. The KEGG database offers a collection of different pathways and terms (Kanehisa et al. 2012).

A GSEA on the common LRC GEP (including ALL-199 and ALL-265) was performed with all available KEGG terms. The highly significant terms are summarized in Figure 27. All significantly downregulated KEGG terms are associated with cell cycle and proliferation confirming the dormant state of LRC.

In the upregulated KEGG terms cell adhesions molecules and cytokine-cytokine receptor interactions were highly enriched in GEP of LRC as compared to non-LRC. However, no specific pathway with a high enrichment score was significantly upregulated in LRC.

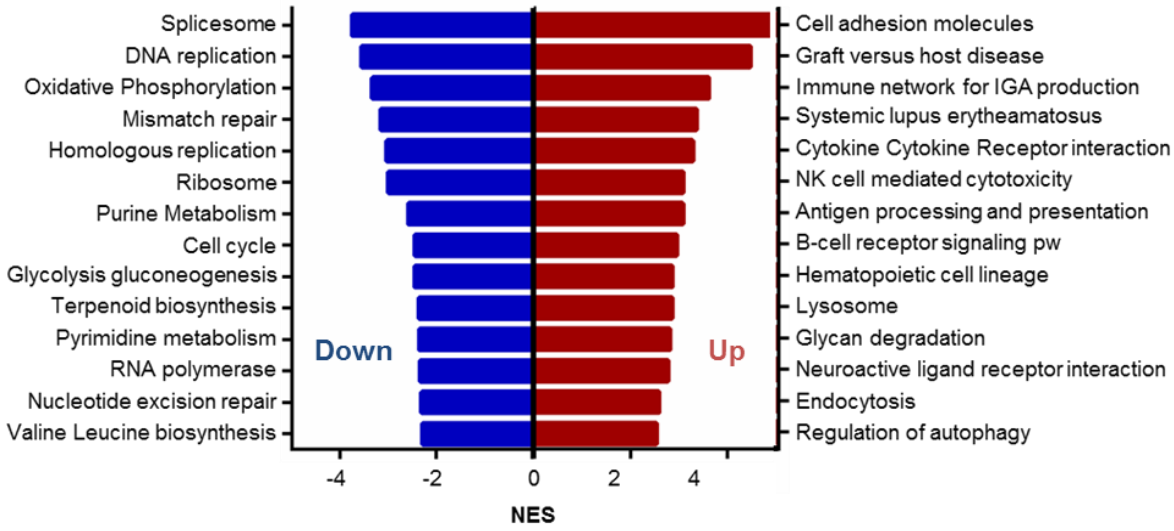

Figure 27: KEGG pathways for proliferation are downregulated and cell-cell interactions are upregulated in LRC.

Significantly enriched KEGG pathways (padj < 0.01) are listed as determined by gene set enrichment analysis (GSEA). All RNA-seq data from ALL-199 and ALL-265 are combined for one common LRC GEP. Bars show the normalized enrichment score (NES).

The metabolism in dormant cells differ highly from proliferating cells, for example in expression levels of genes, which are involved in the cell cycle (Whitfield et al. 2006). Therefore, the major difference of the GEP of LRC compared to non-LRC was associated with the dormant state of LRC.

4.3.1.3 Patient signatures with challenging features are enriched in LRC

To obtain a better idea about the challenging role of LRC, I next investigated the association of the LRC gene expression profile with patients' signatures. Therefore, GSEA was performed with published patients' gene signatures. All gene signatures contained only highly significantly upregulated genes.

First, a gene signature of ALL with high risk for relapse was correlated with the LRC GEP (see Figure 28A). In this signature gene expression profiles from 207 uniformly treated children with ALL were obtained before therapy start, and 15 genes were identified as high risk genes for relapse by consideration of patients' outcome (Kang et al. 2010). 11 out of the 15 genes were also detected in the RNA-seq data of LRC. These 11 genes were significantly upregulated in LRC indicated by the high enrichment of this gene signature with the LRC GEP. Unfortunately, the role of these enriched genes cannot be classified to one specific cellular function.

Next, a gene set from dormant CD34$^+$ CML populations was compared with the GEP of LRC. This gene signature was obtained by profiling dormant CD34$^+$ CML patient populations against dividing CD34$^+$ CML cells (Graham et al. 2007), and was also enriched more in LRC than non-LRC. This result confirmed the quiescent phenotype of LRC (see Figure 28B). Furthermore, a leukemia stem cell (LSC) signature, created by the comparison of LSC and hematopoietic stem cells (HSC), was enriched in upregulated genes of LRC (see Figure 28C) (Saito et al. 2010). The detection of LSC in patients is associated with worse prognosis, leading to the hypothesis that also the presence of LRC might be a bad prognosis factor.

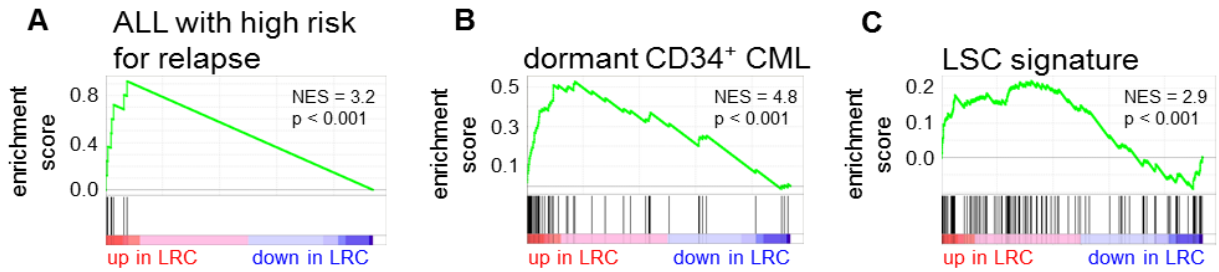

Figure 28: LRC GEP shows a high correlation with published critical patients' signatures.
Gene set enrichment analysis (GSEA) for published signatures on high risk ALL cells (Kang et al. 2010), dormant CD34$^+$ CML (Graham et al. 2007) and leukemia stem cells (Saito et al. 2010) were performed. All RNA-seq data from ALL-199 and ALL-265 are combined for one common LRC GEP. Adapted from (Ebinger, Özdemir et al. 2016).

Taken together, all critical patients' signatures for ALL high risk, dormancy and malignant stemness, are significantly enriched in the GEP of LRC compared to non-LRC. These results indicate that LRC resemble a high-risk population in ALL. The LRC mouse model can be used as a novel platform to develop new treatment strategies for eliminating challenging cells in the ALL therapy.

4.3.2 Gene expression profiles of PDX MRD cells

Next, GEP of chemotherapy-resistant PDX MRD cells and untreated control cells for the samples ALL-199 and ALL-265 was determined by RNA-seq in order to understand the challenging feature of chemotherapy resistance on transcriptome level (see 4.3.1).

PDX MRD cells were generated by polychemotherapy as described 4.1.1 and the cells were isolated from the bone marrow by making use of the transgenes (truncated NGFR for MACS enrichment and mCherry for FACS enrichment). From the bone marrow of a chemotherapy treated mouse around 40,000 PDX MRD cells (0.1% of PDX cells in the bone marrow) were isolated and sorted either directly into lysis buffer for bulk RNA-seq or into patient medium for single cell RNA-seq (see Figure 29).

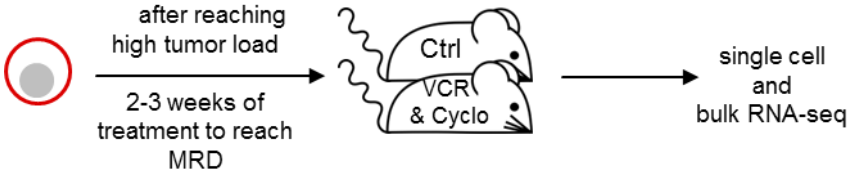

Figure 29: Scheme for generating PDX MRD and control cells for RNA-seq analysis.
$1x10^6$ freshly isolated or thawed transgenic PDX cells were injected into each mouse. PDX cells were positive for the following transgenes: mCherry, truncated NGFR and firefly luciferase. Leukemia engraftment and therapy effects were followed by *in vivo* imaging. After reaching high tumor load chemotherapy was initiated. VCR (0.25 mg/kg; i.v.) and Cyclo (100 mg/kg; i.p.) were injected weekly as combination therapy. The untreated control group received PBS. At MRD level of about 0.1% blasts in the bone marrow after 2-3 weeks of treatment, mice were sacrificed and the isolated PDX cells from the bone marrow were sorted either in 10 µl patient medium with 1,000 cells for single cell RNA-seq or in 80 µl TCL-buffer with 2,000 cells for bulk RNA-seq. Adapted from (Ebinger, Özdemir et al. 2016).

4.3.2.1 GEP of PDX MRD cells are distinguished from the controls

Single cell RNA-seq was performed with the ALL-199 PDX MRD cells. GEP of 90 MRD and 31 control single cells were obtained. To compare the GEP of both populations, a heatmap with hierarchical clustering and a PCA were performed as described before in 4.3.1.1.

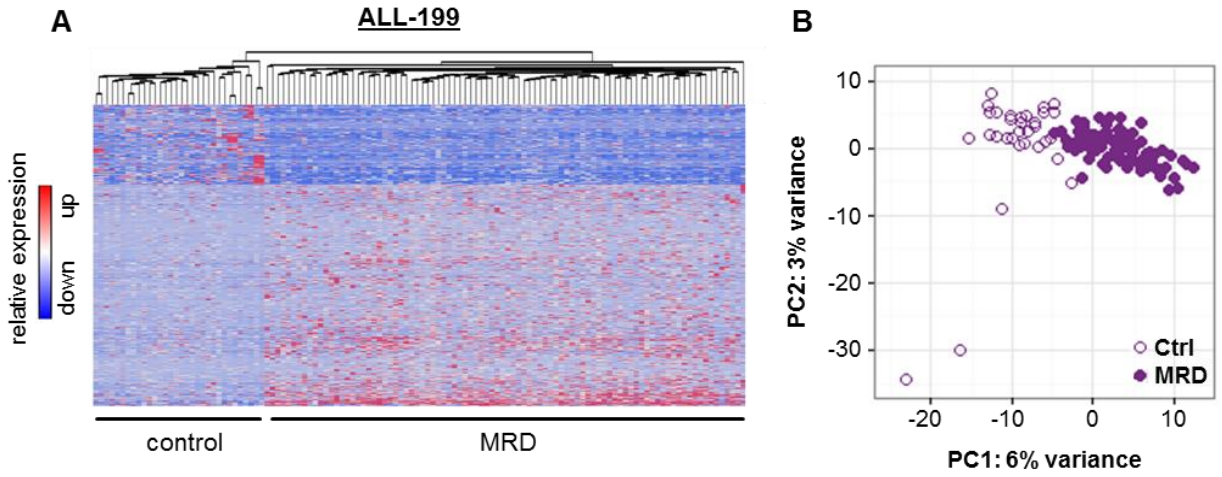

Figure 30: GEP of PDX MRD and untreated control cells from ALL-199 are clearly distinct in single cell RNA-seq.

For each PDX MRD and control sample, PDX cells of one mouse were sorted for single cell RNA-seq. (A) Hierarchical clustering and gene expression heatmap across the 500 most differentially expressed genes (padj < 0.01) in 90 PDX MRD and 31 control single cells were performed. Values were plotted relative to the average of untreated control cells. (B) PCA of the 500 most variable genes in all 121 single cells is shown. Each dot indicates a single cell. Adapted from (Ebinger, Özdemir et al. 2016).

The heatmap of the 500 most differentially expressed genes indicated that the PDX MRD cells differed from the untreated control cells and displayed a more homogenous population compared to control cells. Furthermore, both populations were clearly distinguishable in the PCA, although an overlap between both PDX populations was observed (see Figure 30).

Bulk RNA-seq data was obtained for both PDX MRD samples (ALL-199 and ALL-265). In order to characterize the PDX MRD cells independent of any specific PDX sample features, all bulk RNA-seq data of both PDX samples were combined to one common PDX MRD GEP for further analysis (see 3.5.1). The 250 most significantly differentially expressed genes were plotted as a heatmap. The overlap between both PDX samples was not high. The highest upregulated genes in one sample were not the same in the other sample. However, the direction of the regulation was always the same indicating a common gene expression between the different PDX MRD samples (see Figure 31A).

Additionally, the PCA with the 500 most variable genes of all bulk RNA-seq data confirmed the diversity between the two PDX samples, ALL-199 and ALL-265. The first component (PC1) with 87% variance separated both PDX samples. The sample ALL-199 was localized on the left side of the PCA and on the right side ALL-265. Nevertheless, both PDX MRD populations differed from their controls with a variance of 4% in the second component (PC2) and thereby showed a small overlap within gene expressions for PDX MRD cells independent to the PDX sample (see Figure 31).

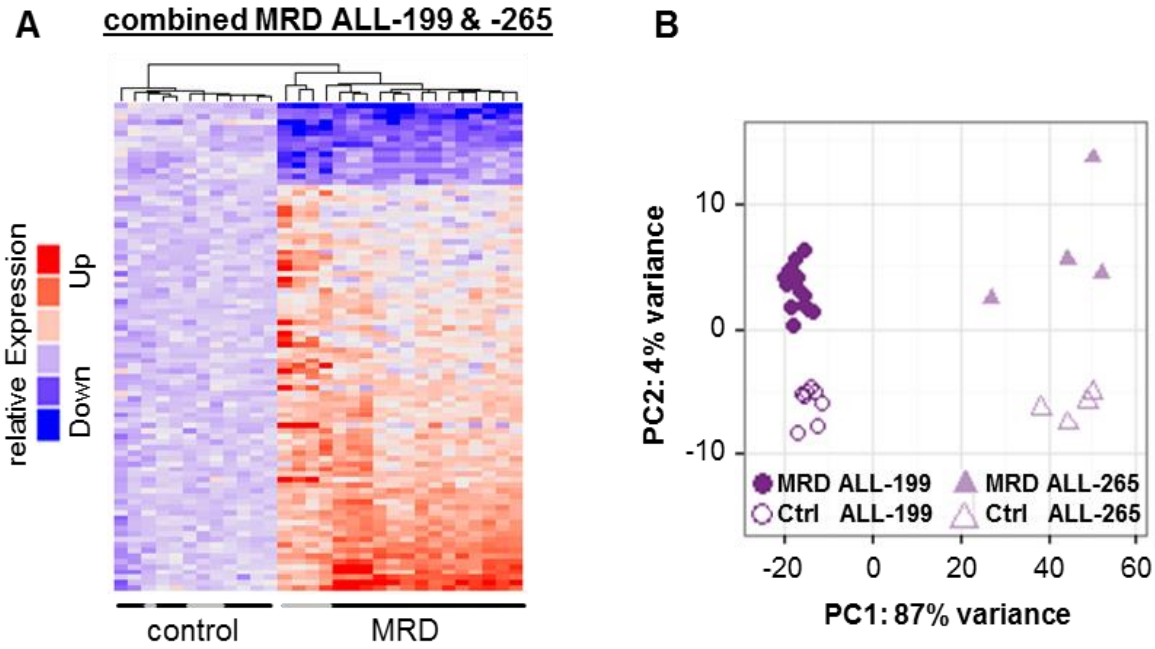

Figure 31: ALL-199 and ALL-265 differ highly in their GEP, whereas the PDX MRD GEP are similar.
(A) Combined PDX MRD hierarchical clustering and gene expression of ALL-199 and ALL-265 are depicted in a heatmap across the 250 most differentially expressed genes (padj < 0.01; PDX MRD/Ctrl of ALL-265:each n=4; PDX Ctrl of ALL-199: n=8; PDX MRD of ALL-199: n=14). Values are plotted relative to the average of the control. ALL-265 bulk samples are symbolized in grey lines and ALL-199 bulk samples resulted in black lines. (B) PCA of the 500 most variable genes was performed for all 30 bulk samples. Each symbol indicates a bulk sample.

In summary, the GEP of both PDX MRD populations differed from the untreated controls. Although a substantial difference in gene expression was observed between the two PDX samples ALL-199 and ALL-265, the existing overlap between the two PDX MRD populations enabled determining a common PDX MRD GEP signature for both samples.

4.3.2.2 KEGG terms belonging to metabolism are downregulated in PDX MRD cells

Next, a KEGG pathway enrichment analysis was performed using the common PDX MRD GEP of both PDX samples (ALL-199 and ALL-265) in order to identify the changes in the transcriptome of the PDX MRD cells induced by chemotherapy. Besides, the final question was to understand the chemotherapy resistance in the PDX MRD cells by using this bioinformatic analysis.

KEGG terms for metabolism and proliferation were the most significant downregulated terms in the MRD population. In contrast, the cytokine-cytokine receptor interaction and cell adhesion molecule terms were upregulated in GEP of PDX MRD cells compared to the

untreated controls. Furthermore, some pathways were also significantly enriched in the upregulated genes of PDX MRD cells, for example the JAK-STAT pathway and diverse chemokine signaling pathways (see Figure 32).

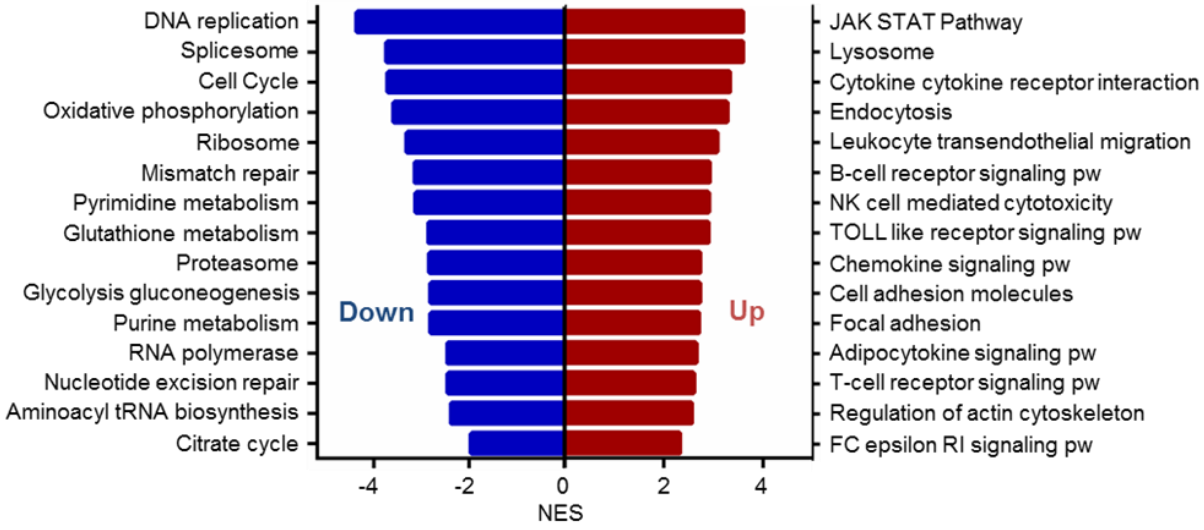

Figure 32: KEGG pathways for proliferation are downregulated in the GEP of PDX MRD cells.
Significantly enriched KEGG pathways (padj < 0.01) were listed as determined by GSEA. All RNA-seq data from ALL-199 and ALL-265 are combined for one common PDX MRD GEP. Bars show the normalized enrichment score (NES).

The results from the PDX MRD KEGG pathway analysis let assume a dormant state of the PDX MRD cells due to the downregulation of cell cycle associated KEGG terms. Chemotherapy resistance in the PDX MRD cells might be based on this dormant phenotype. Furthermore, the high upregulation of KEGG terms for microenvironment interactions indicate the dependency of the PDX MRD cells to the bone marrow environment.

4.3.2.3 PDX MRD cells exhibit a dormant GEP

The KEGG pathway analysis indicated a low metabolic and low cell cycle activity in the PDX MRD cells compared to untreated control cells. To investigate this observation GSEA were performed with gene signatures of E2F and MYC targets from the Molecular Signatures Database (Liberzon et al. 2015). The two gene signatures contain genes, which are upregulated by the transcription factors E2F or MYC. The downregulation of the E2F and MYC target genes correlated with a dormant and low proliferating cell cycle state (Dimova & Dyson. 2005; Zeller et al. 2003). In contrast, genes with pretended controversial functions are also summarized to one KEGG term. Therefore, these two signatures confirm more specifically and precisely the low cell cycle activity in the PDX MRD cells than KEGG terms.

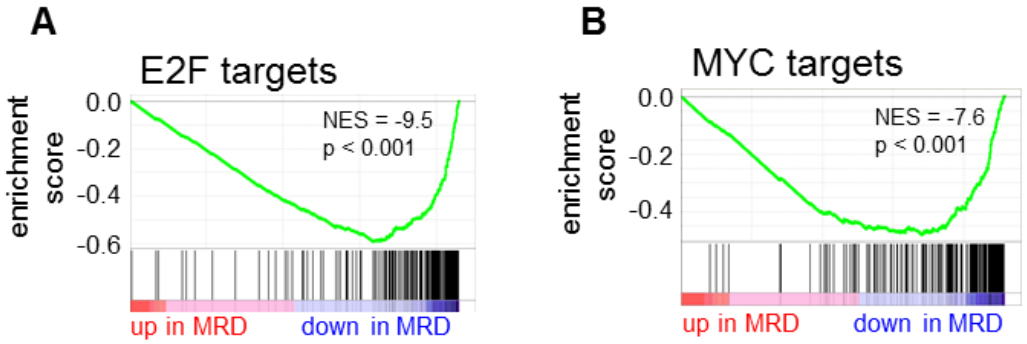

Figure 33: PDX MRD cells exhibit a dormant GEP.
GSEA for E2F and MYC targets from Molecular Signatures Database (MSigDB) were performed (Liberzon et al. 2015). All bulk RNA-seq data from ALL-199 and ALL-265 were combined for one common PDX MRD GEP. Adapted from (Ebinger, Özdemir et al. 2016).

Targets genes from E2F and MYC were highly significant downregulated in the GEP of PDX MRD cells in the GSEA (see Figure 33). This observation correlated the PDX MRD GEP with a dormant phenotype. In conclusion, the combination chemotherapy over several weeks selected for PDX cells with low cell cycle activity.

4.3.3 Gene expression profiles of LRC and PDX MRD cells are similar

PDX MRD GEP correlates with a dormant phenotype and LRC are selected by their dormant state. Therefore, possible similarities in GEP of these two populations were investigated.
GSEA with the LRC signature (see Figure 39) was performed on the PDX MRD GEP, and all single cell RNA-seq data of LRC and PDX MRD cells were combined in one PCA in order to identify similarities and differences between the different PDX populations with challenging features.
The LRC signature was significantly enriched in the GEP of PDX MRD cells. Significantly upregulated genes in LRC were also mostly upregulated in PDX MRD cells (see Figure 34A). Furthermore, GEP of LRC and PDX MRD single cells were clearly distinguishable from their either proliferating or untreated controls in the PCA. All 105 dormant and chemotherapy-resistant single cells of LRC and PDX MRD cells were uniformly localized in the lower part of the PCA in contrast to the proliferating, untreated control PDX cells, which were localized in the upper part (see Figure 34B).

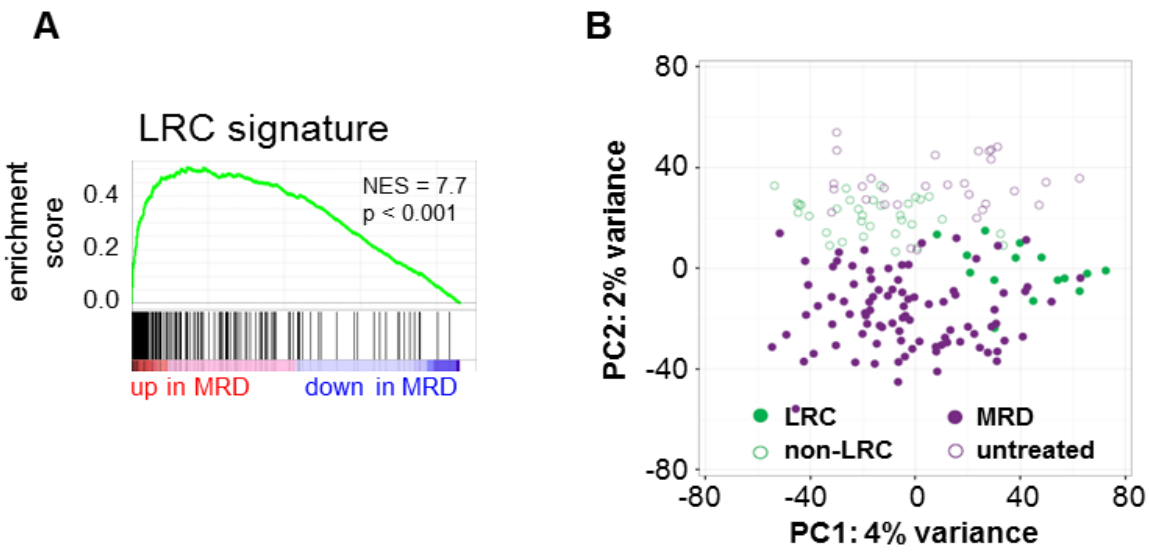

Figure 34: High correlation between the GEP of LRC and PDX MRD cells.
(A) GSEA with the LRC signature was performed on the combined PDX MRD GEP. (B) All single cell RNA-seq data from ALL-265 LRC/non-LRC and ALL-199 MRD/control cells are plotted using all shared expressed genes. Each dot indicates a single cell. Adapted from (Ebinger, Özdemir et al. 2016).

Taken together, LRC constitute a small subpopulation of dormant PDX cells during engraftment of the leukemia. In comparison, the PDX MRD cells are a population of chemotherapy treated cells. Modern next generation sequencing techniques including single cell RNA-seq enabled comparing both populations despite the fact that only very minor cell numbers were available for analysis. The data of GEP showed that the two populations associated either with dormancy or drug resistance show high similarities and share adverse and clinically challenging features.

4.4 LRC and PDX MRD cells resemble primary patient MRD cells

In the ALL PDX mouse model two distinct and clinically relevant populations were described. LRC were identified by dormancy during leukemia engraftment, whereas drug resistance in long-term chemotherapy characterized PDX MRD cells.

As a last step, I aimed at estimating the relevance of these challenging PDX populations from the mouse model to patients' disease. In patients MRD cells are the most challenging cells for the treatment of leukemia and correlate with a high risk for relapse and a poor prognosis (see 1.1.2) (Conter et al. 2010; van Dongen et al. 2015).

Five patient samples at diagnosis and corresponding MRD samples were provided and sorted for RNA-seq by Prof. Renate Panzer-Grümayer and colleagues (St. Anna Kinderspital,

Vienna; see 2.1). These samples were derived from children with newly diagnosed B-cell precursor ALL at time point of diagnosis and after the first block of chemotherapy and regeneration at day 33. Cells were sequenced by our cooperation partner Prof. Wolfgang Enard. GEP of primary MRD cells were compared with matched diagnosis samples (see Figure 35A). The sequencing quality from 3 out of 5 primary MRD samples was of sufficient quality for further analysis. All 220 significantly differentially expressed genes are plotted in the heatmap shown in Figure 35B. The gene expression of diagnosis and MRD samples differed. The GEP of primary MRD samples was associated with a dormant phenotype in GSEA compared to GEP of diagnosis samples (see Figure 40 in the appendix).

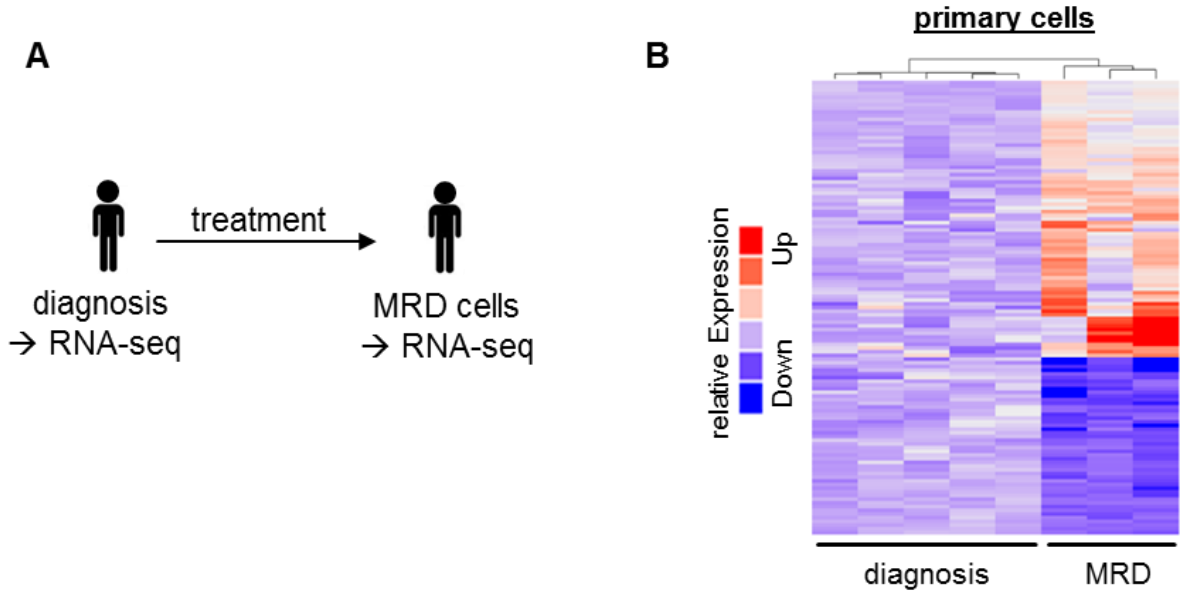

Figure 35: GEP from diagnosis and MRD of primary ALL samples are distinct.
(A) Bulk RNA-seq was performed from primary diagnosis (n=5) and primary MRD (n=3) samples. Primary MRD samples were obtained after 33 days of treatment onset. 2,000 cells were sorted into 80 µl TCL-buffer for bulk RNA-seq. (B) Hierarchical clustering and gene expression heatmap across all differentially expressed genes (padj < 0.05) is shown. Values were plotted relative to the average of diagnosis. Adapted from (Ebinger, Özdemir et al. 2016).

After obtaining RNA-seq data from primary MRD samples the next step was to show the relevance of LRC and PDX MRD cells to patients' disease. In the first approach the LRC signature (see Figure 39 in the appendix) was used for GSEA in order to compare GEP of primary MRD cells with the PDX cells. The LRC signature was significantly enriched in the primary MRD GEP (see Figure 36A). Furthermore, in the second approach all GEP from RNA-seq bulk samples, including LRC, PDX MRD cells and patient MRD cells, were plotted with all the controls in one PCA. All the bulk samples with the challenging features were localized within the same cluster. The first variance (PC1) shows the difference between GEP

of LRC, PDX MRD and primary MRD bulk samples on the left side of the PCA and the control bulk samples on the right side (see Figure 36B).

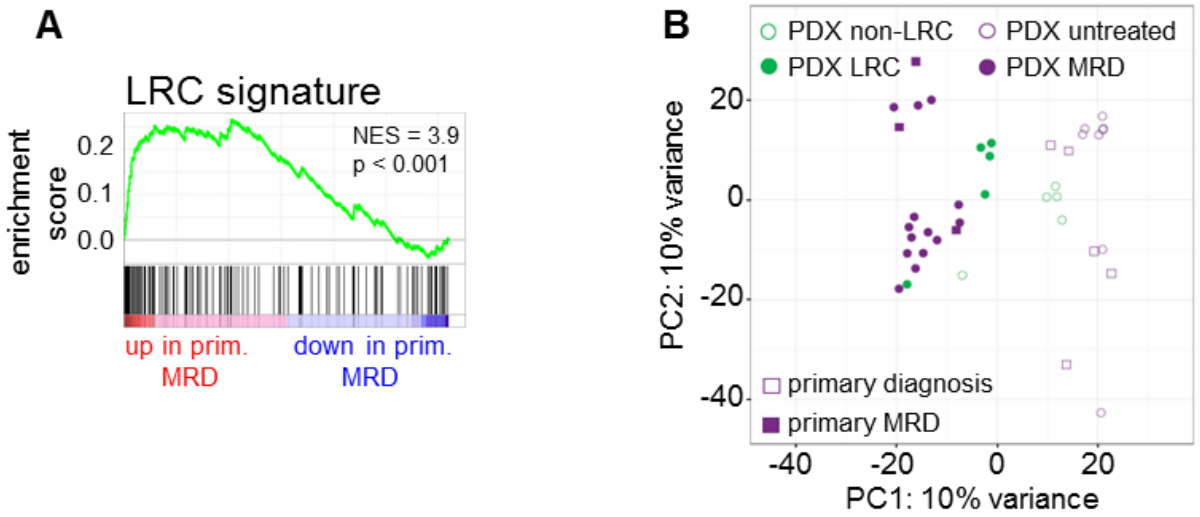

Figure 36: GEP of dormant and chemotherapy-resistant PDX cells show a high correlation with the GEP of primary MRD cells.
(A) GSEA with the LRC signature was performed on the primary MRD GEP. (B) All bulk RNA-seq data from LRC, PDX MRD, primary MRD and their controls are plotted using all shared expressed genes. Each symbol indicates a bulk sample. Adapted from (Ebinger, Özdemir et al. 2016).

GEP of LRC and PDX MRD cells correlated significantly with GEP of primary MRD samples. Thus, the two PDX populations with the challenging features of dormancy and chemotherapy resistance reflect patients' disease at the stage of MRD on the transcriptome level. Both PDX NSG mouse models provide a novel platform for studying patients' MRD in further functional studies.

Taken together, in the present work I established several preclinical PDX mouse models of chemotherapy and treatment resistance and were able to show that dormant ALL cells during engraftment localize to the same endosteal bone marrow region as normal hematopoietic stem cells. In contrast, the PDX MRD cells are localized more to perivascular regions after surviving long-term chemotherapy. Gene expression profiles revealed that dormant and drug resistant PDX ALL cells in the bone marrow display substantial similarities to similar cells in patients. Thus, the PDX models can be used in the future to better characterize and finally efficiently treat treatment resistant tumor cells in patients with ALL.

5 Discussion

Acute lymphoblastic leukemia (ALL) patients reach often remission upon initial treatment with cytostatic drugs (Inaba et al. 2013; Pui et al. 2008). Remaining leukemic cells in remission, which are defined as minimal residual disease (MRD) cells, indicate a high risk for relapse resulting in poor prognosis. Novel therapies targeting MRD cells are urgently needed for the improvement of patients' treatment (Buckley et al. 2013).
However, the biology of MRD cells is currently not very well understood. In clinics, MRD cells are detected in bone marrow aspirates but are not functionally characterized (Bruggemann et al. 2010). So far in one trial a dormant subpopulation of patients' MRD cells was identified in bone marrow aspirates, but was not further analyzed (Lutz et al. 2013).

In the present study, I established a novel patient-derived xenograft (PDX) mouse model that mimics patients' MRD. This model enables us for the first time to perform functional studies on these cells and provides new insights into the characteristics of MRD cells. Furthermore, the recently established label retaining cell (LRC) mouse model for identification of dormant PDX ALL cells was also characterized and compared with the PDX MRD mouse model in order to understand the relation between dormancy and chemotherapy resistance in ALL.

5.1 PDX MRD mouse model mimics patients' MRD in ALL

The feasibility to study the biology of patients' MRD is limited by the minute numbers of remaining leukemic cells isolated from bone marrow aspirates. In addition, the identification of the MRD cells from healthy bone marrow is challenging and inefficient in FACS due to the high phenotypic MRD variability regarding cell surface markers (van Dongen et al. 2015). To overcome these limitations, the PDX MRD mouse model was established. The transgenes (mCherry, truncated NGFR, luciferase) introduced in the PDX cells, simplified the detection and isolation of remaining chemotherapy treated leukemic cells in the xenograft model.
While PDX models in acute leukemia are mostly used for preclinical treatment trials and for studying the role of the bone marrow environment, the PDX MRD mouse model provides a tool for the characterization of a critical cell population in patients' treatment (Gao et al. 2015; Liem et al. 2004; Townsend et al. 2016). This established mouse model is the first mouse model mimicking the MRD in acute leukemia. Several groups established also an acute leukemia PDX model in which the leukemia was treated by chemotherapy. However,

the focus of these studies was set on simulation of standard chemotherapy. Treatment responses of the induction chemotherapy were analyzed rather than the functional characterization of remaining leukemic cells after treatment. Nevertheless, these studies demonstrate the relevance of the PDX model for the prediction of therapeutic agents in clinics. The same anti-leukemic effects of cytostatic drugs are observed in patient as well as in the xenograft mouse model (Liem et al. 2004; Samuels et al. 2014; Zuber et al. 2009). This close proximity in treatment effects between mouse and human was made use for the establishment of the PDX model mimicking MRD.

Thus, the PDX MRD mouse model is based on the treatment with conventional cytostatic drugs in ALL therapies in order to reach the MRD level (of less than 0.1% blasts in the bone marrow) as close as possible to clinics. The combination therapy of Vincristine (VCR) and Cyclophosphamide (Cyclo) and treatment over prolonged periods of time reduce high tumor loads to MRD level in contrast to monotherapies (see Figure 9). The used drug concentrations in the PDX MRD model are based on optimized treatment protocols for ALL (see Table 8 in methods). The leukemia is decreased by more or less the same chemotherapeutic stress as in patients. Several studies showed that a specific cellular response to cytostatic drugs depends on the used drug concentrations (Meng et al. 2007; Morgan & Holguin. 2002). Consequently, the cellular response of the PDX MRD cells to chemotherapy might be the same like in patients due to the same provided chemotherapeutic stress.

The initial induction therapy in patients is based on a polychemotherapy and takes usually 4-6 weeks until remission and detection of the first remaining MRD cells. A combination therapy of more than two cytostatic drugs, as it is used in patients, is not feasible in mice due to high toxicity. A reason for this limitation is most likely the different metabolic activity in humans and mice as the higher metabolic activity in mice causes different pharmacokinetics of the used cytostatic drugs (Demetrius. 2005; Nair et al. 2016; Sharma & McNeill. 2009). Nevertheless, the combination therapy with VCR and Cyclo was administered for 2-3 weeks under clinical relevant drug concentrations. The established PDX MRD model is as close as possible to patients' treatment and MRD.

In order to demonstrate the clinical relevance of the PDX MRD and the LRC mouse model, gene expression profiles (GEP) of the PDX cells and primary MRD cells were analyzed. MRD cells are the most critical cell population of patients' treatment. They are chemotherapy-resistant, dormant and highly self-regenerative (Buckley et al. 2013; Lutz et al.

2013). These features related also to LRC and PDX MRD cells, which were shown in the functional *in vivo* studies (see 4.1; Ebinger, Özdemir et al. 2016).

So far no GEP of primary ALL MRD cells existed. In clinics the MRD cells are identified to monitor therapy efficiencies but have not been isolated for further studies (Bruggemann et al. 2010). With the help of our cooperation partners (Prof. Renate Panzer-Grümayer and Prof. Wolfgang Enard), GEP of primary ALL MRD cells could be obtained for the first time. A comparative RNA-seq data analysis of LRC, PDX MRD cells and primary MRD cells demonstrates a significant correlation between all populations (see Figure 36). PDX cells with challenging features of dormancy and chemotherapy resistance display a similar gene expression profile as primary MRD cells. In conclusion, both minor cell populations in the two distinct PDX mouse models mimic features of patients' MRD cells. Additionally, several studies report also a high correlation in GEP between PDX cells and primary malignant cells and underline the proximity of the PDX models to patients' disease as for example in lung cancer biology or in acute leukemia (Daniel et al. 2009; Wong et al. 2014). These results confirm the relevance and ability of the PDX models for characterizing patients' diseases *in vivo*.

In conclusion, the established PDX MRD mouse model provides an unique tool to study the biology of MRD as close as possible to patients' MRD.

5.2 Detection of acquired chemotherapy resistance in the PDX model

The initial treatment after diagnosis is often successful in ALL patients. The leukemia burden is drastically reduced and consequently patients reach the remission. However, remaining MRD cells often give relapses with poor outcome due to chemotherapy resistance (Foo & Michor. 2014; Inaba et al. 2013; Pui et al. 2008). The evolution of chemotherapy resistance is poorly understood and so far no model exists to study this critical aspect in ALL biology. In functional studies of the PDX MRD model first evidences for evolution of chemotherapy resistance in ALL was observed.

The two used PDX samples, ALL-199 and ALL-265, exhibit different sensitivities to VCR during long-term treatment. Over three months a VCR resistant subpopulation in ALL-265 remained stable despite weekly treatment. In contrast, PDX ALL-199 cells were immediately eradicated by the same therapy (see Figure 10). Genetic differences between the PDX samples are most probably the reason for the different VCR sensitivities.

The VCR resistance in ALL-265 is either based on a resistant subpopulation within the sample or an acquired resistance favored by genetic alterations. In the PDX models the conservation of heterogeneity was already known and proven. PDX samples can consist of different subpopulations, which are not lost during passaging in mice (Cassidy et al. 2015). Furthermore, the mechanism for VCR resistance is also described for PDX B-ALL cells. The mode of action of VCR is based on binding to tubulin resulting in microtubule destabilization followed with mitotic arrest and cell death (Owellen et al. 1972). Ong and colleagues demonstrated that VCR resistant PDX B-ALL cells exhibit an increased level of polymerized tubulin. Mechanisms regulating the microtubule stability are involved in VCR resistance (Ong et al. 2008). However, this experiment in the present work cannot provide insights into the question whether the long-term VCR therapy selected either for a subpopulation with a genotype favoring the acquisition of VCR resistance or for an existing resistant subpopulation in ALL-265. Nevertheless, the formation of a VCR resistant population for several months was observed *in vivo*. This model can be used for further studies in order to understand treatment failures based on chemotherapy resistance.

In contrast, the established PDX MRD model suggests an acquired chemotherapy resistance. PDX MRD cells were generated by the combination therapy with VCR and Cyclo, and were re-passaged. In the next *in vivo* treatment round with the same therapy the PDX MRD cells were slightly more resistant than the control cells, which were treated to MRD level for the first time. At the end of the therapy 2.5-fold more PDX MRD cells were detectable in the bone marrow compared to the control cells (see Figure 12). Homing and engraftment of both groups were identical. This observation is also consistent with the reported high leukemia stem cell (LSC) frequency in ALL. The ability of self-renewal is conserved in all ALL cells independent of any subpopulations. Therefore no differences in homing and engraftment was expected in this experiment (Abdullah & Chow. 2013; le Viseur et al. 2008; Morisot et al. 2010; Pal et al. 2016).

Predetermination might be the (or one) reason for the significant increase of remaining cells in the PDX MRD group, and can be explained by epigenetic mechanisms. Bhatla and colleagues suggested also that chemotherapy resistance in B-ALL may be driven by epigenetic changes (Bhatla et al. 2012). After first round of treatment the PDX cells might obtain an epigenetic predetermination resulting in faster adaption to the next round of chemotherapeutic stress. Most probably such a predetermination in the leukemic cells is based

on acquiring faster a dormant state in order to get resistant towards chemotherapy as the GEP of PDX MRD cells suggests a dormant phenotype (see Figure 33).
A selection for a resistant subpopulation during the first treatment round is unlikely. The PDX MRD cells were as sensitive to chemotherapy at the beginning of the second treatment round as the control cells; otherwise the PDX MRD cells would show a clear drug resistance in the next passage. In the PDX MRD model three weeks of combination therapy with two drugs was sufficient to exhibit the process of acquiring chemotherapy resistance. To the best of our knowledge this model provides the first tool to monitor and study the evolution of chemotherapy resistance in ALL *in vivo*.
Our data indicate that chemotherapy resistance in ALL-265 is acquired over a long period of drug treatment rather than the existence of a drug resistant subpopulation.

5.3 Bone marrow mediated dormancy is crucial for chemotherapy resistance

The functional LRC and PDX MRD studies reveal the importance of the bone marrow microenvironment. In both *in vivo* models a high plasticity between the PDX cells is observed. The two critical populations of LRC and PDX MRD cells are able to re-engraft in mice with the same efficiency as untreated and dividing control cells. No isolated cell population is enriched for self-renewal or stemness in the next mouse passage compared to the control cells. Besides, dormant LRC or chemotherapy-resistant PDX MRD cells arise even within the control cell population in the next passage (see 4.1.3; Ebinger, Özdemir et al. 2016). The observed high plasticity in the two PDX mouse models is consistent with the non-hierarchical and random ALL stem cell model as described before in 5.2. No ALL stem cell population, enriched in self-renewal, has been identified so far (le Viseur et al. 2008; Morisot et al. 2010).
Our two distinct mouse models for identification of LRC and PDX MRD cells show microenvironment mediated dormancy and chemotherapy resistance (Ebinger, Özdemir et al. 2016). Consequently, the localization of LRC and PDX MRD cells within the bone marrow were analyzed to understand the role of the microenvironment for the critical acquired features of dormancy and chemotherapy resistance.

In the LRC model the dormant subpopulation of PDX cells localizes close to the endosteum in both samples, ALL-199 and ALL-265. During homing and engraftment the PDX cells

interact with the endosteal region in order to settle within the niche. Most probably the interaction with the bone marrow environment stimulates these cells to become quiescent. Some unidentified factors such as cytokines and cell surface receptors within in the niche might contribute to the induction of dormancy. This hypothesis is supported by our findings that in GSEA (gene set enrichment analysis) terms for cell surface and cytokine cytokine interactions are highly upregulated in LRC indicating the necessity of LRC-microenvironment interactions for dormancy (see Figure 27 in the results). Several groups also described the role of the endosteum in diverse hematopoietic disorders for the induction of dormancy. Osteoblasts and osteoclasts, which are the characteristic cells of the endosteum, are responsible for harboring dormant malignant cells by expressing diverse cytokines. (Boyerinas et al. 2013; Chen et al. 2014; Lawson et al. 2015).

In contrast to LRC, the chemotherapy resistance *in vivo* initially let to the identification of PDX MRD cells. However, the observed resistance in the PDX MRD model is based most probably on the dormant state of PDX MRD cells. GEP of these cells clearly indicate a non-dividing phenotype. Gene sets including E2F- and MYC target genes are highly downregulated in PDX MRD cells, which associates these cells with dormancy (Dimova & Dyson. 2005; Liberzon et al. 2015; Zeller et al. 2003). This acceptance is also confirmed by GEP of the sorted primary MRD cells, which exhibit also a dormant phenotype. Therefore, an endosteal cell localization was assumed for the remaining leukemic cells after ploychemotherapy. Besides, drug resistance in the bone marrow is associated with localization close to the endosteum (Duan et al. 2014; Jin et al. 2008).

However, the PDX MRD cells from both samples, ALL-199 and ALL-265, are randomly distributed in the perivascular regions of the bone marrow without accumulation in the endosteum like observed for LRC. There is a clear discrepancy between the localization of PDX MRD cells and LRC.

Recently, Hawkins and colleagues were the first to describe the localization of chemotherapy treated T-ALL PDX cells. Using intravital microscopy and analyzing the entire calvarium bone marrow in real time, a stochastic mechanism for chemotherapy resistance in T-ALL was developed. The remaining PDX cells during and after treatment are randomly distributed in their model. No specific accumulation pattern in the bone marrow was identified confirming the PDX MRD localization results (Hawkins et al. 2016). Furthermore, the authors observed a nearly complete depletion of osteoblasts during high tumor load in mice. In patients' bone

marrow aspirates with more than 75% blast infiltration the loss of osteoblasts was also confirmed by Hawkins and colleagues (Hawkins et al. 2016).

This described dramatic change of the endosteal region can be translated to our PDX model and can explain why the dormant PDX MRD cell population is not localized to the endosteum but is rather randomly distributed in the bone marrow. At day 10 after cell injection the leukemia in both samples was less than 1% of the entire bone marrow population (Ebinger, Özdemir et al. 2016). The structure of endosteal region including the osteoblasts should not undergo a drastic change at this early time point. As one possible explanation, the endosteum might provide a niche for untreated ALL cells such as LRC, but osteoblast depletion changes the endosteum dramatically disabling a protective niche in the post-treatment situation of PDX MRD cells.

A yet undefined niche for dormancy could influence the perivascular localization of the PDX MRD cells. In the last decades the endosteum was associated with localization of dormant HSC. Even osteoblasts were described as the key component of the niche supporting HSC maintenance (Guezguez et al. 2013; Haylock et al. 2007; Xie et al. 2009; Zhang et al. 2003). In contrast, Kiel and colleagues doubted the influence of osteoblasts on HSC (Kiel et al. 2007). Furthermore, Ding and Morrison were able to show two distinct niches of HSC and early lymphoid progenitors (ELP) in the bone marrow. HSC localized in a perivascular niche and ELP in an endosteal niche (Ding & Morrison. 2013). Nevertheless, the endosteal niche harboring ELP has to provide factors supporting dormancy due to the reversible quiescent state of ELP (Pelayo et al. 2006). Besides, it has been shown recently, that dividing as well as non-dividing HSC reside in small areas of the perivascular niche indicating an additional niche for dormant cells within the bone marrow (Acar et al. 2015). These controversies indicate that next to the endosteum a second niche for dormancy might exist in perivascular regions in the bone marrow.

New insights in the malignant bone marrow niche are always associated with the healthy hematopoiesis. Leukemic cells always interact with normal healthy bone marrow cells, before capturing niche elements of HSC and disrupting the healthy hematopoiesis (Boyd et al. 2014; Colmone et al. 2008). Therefore, my assumption is that the PDX MRD cells localize in dormant perivascular niches as recently described for HSC (Acar et al. 2015). However, the question remains open, why LRC predominantly use the endosteal niche for dormancy and no other niches during engraftment.

A possible explanation for the endosteal localization of LRC might be an observation during the engraftment at day 3 and day 10 after cell injection. The percentage of PDX cells localized to the endosteum is significantly higher at day 3 compared to day 10. The endosteum seems to contribute mainly to PDX ALL homing and engraftment. Ishikawa and colleagues reported similar observations for the acute myeloid leukemia (AML) in their PDX model (Ishikawa et al. 2007).
During homing in the endosteum, some PDX cells may get dormant and reside as LRC in this niche during engraftment. However, the necessity of the endosteal region for engraftment differs between ALL-199 and ALL-265. ALL-265 is highly enriched in the endosteal region during the first two weeks after cell injection. In contrast, ALL-199 localize to a lower degree to the endosteum. Nevertheless, the LRC and PDX MRD cells of both samples show a similar localization pattern within the bone marrow indicating the importance and the unique functions of these two different niches for dormancy and chemotherapy resistance.

Taken together, dormancy of LRC and PDX MRD cells is based on the interactions with the bone marrow environment. However, both PDX populations localize to different niches. During engraftment LRC reside in the endosteal niche, which is associated with dormancy. At high leukemia burden the endosteal niche undergoes a change due to the depletion of osteoblasts, and consequently the function of this niche to localize dormant cells might be destroyed (Hawkins et al. 2016). The PDX MRD cells, which survive combination chemotherapy for several weeks, predominantly localize in the perivascular regions of the bone marrow suggesting that some areas of the perivascular niche replace the dormant function of the endosteal niche.

5.4 High correlation of GEP from two populations within distinct PDX models is based on dormancy

In this study the method of RNA-seq was used for transcriptome analysis of LRC and PDX MRD cells in order to characterize and understand the challenging features of dormancy and chemotherapy resistance in ALL. The first step towards this aim was to obtain GEP of both critical PDX cell populations. A clear difference in the gene expressions from LRC/PDX MRD cells and their proliferating untreated controls was confirmed by principle component analysis (PCA) and let to the generation of each GEP.

Since almost two decades GEP are used as data sets to explore the relations and associations between different cells, diseases and therapies (Alizadeh et al. 2000; Khan et al. 2001; van 't Veer et al. 2002). Consequently, the GEP of LRC was classified by several gene set enrichment analysis (GSEA) with published gene signatures to confirm the challenging features of LRC observed in the functional studies. The applied gene signatures correlated highly with the LRC GEP, for example genes associated for dormant CML (chronic myeloid leukemia) cells or AML LSC (leukemia stem cell) were enriched in the GEP of LRC (Graham et al. 2007; Saito et al. 2010). The dormant state of LRC shows a similar regulation in the transcriptome like the dormant primary CML cells indicating a universal GEP for dormancy independent of diverse malignancies. Besides, the GEP of LRC includes genes that are involved in stemness, like in the AML LSC. These bioinformatical results confirm the observed LRC features of dormancy and self-renewal in the functional studies (Ebinger, Özdemir et al. 2016).

Due to the high capacity of self-renewal in ALL no gene signatures of sorted ALL subpopulation with challenging features are available (le Viseur et al. 2008). In AML the $CD34^+$ $CD38^-$ cell population is associated with stemness. Therefore, many gene signatures for AML LSC are published (Gal et al. 2006; Gentles et al. 2010; Hackl et al. 2015). However, Kang and colleagues generated a signature for ALL to predict the risk for relapse. This signature for relapse prediction was generated by comparing patients' outcomes and gene expressions before therapy start (Kang et al. 2010). GSEA with this gene signature showed a high enrichment in the GEP of LRC. LRC seems to be a surrogate for relapse inducing cells. Unfortunately, the enriched genes in this signature cannot be assorted to one particular/specific pathway or cellular mechanism in order to understand the risk for relapse in detail.

We were the first who identified and isolated dormant as well as chemotherapy-resistant cells from a single sample by using two distinct PDX models. PDX MRD cells are characterized by chemotherapy resistance after 2-3 weeks of treatment, and LRC are characterized by dormancy during leukemia engraftment. Therefore, it is more surprising that the GEP of both critical PDX populations are similar (see Figure 34). Most probably the similarity of the GEP is based on the dormant phenotype of both populations. GSEA of PDX MRD cells revealed also a dormant phenotype (see Figure 33).

Dormancy seems to be a common and reversible feature in ALL cells like described for HSC (Wilson et al. 2008). Hence, novel therapies aiming to reduce the relapse risk and increase

patients' outcome have to target ALL dormancy. Dormant ALL cells have to be turned into proliferating cells in order to sensitize them towards chemotherapy. Such treatment strategies are also suggested in different hematological disorders. However, the proof of concept for this novel treatment approaches is still missing (Boyerinas et al. 2013; Takeishi et al. 2013).

Functional studies from LRC and PDX MRD cells showed a microenvironment mediated dormant phenotype in ALL (see 4.1.3; Ebinger, Özdemir et al. 2016). Nevertheless, the leukemic cells have to be targeted instead of the bone marrow microenvironment. The high controversy in the bone marrow niche and our limited knowledge about the interaction of bone marrow cells prevent to use the microenvironment as a therapy target (see 5.3) (Boyd et al. 2014; Calvi & Link. 2014; Hawkins et al. 2016). Furthermore, the obtained RNA-seq data of LRC and PDX MRD cells offer an unique platform to identify targets/candidates on the ALL cells.

However, the question remains, whether it is possible to target both critical PDX populations by inhibiting one candidate. The bone marrow localization of LRC and PDX MRD cells are completely different and so the neighboring cells in the two distinct niches are most probably disparate. In contrast, the GEP of LRC and PDX MRD cells are very similar and an overlap of candidates exists for sure. Therefore, the chance might be high that the inhibition of LRC/PDX MRD cell interaction with the niche is possible by using one candidate. The assumption is that both niches of LRC and PDX MRD cells use the identical mechanism for keeping these cells dormant.

5.5 Conclusion and outlook

The present study developed a novel preclinical mouse model and enabled novel insights into the biology of dormant and treatment resistant ALL cells. The data obtained allow the conclusion that resolving resistant cells from their protective bone marrow niche supporting dormancy might sensitize them towards chemotherapy.

The present work allows future studies to prove this concept and to test novel treatment options against MRD in a preclinical setting. The data approximate the global aim to develop novel therapies which eliminate resistant and dormant tumor cells in ALL, to prevent ALL relapse and to finally improve the prognosis of patients with ALL.

6 Appendix

6.1 Supplemental figures

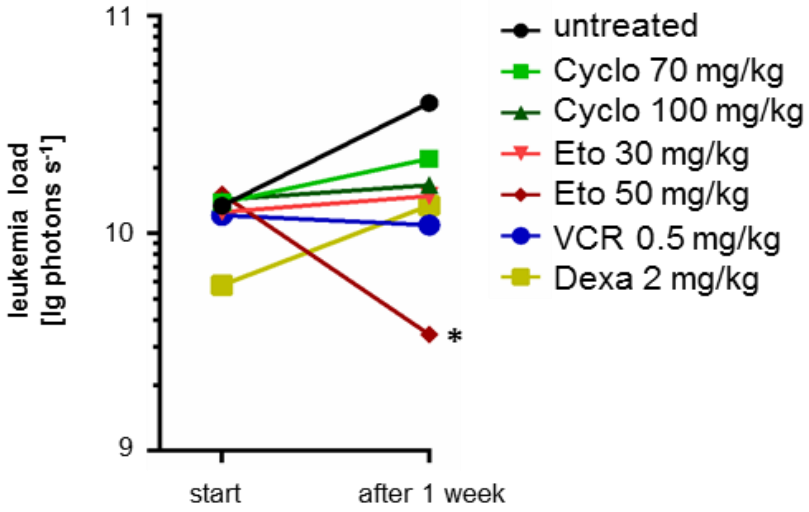

Figure 37: Commonly used cytostatic drugs in patients' ALL therapy show a different and dose-dependent growth inhibition of ALL-265. (related to 4.1.1)

After reaching high tumor load, different cytostatic drugs were applied once a week into mice. Each therapy group consists of two mice. * Eto 50 mg/kg therapy group had to be sacrificed due to high weight loss (> 10% after therapy start).

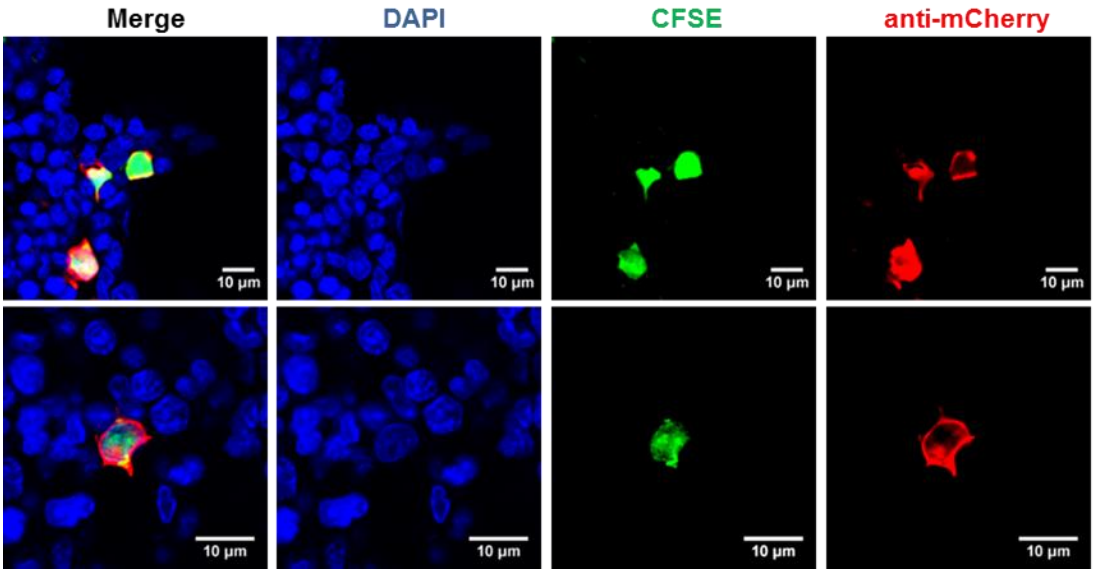

Figure 38: The mCherry antibody staining correlates with the CFSE signal of PDX cells. (related to 4.2.1)

$CFSE^+$ $mCherry^+$ PDX cells were injected into mice. Femurs were fixed with zinc formalin for femur preparation. Fixation destroyed the mCherry signal, but not the CFSE signal. Femur sections of day 3 after cell injection were stained with an anti-mCherry antibody. The CFSE signal at day 3 was strong enough to be detected by confocal microscopy and served as positive control.

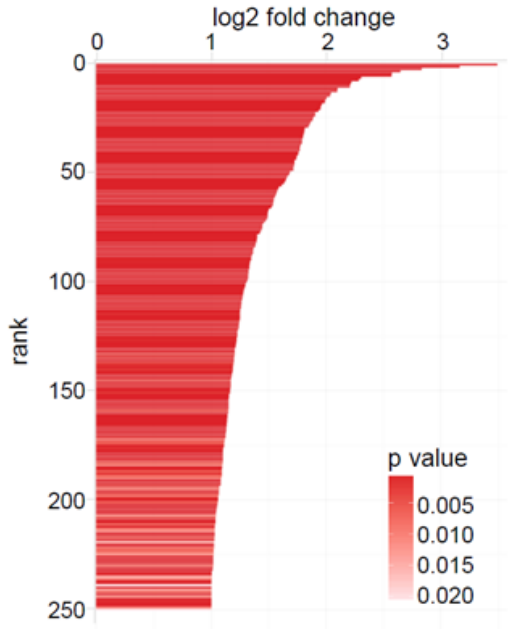

Figure 39: LRC signature from combined RNA-seq data of ALL-199 and ALL-265. (related to 4.3.1)
LRC signature genes (padj < 0.05 and log2 fold-change >1) were derived from combined bulk and single-cell RNA-seq analysis from 6 animals carrying either ALL-265 or ALL-199 and are shown ranked by fold-change and colored by significance. In Table 12 (in the appendix) the genes of the LRC signature are listed. Adapted from (Ebinger, Özdemir et al. 2016).

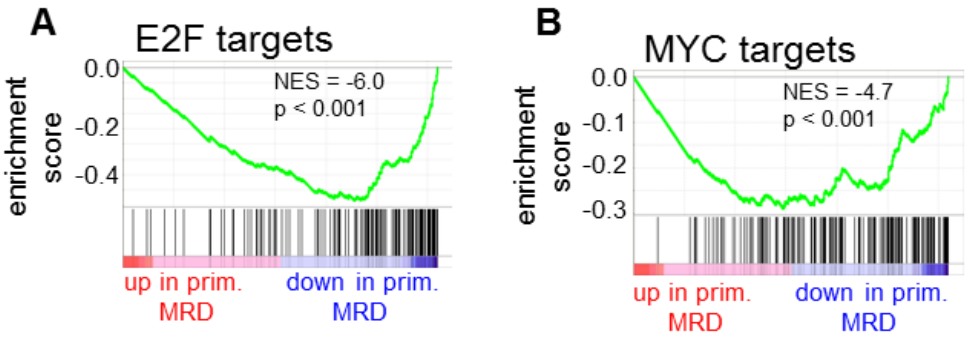

Figure 40: Primary ALL MRD samples are dormant compared to their diagnosis samples. (related to 4.4)
GSEA for E2F and MYC targets from Molecular Signatures Database (MSigDB) (Liberzon et al. 2015) were performed. All bulk RNA-seq data from patients' diagnosis and MRD samples were combined for a primary MRD GEP.

6.2 Supplemental tables

Table 11: Expected absolute and relative LRC numbers in the entire bone marrow/femur based on FACS data (related to 4.2.3)

	ALL-199		
dpi	abs. LRC number	% of LRC to PDX	% of LRC in one femur
day 10	35,000	2%	0.015
day 14	7,000	0.06%	0.003
	ALL-265		
dpi	abs. LRC number in bm	% of LRC to PDX	% of LRC in one femur
day 10	3,000	1.1%	0.001
day 14	2,100	0.02%	0.0007

dpi = days post injection; abs. = absolute; assumption of around $11x10^6$ hematopoietic cells in one femur

Table 12: Common LRC signature (log2 fc > 1 and padj < 0.05) of ALL-199 and ALL-265 (related to Figure 39) Adapted from (Ebinger, Özdemir et al. 2016).

Rank	Gene Name	log2 fc	padj
1	H1F0	3.49	1.17E-45
2	HSD11B1	3.17	3.12E-22
3	NEIL1	2.83	1.72E-23
4	AC116366.5	2.65	2.00E-16
5	MTUS2	2.58	2.45E-17
6	HIST1H2AC	2.57	1.01E-33
7	FLT3	2.30	2.95E-21
8	C10orf10	2.29	1.19E-19
9	CYTL1	2.22	4.16E-60
10	MS4A6A	2.21	4.84E-11
11	CD97	2.21	1.34E-13
12	TMEM173	2.10	2.51E-19
13	NFE2	2.10	1.94E-13
14	NT5E	2.04	8.22E-13
15	CD86	2.04	1.14E-09
16	TP53INP1	2.01	6.96E-14
17	SETBP1	1.99	9.12E-09
18	LGALS1	1.99	4.99E-10
19	GSN	1.97	1.25E-22
20	HSH2D	1.96	5.20E-16
21	RAB37	1.95	2.38E-16
22	ABHD4	1.94	1.14E-11
23	HIST1H4H	1.91	1.26E-10
24	EMR2	1.91	4.26E-08
25	ENSG00000229164	1.89	2.47E-12
26	EMP1	1.89	6.49E-12
27	ITGA6	1.87	4.50E-18
28	LINC00114	1.86	3.59E-09
29	HRK	1.85	1.51E-07
30	CST7	1.82	1.26E-07
31	MYO1F	1.81	6.28E-10
32	PDGFA	1.81	2.11E-07
33	NOTCH2	1.81	8.35E-13
34	SERPINE1	1.80	1.83E-07
35	FAIM3	1.80	4.01E-20
36	NRXN3	1.80	3.73E-07
37	TOX2	1.79	4.63E-07
38	NCF1C	1.78	1.29E-12
39	HIST2H2BE	1.77	5.41E-14
40	DUSP26	1.77	6.33E-07
41	C15orf52	1.76	9.58E-08
42	CD70	1.75	4.89E-09
43	METTL7A	1.74	7.41E-11
44	LINC00707	1.74	3.52E-08
45	MYRIP	1.72	6.08E-10
46	SAMHD1	1.72	3.95E-14
47	NCF1B	1.72	4.66E-13
48	RP11-473M20.9	1.71	7.25E-08
49	TNFSF4	1.71	2.01E-07
50	RIN2	1.68	9.90E-09
51	TPST1	1.68	2.88E-08
52	SERPING1	1.66	8.31E-08
53	PIK3IP1	1.65	2.72E-16
54	NCF1	1.65	3.95E-14
55	ADAM19	1.63	1.38E-07
56	DHRS7	1.61	4.66E-13
57	P4HA2	1.59	3.06E-08
58	DNASE2	1.58	1.17E-05

59	ADAM8	1.57	4.48E-06
60	CD1C	1.56	9.35E-11
61	MYLIP	1.55	3.81E-11
62	SDK2	1.55	6.26E-06
63	LINC01021	1.54	2.33E-06
64	IL24	1.54	1.71E-05
65	PLEKHG1	1.54	6.34E-06
66	HIP1	1.52	3.71E-05
67	Y_RNA	1.50	9.13E-06
68	PTGER4	1.49	3.64E-05
69	ZMAT3	1.49	2.19E-09
70	KLF4	1.49	6.68E-06
71	ARL4C	1.49	3.62E-05
72	FERMT2	1.48	7.36E-05
73	GBP2	1.46	8.50E-05
74	LPAR6	1.45	1.14E-20
75	IL1B	1.45	3.21E-18
76	ZNF555	1.44	2.84E-06
77	TERF2	1.43	4.69E-23
78	FOLR2	1.43	2.20E-06
79	FCGRT	1.40	1.12E-13
80	S100A10	1.40	1.70E-04
81	PAN3	1.40	2.36E-17
82	LRMP	1.40	1.34E-20
83	NOTCH2NL	1.39	1.60E-04
84	CDKN2D	1.38	1.05E-15
85	CTSH	1.37	6.18E-14
86	DUSP1	1.37	5.47E-10
87	OSBPL10	1.37	8.69E-05
88	ANTXR1	1.36	1.14E-04
89	FOSB	1.35	8.89E-06
90	SELM	1.35	2.26E-04
91	OSER1-AS1	1.34	4.08E-04
92	LGR6	1.34	1.42E-04
93	C10orf25	1.33	1.20E-05
94	RHOC	1.33	3.39E-05
95	PLAUR	1.33	4.85E-07
96	FBXO25	1.33	2.08E-04
97	B3GNT5	1.32	4.35E-04
98	ENSG00000117289	1.32	1.36E-12
99	CLMN	1.32	4.80E-06
100	FAM3C	1.31	4.11E-07
101	CA5B	1.30	5.54E-08
102	LYST	1.30	1.83E-07
103	RASSF4	1.29	1.71E-04
104	RGS16	1.28	1.34E-04
105	SH3BP2	1.28	3.32E-08
106	TNFRSF10D	1.28	5.70E-05
107	PPP1R15A	1.28	8.19E-09
108	ITGAM	1.27	9.23E-04
109	MACROD2	1.27	7.80E-05
110	ITGB2	1.27	8.88E-08
111	GADD45B	1.26	1.84E-07
112	HGSNAT	1.26	7.85E-04
113	CLEC4E	1.26	3.31E-04
114	IPCEF1	1.26	2.47E-12
115	PLXNB1	1.25	1.30E-03
116	CRMP1	1.25	1.24E-05
117	LGALS3BP	1.25	4.55E-13
118	SULF2	1.25	1.18E-03
119	N4BP2L1	1.25	8.36E-07
120	C16orf54	1.24	6.83E-10
121	NEAT1	1.24	7.66E-11
122	CEP112	1.24	4.56E-04
123	TIMP1	1.23	1.29E-09
124	SMAD3	1.23	3.45E-06
125	OAS1	1.23	9.07E-07
126	RASAL2	1.22	1.57E-04
127	FOS	1.22	8.28E-04
128	THEMIS2	1.22	7.43E-09
129	AC005154.6	1.22	4.05E-05
130	CXCR4	1.22	6.43E-10
131	CSRNP2	1.21	1.95E-04
132	CD44	1.21	6.85E-09
133	TNFAIP2	1.21	2.22E-03
134	GPR183	1.21	1.18E-03
135	SPRY1	1.20	1.37E-03
136	TSC22D3	1.20	7.17E-10
137	RP11-154D3.1	1.20	2.33E-03
138	PLXND1	1.19	1.71E-03
139	LSP1	1.19	4.49E-05
140	ID2	1.19	1.92E-03
141	YPEL2	1.19	3.78E-04
142	LINC01013	1.18	2.55E-09
143	ENSG00000182217	1.18	8.67E-08
144	ENSG00000183941	1.17	7.75E-08
145	CTD-3252C9.4	1.17	3.26E-03
146	MS4A7	1.17	1.39E-04
147	BHLHE40	1.17	1.21E-03
148	TLR1	1.17	5.47E-05
149	HSPB1	1.16	5.70E-10
150	ANKRD28	1.16	5.80E-07
151	RAP1GAP2	1.16	2.00E-03
152	HLA-E	1.15	3.21E-18
153	GIMAP4	1.15	1.66E-05
154	DDIT4L	1.15	6.09E-10
155	BTG1	1.15	3.21E-07
156	CD37	1.15	2.07E-05
157	HCST	1.15	1.58E-05
158	HVCN1	1.15	1.88E-08
159	KIAA1407	1.15	4.51E-03
160	RP11-325F22.2	1.14	3.69E-04
161	RYBP	1.14	5.63E-07
162	ENSG00000163386	1.14	7.60E-07
163	EMP3	1.14	3.39E-05
164	ANTXR2	1.14	2.49E-06
165	SMAGP	1.13	3.71E-06
166	HIST1H1C	1.13	1.58E-09
167	KLF6	1.13	1.40E-06
168	LITAF	1.13	1.42E-06
169	ARID5B	1.12	2.04E-07
170	LINC-PINT	1.12	2.25E-04
171	CBR3	1.12	7.85E-04
172	SFXN3	1.12	5.04E-03
173	RP11-474J18.1	1.11	5.38E-03
174	NR4A1	1.11	6.30E-03

175	HIST1H2BK	1.11	7.97E-08
176	RAB29	1.10	1.58E-03
177	NEGR1	1.10	2.22E-04
178	GCSAM	1.10	4.30E-05
179	TGFBR2	1.10	6.20E-05
180	ICAM3	1.10	1.70E-04
181	PSAT1	1.10	2.53E-08
182	ARMCX4	1.10	1.92E-03
183	IGFBP7	1.10	6.35E-03
184	AMICA1	1.09	6.80E-03
185	F11R	1.09	2.73E-04
186	IFITM3	1.09	8.49E-08
187	RP11-556E13.1	1.09	6.34E-03
188	PSAT1P3	1.09	1.24E-03
189	PCNXL2	1.09	7.63E-03
190	RYK	1.08	8.32E-03
191	EFNA1	1.08	3.59E-05
192	KLF3	1.08	3.55E-05
193	NEDD9	1.08	1.08E-03
194	HSBP1L1	1.07	2.93E-03
195	CDC42EP3	1.07	9.17E-03
196	CMTM2	1.06	1.47E-06
197	CECR1	1.06	1.65E-03
198	CASC15	1.06	1.04E-02
199	SYNE2	1.06	9.08E-04
200	TMCO4	1.06	3.53E-04
201	RHOB	1.06	7.70E-03
202	RGL1	1.05	2.79E-08
203	FOSL2	1.05	1.58E-04
204	ENSG00000183558	1.05	8.21E-05
205	CD9	1.04	1.10E-09
206	ZNF252P	1.04	1.59E-06
207	SPNS3	1.04	1.00E-02
208	HSPB1P2	1.04	2.51E-03
209	ARHGEF3	1.04	6.03E-04
210	C9orf89	1.04	1.24E-04
211	DPEP1	1.03	7.85E-03
212	RP11-301G19.1	1.03	1.52E-07
213	GDPD1	1.03	9.85E-03
214	PCDH9	1.03	1.15E-02
215	HIST2H2AA4	1.03	1.23E-04
216	MX1	1.03	3.31E-04
217	CAP2	1.03	4.68E-03
218	KIAA2026	1.03	4.82E-05
219	TEX41	1.02	1.47E-02
220	CAPG	1.02	1.45E-10
221	PLP2	1.02	2.53E-05
222	ZNF441	1.02	1.03E-02
223	ATF3	1.02	6.04E-03
224	ZBTB20	1.02	9.32E-03
225	IRAK2	1.02	1.34E-02
226	SPTA1	1.02	1.61E-04
227	RP4-725G10.4	1.02	1.27E-06
228	CAPN2	1.02	3.59E-04
229	S100A6	1.02	3.45E-09
230	WWC3	1.02	8.93E-03
231	ZCCHC7	1.01	9.36E-13
232	HLA-G	1.01	4.50E-09
233	RNASET2	1.00	5.45E-10
234	HLA-W	1.00	6.03E-04
235	ZBTB4	1.00	1.54E-02
236	FAM3C2	1.00	1.14E-02
237	HSPB1P1	1.00	4.69E-04
238	UBXN11	1.00	3.56E-04
239	TP53INP2	1.00	1.94E-02
240	XAF1	1.00	1.08E-04
241	ZFP36	1.00	1.09E-02
242	KCTD7	1.00	5.88E-03
243	RP11-705C15.2	1.00	3.71E-05
244	GLDC	1.00	1.02E-02
245	KLHL24	1.00	6.51E-05
246	GCHFR	1.00	1.20E-03
247	C20orf194	1.00	3.31E-04
248	IGLL1	1.00	6.68E-12
249	PLXNC1	1.00	1.12E-02
250	IL3RA	1.00	2.07E-02

6.3 R-packages and version numbers

R version 3.3.1 (2016-06-21)
Platform: x86_64-w64-mingw32/x64 (64-bit)
Running under: Windows >= 8 x64 (build 9200)

locale:
[1] LC_COLLATE=German_Germany.1252 LC_CTYPE=German_Germany.1252
[3] LC_MONETARY=German_Germany.1252 LC_NUMERIC=C
[5] LC_TIME=German_Germany.1252

attached base packages:
[1] grid parallel stats4 stats graphics grDevices
[7] utils datasets methods base

other attached packages:
[1] BiocInstaller_1.22.3 org.Hs.eg.db_3.3.0
[3] AnnotationDbi_1.34.4 ggplot2_2.1.0
[5] ComplexHeatmap_1.10.2 DESeq2_1.14.0
[7] SummarizedExperiment_1.2.3 Biobase_2.32.0
[9] GenomicRanges_1.24.3 GenomeInfoDb_1.8.7
[11] IRanges_2.6.1 S4Vectors_0.10.3
[13] BiocGenerics_0.18.0

loaded via a namespace (and not attached):
[1] mclust_5.2 Rcpp_0.12.7 locfit_1.5-9.1
[4] mvtnorm_1.0-5 lattice_0.20-33 circlize_0.3.9
[7] class_7.3-14 plyr_1.8.4 chron_2.3-47
[10] acepack_1.4.1 RSQLite_1.0.0 GlobalOptions_0.0.10
[13] zlibbioc_1.18.0 diptest_0.75-7 data.table_1.9.6
[16] annotate_1.50.1 whisker_0.3-2 kernlab_0.9-25
[19] GetoptLong_0.1.5 rpart_4.1-10 Matrix_1.2-6
[22] splines_3.3.1 BiocParallel_1.6.6 geneplotter_1.50.0
[25] foreign_0.8-67 RCurl_1.95-4.8 munsell_0.4.3
[28] shape_1.4.2 nnet_7.3-12 gridExtra_2.2.1
[31] Hmisc_3.17-4 dendextend_1.3.0 XML_3.98-1.4
[34] MASS_7.3-45 bitops_1.0-6 xtable_1.8-2
[37] gtable_0.2.0 DBI_0.5-1 magrittr_1.5
[40] scales_0.4.0 XVector_0.12.1 genefilter_1.54.2
[43] flexmix_2.3-13 latticeExtra_0.6-28 robustbase_0.92-6
[46] Formula_1.2-1 rjson_0.2.15 RColorBrewer_1.1-2
[49] tools_3.3.1 fpc_2.1-10 trimcluster_0.1-2
[52] DEoptimR_1.0-6 survival_2.39-5 colorspace_1.2-7
[55] cluster_2.0.5 prabclus_2.2-6 modeltools_0.2-21

7 List of tables and figures

List of tables

List of figures

8 Abbreviations

°C	degree Celsius
µm	micrometre (10^{-6} m)
ALL	acute lymphoblastic leukemia
APC	allophycocyanin
BCP	B-cell precursor
BM	bone marrow
BSA	bovine serum albumin
CAR	CXCL12-abundant reticular
CD	cluster of differentiation
cDNA	complementary deoxyribonucleic acid
CFSE	carboxyfluorescein succinimidyl ester
cm	centrimetre (10^{-2} m)
CML	chronic myelogenous leukemia
CSC	cancer stem cell
ctrl	control
Cyclo	Cyclophosphamide
d	days
DAPI	4′,6-Diamidin-2-phenylindol
dd H_20	double-distilled water
DE	differential expression
Dexa	Dexamethasone
DMSO	Dimethylsulfoxid
DNA	deoxyribonucleic acid
EDTA	Ethylenediaminetetraacetic acid
ELP	early lymphoid progenitor
Eto	Etoposide
F	female
FACS	fluorescence-activated cell scanning
fc	fold change
FCS	fetal calf serum
FSC	forward scatter
g	relative centrifugal force
g	gram
GEO	gene expression omnibus
GEP	gene expression profile
GSEA	gene set enrichment analysis
h	hour
HPC	hematopoietic progenitor cell
HSC	hematopoietic stem cell
Hz	Hertz (60/min)
i.p.	intraperitoneal
i.v.	intravenous

IHC	immunohistochemistry
KEGG	Kyoto Encyclopedia of Genes and Genomes
kg	kilo gram (10^3 g)
lg	logarithm
LIC	leukemia initiating cell
LRC	label retaining cell
LSC	leukemia stem cell
m	meter
M	molecular mass
MACS	Magnetic Activated Cell Sorting
mg	milligram (10^{-3} gram)
min	minute
ml	millilitre (10^{-3} litre)
mM	millimolar (10^{-3} molecular mass)
MRD	minimal residual disease
mRNA	messenger ribonucleic acid
MSC	mesenchymal stem cell
MSigDB	Molecular Signatures Database
n	absolute number
na	not available
NES	normalized enrichment score
NGFR	human low affinity nerve growth factor receptor
nm	nanometer (10^{-9} m)
NSG	NOD scid gamma
padj	p-value adjusted
PBE	PBS including EDTA
PBS	phosphate buffered saline
PC	principle component
PCA	principle component analysis
PCR	polymerase chain reaction
PDX	patient-derived xenograft
PE	Phycoerythrin
pen/strep	penicillin streptomycin
RNA-seq	ribonucleic acid sequencing
RT	room temperature
s	second
sr	steradian
SSC	side scatter
untr.	untreated
UV	ultraviolett
v/v	volume/volume
VCR	Vincristine
VSD	variance stabilizing data
w/v	weigth/volume

9 References

Abdullah LN, Chow EK (2013) Mechanisms of chemoresistance in cancer stem cells. *Clinical and translational medicine* 2**:** 3

Acar M, Kocherlakota KS, Murphy MM, Peyer JG, Oguro H, Inra CN, Jaiyeola C, Zhao Z, Luby-Phelps K, Morrison SJ (2015) Deep imaging of bone marrow shows non-dividing stem cells are mainly perisinusoidal. *Nature* 526**:** 126-130

Alizadeh AA, Eisen MB, Davis RE, Ma C, Lossos IS, Rosenwald A, Boldrick JC, Sabet H, Tran T, Yu X, Powell JI, Yang L, Marti GE, Moore T, Hudson J, Jr., Lu L, Lewis DB, Tibshirani R, Sherlock G, Chan WC et al (2000) Distinct types of diffuse large B-cell lymphoma identified by gene expression profiling. *Nature* 403**:** 503-511

Arai F, Suda T (2007) Regulation of hematopoietic stem cells in the osteoblastic niche. *Advances in experimental medicine and biology* 602**:** 61-67

Bacher R, Kendziorski C (2016) Design and computational analysis of single-cell RNA-sequencing experiments. *Genome biology* 17**:** 63

Barrett DM, Seif AE, Carpenito C, Teachey DT, Fish JD, June CH, Grupp SA, Reid GS (2011) Noninvasive bioluminescent imaging of primary patient acute lymphoblastic leukemia: a strategy for preclinical modeling. *Blood* 118**:** e112-117

Bassan R, Hoelzer D (2011) Modern therapy of acute lymphoblastic leukemia. *Journal of clinical oncology : official journal of the American Society of Clinical Oncology* 29**:** 532-543

Basso G, Veltroni M, Valsecchi MG, Dworzak MN, Ratei R, Silvestri D, Benetello A, Buldini B, Maglia O, Masera G, Conter V, Arico M, Biondi A, Gaipa G (2009) Risk of relapse of childhood acute lymphoblastic leukemia is predicted by flow cytometric measurement of residual disease on day 15 bone marrow. *Journal of clinical oncology : official journal of the American Society of Clinical Oncology* 27**:** 5168-5174

Bhatla T, Wang J, Morrison DJ, Raetz EA, Burke MJ, Brown P, Carroll WL (2012) Epigenetic reprogramming reverses the relapse-specific gene expression signature and restores chemosensitivity in childhood B-lymphoblastic leukemia. *Blood* 119**:** 5201-5210

Bomken S, Buechler L, Rehe K, Ponthan F, Elder A, Blair H, Bacon CM, Vormoor J, Heidenreich O (2013) Lentiviral marking of patient-derived acute lymphoblastic leukaemic cells allows in vivo tracking of disease progression. *Leukemia* 27**:** 718-721

Borowitz MJ, Devidas M, Hunger SP, Bowman WP, Carroll AJ, Carroll WL, Linda S, Martin PL, Pullen DJ, Viswanatha D, Willman CL, Winick N, Camitta BM, Children's Oncology G (2008) Clinical significance of minimal residual disease in childhood acute lymphoblastic leukemia and its relationship to other prognostic factors: a Children's Oncology Group study. *Blood* 111**:** 5477-5485

Boyd AL, Campbell CJ, Hopkins CI, Fiebig-Comyn A, Russell J, Ulemek J, Foley R, Leber B, Xenocostas A, Collins TJ, Bhatia M (2014) Niche displacement of human leukemic stem cells uniquely allows their competitive replacement with healthy HSPCs. *The Journal of experimental medicine* 211**:** 1925-1935

Boyerinas B, Zafrir M, Yesilkanal AE, Price TT, Hyjek EM, Sipkins DA (2013) Adhesion to osteopontin in the bone marrow niche regulates lymphoblastic leukemia cell dormancy. *Blood* 121**:** 4821-4831

Brower V (2016) Phase 1/2 study of blinatumomab in relapsed paediatric ALL. *The Lancet Oncology*

Bruggemann M, Raff T, Kneba M (2012) Has MRD monitoring superseded other prognostic factors in adult ALL? *Blood* 120**:** 4470-4481

Bruggemann M, Schrauder A, Raff T, Pfeifer H, Dworzak M, Ottmann OG, Asnafi V, Baruchel A, Bassan R, Benoit Y, Biondi A, Cave H, Dombret H, Fielding AK, Foa R, Gokbuget N, Goldstone AH, Goulden N, Henze G, Hoelzer D et al (2010) Standardized MRD quantification in European ALL trials: proceedings of the Second International Symposium on MRD assessment in Kiel, Germany, 18-20 September 2008. *Leukemia* 24**:** 521-535

Buckley SA, Appelbaum FR, Walter RB (2013) Prognostic and therapeutic implications of minimal residual disease at the time of transplantation in acute leukemia. *Bone marrow transplantation* 48**:** 630-641

Calvi LM, Adams GB, Weibrecht KW, Weber JM, Olson DP, Knight MC, Martin RP, Schipani E, Divieti P, Bringhurst FR, Milner LA, Kronenberg HM, Scadden DT (2003) Osteoblastic cells regulate the haematopoietic stem cell niche. *Nature* 425**:** 841-846

Calvi LM, Link DC (2014) Cellular complexity of the bone marrow hematopoietic stem cell niche. *Calcified tissue international* 94**:** 112-124

Campana D (2010) Minimal residual disease in acute lymphoblastic leukemia. *Hematology American Society of Hematology Education Program* 2010**:** 7-12

Cassidy JW, Caldas C, Bruna A (2015) Maintaining Tumor Heterogeneity in Patient-Derived Tumor Xenografts. *Cancer research* 75**:** 2963-2968

Chen Z, Orlowski RZ, Wang M, Kwak L, McCarty N (2014) Osteoblastic niche supports the growth of quiescent multiple myeloma cells. *Blood* 123**:** 2204-2208

Cheung AM, Nguyen LV, Carles A, Beer P, Miller PH, Knapp DJ, Dhillon K, Hirst M, Eaves CJ (2013) Analysis of the clonal growth and differentiation dynamics of primitive barcoded human cord blood cells in NSG mice. *Blood* 122**:** 3129-3137

Chiarini F, Lonetti A, Evangelisti C, Buontempo F, Orsini E, Evangelisti C, Cappellini A, Neri LM, McCubrey JA, Martelli AM (2016) Advances in understanding the acute lymphoblastic leukemia bone marrow microenvironment: From biology to therapeutic targeting. *Biochimica et biophysica acta* 1863**:** 449-463

Clappier E, Gerby B, Sigaux F, Delord M, Touzri F, Hernandez L, Ballerini P, Baruchel A, Pflumio F, Soulier J (2011) Clonal selection in xenografted human T cell acute lymphoblastic leukemia recapitulates gain of malignancy at relapse. *The Journal of experimental medicine* 208**:** 653-661

Clevers H (2011) The cancer stem cell: premises, promises and challenges. *Nature medicine* 17**:** 313-319

Cobaleda C, Sanchez-Garcia I (2009) B-cell acute lymphoblastic leukaemia: towards understanding its cellular origin. *BioEssays : news and reviews in molecular, cellular and developmental biology* 31**:** 600-609

Colmone A, Amorim M, Pontier AL, Wang S, Jablonski E, Sipkins DA (2008) Leukemic Cells Create Bone Marrow Niches That Disrupt the Behavior of Normal Hematopoietic Progenitor Cells. *Science* 322**:** 1861-1865

Conter V, Bartram CR, Valsecchi MG, Schrauder A, Panzer-Grumayer R, Moricke A, Arico M, Zimmermann M, Mann G, De Rossi G, Stanulla M, Locatelli F, Basso G, Niggli F, Barisone E, Henze G, Ludwig WD, Haas OA, Cazzaniga G, Koehler R et al (2010) Molecular response to treatment redefines all prognostic factors in children and adolescents with B-cell precursor acute lymphoblastic leukemia: results in 3184 patients of the AIEOP-BFM ALL 2000 study. *Blood* 115**:** 3206-3214

Cooper SL, Brown PA (2015) Treatment of pediatric acute lymphoblastic leukemia. *Pediatric clinics of North America* 62**:** 61-73

Coustan-Smith E, Song G, Clark C, Key L, Liu P, Mehrpooya M, Stow P, Su X, Shurtleff S, Pui CH, Downing JR, Campana D (2011) New markers for minimal residual disease detection in acute lymphoblastic leukemia. *Blood* 117**:** 6267-6276

Daniel VC, Marchionni L, Hierman JS, Rhodes JT, Devereux WL, Rudin CM, Yung R, Parmigiani G, Dorsch M, Peacock CD, Watkins DN (2009) A primary xenograft model of small-cell lung cancer reveals irreversible changes in gene expression imposed by culture in vitro. *Cancer research* 69**:** 3364-3373

Demetrius L (2005) Of mice and men. When it comes to studying ageing and the means to slow it down, mice are not just small humans. *EMBO reports* 6 Spec No**:** S39-44

Dimova DK, Dyson NJ (2005) The E2F transcriptional network: old acquaintances with new faces. *Oncogene* 24**:** 2810-2826

Ding L, Morrison SJ (2013) Haematopoietic stem cells and early lymphoid progenitors occupy distinct bone marrow niches. *Nature* 495**:** 231-235

Duan CW, Shi J, Chen J, Wang B, Yu YH, Qin X, Zhou XC, Cai YJ, Li ZQ, Zhang F, Yin MZ, Tao Y, Mi JQ, Li LH, Enver T, Chen GQ, Hong DL (2014) Leukemia propagating cells rebuild an evolving niche in response to therapy. *Cancer cell* 25**:** 778-793

Dull T, Zufferey R, Kelly M, Mandel RJ, Nguyen M, Trono D, Naldini L (1998) A third-generation lentivirus vector with a conditional packaging system. *Journal of virology* 72**:** 8463-8471

Ebinger S, Ozdemir EZ, Ziegenhain C, Tiedt S, Castro Alves C, Grunert M, Dworzak M, Lutz C, Turati VA, Enver T, Horny HP, Sotlar K, Parekh S, Spiekermann K, Hiddemann W, Schepers A, Polzer B, Kirsch S, Hoffmann M, Knapp B et al (2016) Characterization of Rare, Dormant, and Therapy-Resistant Cells in Acute Lymphoblastic Leukemia. *Cancer cell*

Ehninger A, Trumpp A (2011) The bone marrow stem cell niche grows up: mesenchymal stem cells and macrophages move in. *The Journal of experimental medicine* 208**:** 421-428

Esparza SD, Sakamoto KM (2005) Topics in pediatric leukemia--acute lymphoblastic leukemia. *MedGenMed : Medscape general medicine* 7**:** 23

Essers MA, Trumpp A (2010) Targeting leukemic stem cells by breaking their dormancy. *Molecular oncology* 4**:** 443-450

Ferrando AA, Armstrong SA, Neuberg DS, Sallan SE, Silverman LB, Korsmeyer SJ, Look AT (2003) Gene expression signatures in MLL-rearranged T-lineage and B-precursor acute leukemias: dominance of HOX dysregulation. *Blood* 102**:** 262-268

Fiser K, Sieger T, Schumich A, Wood B, Irving J, Mejstrikova E, Dworzak MN (2012) Detection and monitoring of normal and leukemic cell populations with hierarchical clustering of flow cytometry data. *Cytometry Part A : the journal of the International Society for Analytical Cytology* 81**:** 25-34

Foo J, Michor F (2014) Evolution of acquired resistance to anti-cancer therapy. *Journal of theoretical biology* 355**:** 10-20

Fry TJ, Aplan PD (2015) A robust in vivo model for B cell precursor acute lymphoblastic leukemia. *The Journal of clinical investigation* 125**:** 3427-3429

Gal H, Amariglio N, Trakhtenbrot L, Jacob-Hirsh J, Margalit O, Avigdor A, Nagler A, Tavor S, Ein-Dor L, Lapidot T, Domany E, Rechavi G, Givol D (2006) Gene expression profiles of AML derived stem cells; similarity to hematopoietic stem cells. *Leukemia* 20**:** 2147-2154

Gao H, Korn JM, Ferretti S, Monahan JE, Wang Y, Singh M, Zhang C, Schnell C, Yang G, Zhang Y, Balbin OA, Barbe S, Cai H, Casey F, Chatterjee S, Chiang DY, Chuai S, Cogan SM, Collins SD, Dammassa E et al (2015) High-throughput screening using patient-derived tumor xenografts to predict clinical trial drug response. *Nature medicine* 21**:** 1318-1325

Gentles AJ, Plevritis SK, Majeti R, Alizadeh AA (2010) Association of a leukemic stem cell gene expression signature with clinical outcomes in acute myeloid leukemia. *Jama* 304**:** 2706-2715

Gopalakrishnapillai A, Kolb EA, Dhanan P, Bojja AS, Mason RW, Corao D, Barwe SP (2016) Generation of Pediatric Leukemia Xenograft Models in NSG-B2m Mice: Comparison with NOD/SCID Mice. *Frontiers in oncology* 6**:** 162

Graham SM, Vass JK, Holyoake TL, Graham GJ (2007) Transcriptional analysis of quiescent and proliferating CD34+ human hemopoietic cells from normal and chronic myeloid leukemia sources. *Stem cells* 25**:** 3111-3120

Greaves M (2013) Cancer stem cells as 'units of selection'. *Evolutionary applications* 6**:** 102-108

Greaves MF, Wiemels J (2003) Origins of chromosome translocations in childhood leukaemia. *Nature reviews Cancer* 3**:** 639-649

Guezguez B, Campbell Clinton JV, Boyd Allison L, Karanu F, Casado Fanny L, Di Cresce C, Collins Tony J, Shapovalova Z, Xenocostas A, Bhatia M (2013) Regional Localization within the Bone Marrow Influences the Functional Capacity of Human HSCs. *Cell stem cell* 13**:** 175-189

Hackl H, Steinleitner K, Lind K, Hofer S, Tosic N, Pavlovic S, Suvajdzic N, Sill H, Wieser R (2015) A gene expression profile associated with relapse of cytogenetically normal acute myeloid leukemia is enriched for leukemia stem cell genes. *Leukemia & lymphoma* 56**:** 1126-1128

Hawkins ED, Duarte D, Akinduro O, Khorshed RA, Passaro D, Nowicka M, Straszkowski L, Scott MK, Rothery S, Ruivo N, Foster K, Waibel M, Johnstone RW, Harrison SJ, Westerman DA, Quach H, Gribben J, Robinson MD, Purton LE, Bonnet D et al (2016) T-cell acute leukaemia exhibits dynamic interactions with bone marrow microenvironments. *Nature* 538**:** 518-522

Haylock DN, Williams B, Johnston HM, Liu MC, Rutherford KE, Whitty GA, Simmons PJ, Bertoncello I, Nilsson SK (2007) Hemopoietic stem cells with higher hemopoietic potential reside at the bone marrow endosteum. *Stem cells* 25**:** 1062-1069

Hidalgo M, Amant F, Biankin AV, Budinska E, Byrne AT, Caldas C, Clarke RB, de Jong S, Jonkers J, Maelandsmo GM, Roman-Roman S, Seoane J, Trusolino L, Villanueva A (2014) Patient-derived xenograft models: an emerging platform for translational cancer research. *Cancer discovery* 4**:** 998-1013

Hutter G, Nickenig C, Garritsen H, Hellenkamp F, Hoerning A, Hiddemann W, Dreyling M (2004) Use of polymorphisms in the noncoding region of the human mitochondrial genome to identify potential contamination of human leukemia-lymphoma cell lines. *The hematology journal : the official journal of the European Haematology Association* 5**:** 61-68

Inaba H, Greaves M, Mullighan CG (2013) Acute lymphoblastic leukaemia. *Lancet* 381**:** 1943-1955

Ishikawa F (2013) Modeling normal and malignant human hematopoiesis in vivo through newborn NSG xenotransplantation. *International journal of hematology* 98**:** 634-640

Ishikawa F, Yoshida S, Saito Y, Hijikata A, Kitamura H, Tanaka S, Nakamura R, Tanaka T, Tomiyama H, Saito N, Fukata M, Miyamoto T, Lyons B, Ohshima K, Uchida N, Taniguchi S, Ohara O, Akashi K, Harada M, Shultz LD (2007) Chemotherapy-resistant human AML stem cells home to and engraft within the bone-marrow endosteal region. *Nature biotechnology* 25**:** 1315-1321

Iwasaki H, Suda T (2009) Cancer stem cells and their niche. *Cancer science* 100**:** 1166-1172

Jin L, Tabe Y, Konoplev S, Xu Y, Leysath CE, Lu H, Kimura S, Ohsaka A, Rios MB, Calvert L, Kantarjian H, Andreeff M, Konopleva M (2008) CXCR4 up-regulation by imatinib induces chronic myelogenous leukemia (CML) cell migration to bone marrow stroma and promotes survival of quiescent CML cells. *Molecular cancer therapeutics* 7**:** 48-58

Kamel-Reid S, Letarte M, Sirard C, Doedens M, Grunberger T, Fulop G, Freedman MH, Phillips RA, Dick JE (1989) A model of human acute lymphoblastic leukemia in immune-deficient SCID mice. *Science* 246**:** 1597-1600

Kanehisa M, Goto S, Sato Y, Furumichi M, Tanabe M (2012) KEGG for integration and interpretation of large-scale molecular data sets. *Nucleic acids research* 40**:** D109-114

Kang H, Chen IM, Wilson CS, Bedrick EJ, Harvey RC, Atlas SR, Devidas M, Mullighan CG, Wang X, Murphy M, Ar K, Wharton W, Borowitz MJ, Bowman WP, Bhojwani D, Carroll WL, Camitta BM, Reaman GH, Smith MA, Downing JR et al (2010) Gene expression classifiers for relapse-free survival and minimal residual disease improve risk classification and outcome prediction in pediatric B-precursor acute lymphoblastic leukemia. *Blood* 115**:** 1394-1405

Kantarjian H, Thomas D, Jorgensen J, Jabbour E, Kebriaei P, Rytting M, York S, Ravandi F, Kwari M, Faderl S, Rios MB, Cortes J, Fayad L, Tarnai R, Wang SA, Champlin R, Advani A, O'Brien S (2012) Inotuzumab ozogamicin, an anti-CD22-calecheamicin conjugate, for refractory and relapsed acute lymphocytic leukaemia: a phase 2 study. *The Lancet Oncology* 13**:** 403-411

Khan J, Wei JS, Ringner M, Saal LH, Ladanyi M, Westermann F, Berthold F, Schwab M, Antonescu CR, Peterson C, Meltzer PS (2001) Classification and diagnostic prediction of cancers using gene expression profiling and artificial neural networks. *Nature medicine* 7**:** 673-679

Kiel MJ, Radice GL, Morrison SJ (2007) Lack of evidence that hematopoietic stem cells depend on N-cadherin-mediated adhesion to osteoblasts for their maintenance. *Cell stem cell* 1**:** 204-217

Kim JH, Lee SR, Li LH, Park HJ, Park JH, Lee KY, Kim MK, Shin BA, Choi SY (2011) High cleavage efficiency of a 2A peptide derived from porcine teschovirus-1 in human cell lines, zebrafish and mice. *PloS one* 6**:** e18556

Kode A, Manavalan JS, Mosialou I, Bhagat G, Rathinam CV, Luo N, Khiabanian H, Lee A, Murty VV, Friedman R, Brum A, Park D, Galili N, Mukherjee S, Teruya-Feldstein J, Raza A, Rabadan R, Berman E, Kousteni S (2014) Leukaemogenesis induced by an activating [bgr]-catenin mutation in osteoblasts. *Nature* 506**:** 240-244

Kong Y, Yoshida S, Saito Y, Doi T, Nagatoshi Y, Fukata M, Saito N, Yang SM, Iwamoto C, Okamura J, Liu KY, Huang XJ, Lu DP, Shultz LD, Harada M, Ishikawa F (2008) CD34+CD38+CD19+ as well as CD34+CD38-CD19+ cells are leukemia-initiating cells with self-renewal capacity in human B-precursor ALL. *Leukemia* 22**:** 1207-1213

Kreso A, Dick JE (2014) Evolution of the cancer stem cell model. *Cell stem cell* 14**:** 275-291

Kunz JB, Rausch T, Bandapalli OR, Eilers J, Pechanska P, Schuessele S, Assenov Y, Stutz AM, Kirschner-Schwabe R, Hof J, Eckert C, von Stackelberg A, Schrappe M, Stanulla M, Koehler R, Avigad S, Elitzur S, Handgretinger R, Benes V, Weischenfeldt J et al (2015) Pediatric T-cell lymphoblastic leukemia evolves into relapse by clonal selection, acquisition of mutations and promoter hypomethylation. *Haematologica* 100**:** 1442-1450

Lapidot T, Sirard C, Vormoor J, Murdoch B, Hoang T, Caceres-Cortes J, Minden M, Paterson B, Caligiuri MA, Dick JE (1994) A cell initiating human acute myeloid leukaemia after transplantation into SCID mice. *Nature* 367**:** 645-648

Lawson MA, McDonald MM, Kovacic N, Hua Khoo W, Terry RL, Down J, Kaplan W, Paton-Hough J, Fellows C, Pettitt JA, Neil Dear T, Van Valckenborgh E, Baldock PA, Rogers MJ, Eaton CL, Vanderkerken K, Pettit AR, Quinn JM, Zannettino AC, Phan TG et al (2015) Osteoclasts control reactivation of dormant myeloma cells by remodelling the endosteal niche. *Nature communications* 6**:** 8983

le Viseur C, Hotfilder M, Bomken S, Wilson K, Rottgers S, Schrauder A, Rosemann A, Irving J, Stam RW, Shultz LD, Harbott J, Jurgens H, Schrappe M, Pieters R, Vormoor J (2008) In childhood acute lymphoblastic

leukemia, blasts at different stages of immunophenotypic maturation have stem cell properties. *Cancer cell* 14**:** 47-58

Lee EM, Bachmann PS, Lock RB (2007) Xenograft models for the preclinical evaluation of new therapies in acute leukemia. *Leukemia & lymphoma* 48**:** 659-668

Li L, Neaves WB (2006) Normal stem cells and cancer stem cells: the niche matters. *Cancer research* 66**:** 4553-4557

Li S, Kennedy M, Payne S, Kennedy K, Seewaldt VL, Pizzo SV, Bachelder RE (2014) Model of tumor dormancy/recurrence after short-term chemotherapy. *PloS one* 9**:** e98021

Liberzon A, Birger C, Thorvaldsdottir H, Ghandi M, Mesirov JP, Tamayo P (2015) The Molecular Signatures Database (MSigDB) hallmark gene set collection. *Cell systems* 1**:** 417-425

Liem NL, Papa RA, Milross CG, Schmid MA, Tajbakhsh M, Choi S, Ramirez CD, Rice AM, Haber M, Norris MD, MacKenzie KL, Lock RB (2004) Characterization of childhood acute lymphoblastic leukemia xenograft models for the preclinical evaluation of new therapies. *Blood* 103**:** 3905-3914

Lippert TH, Ruoff HJ, Volm M (2014) Could a revision of the current guidelines for cancer drug use improve the quality of cancer treatment? *Therapeutics and clinical risk management* 10**:** 69-72

Lo Celso C, Klein RJ, Scadden DT (2007) Analysis of the hematopoietic stem cell niche. *Current protocols in stem cell biology* Chapter 2**:** Unit 2A 5

Lo Celso C, Scadden DT (2011) The haematopoietic stem cell niche at a glance. *Journal of cell science* 124**:** 3529-3535

Lock RB, Liem N, Farnsworth ML, Milross CG, Xue C, Tajbakhsh M, Haber M, Norris MD, Marshall GM, Rice AM (2002) The nonobese diabetic/severe combined immunodeficient (NOD/SCID) mouse model of childhood acute lymphoblastic leukemia reveals intrinsic differences in biologic characteristics at diagnosis and relapse. *Blood* 99**:** 4100-4108

Love MI, Huber W, Anders S (2014) Moderated estimation of fold change and dispersion for RNA-seq data with DESeq2. *Genome biology* 15**:** 550

Luqmani YA (2005) Mechanisms of drug resistance in cancer chemotherapy. *Medical principles and practice : international journal of the Kuwait University, Health Science Centre* 14 Suppl 1**:** 35-48

Lutz C, Woll PS, Hall G, Castor A, Dreau H, Cazzaniga G, Zuna J, Jensen C, Clark SA, Biondi A, Mitchell C, Ferry H, Schuh A, Buckle V, Jacobsen SE, Enver T (2013) Quiescent leukaemic cells account for minimal residual disease in childhood lymphoblastic leukaemia. *Leukemia* 27**:** 1204-1207

Ma X, Edmonson M, Yergeau D, Muzny DM, Hampton OA, Rusch M, Song G, Easton J, Harvey RC, Wheeler DA, Ma J, Doddapaneni H, Vadodaria B, Wu G, Nagahawatte P, Carroll WL, Chen IM, Gastier-Foster JM, Relling MV, Smith MA et al (2015) Rise and fall of subclones from diagnosis to relapse in pediatric B-acute lymphoblastic leukaemia. *Nature communications* 6**:** 6604

Magee JA, Piskounova E, Morrison SJ (2012) Cancer stem cells: impact, heterogeneity, and uncertainty. *Cancer cell* 21**:** 283-296

Meads MB, Gatenby RA, Dalton WS (2009) Environment-mediated drug resistance: a major contributor to minimal residual disease. *Nature reviews Cancer* 9**:** 665-674

Mellor JD, Brown MP, Irving HR, Zalcberg JR, Dobrovic A (2013) A critical review of the role of Fc gamma receptor polymorphisms in the response to monoclonal antibodies in cancer. *Journal of hematology & oncology* 6**:** 1

Meng F, Henson R, Patel T (2007) Chemotherapeutic stress selectively activates NF-kappa B-dependent AKT and VEGF expression in liver cancer-derived endothelial cells. *American journal of physiology Cell physiology* 293**:** C749-760

Meyer LH, Eckhoff SM, Queudeville M, Kraus JM, Giordan M, Stursberg J, Zangrando A, Vendramini E, Moricke A, Zimmermann M, Schrauder A, Lahr G, Holzmann K, Schrappe M, Basso G, Stahnke K, Kestler HA, Te Kronnie G, Debatin KM (2011) Early relapse in ALL is identified by time to leukemia in NOD/SCID mice and is characterized by a gene signature involving survival pathways. *Cancer cell* 19**:** 206-217

Morgan CD, Holguin MH (2002) Chemotherapeutic stress mediated by certain antitumor antibiotics induces an atypical CD69+ surface phenotype in peripheral T-lymphocytes. *International immunopharmacology* 2**:** 367-380

Morisot S, Wayne AS, Bohana-Kashtan O, Kaplan IM, Gocke CD, Hildreth R, Stetler-Stevenson M, Walker RL, Davis S, Meltzer PS, Wheelan SJ, Brown P, Jones RJ, Shultz LD, Civin CI (2010) High frequencies of leukemia stem cells in poor-outcome childhood precursor-B acute lymphoblastic leukemias. *Leukemia* 24**:** 1859-1866

Morley NJ, Marks DI (2016) Inotuzumab ozogamicin in the management of acute lymphoblastic leukaemia. *Expert Review of Anticancer Therapy* 16**:** 159-164

Morrison SJ, Scadden DT (2014) The bone marrow niche for haematopoietic stem cells. *Nature* 505**:** 327-334

Morrison SJ, Spradling AC (2008) Stem cells and niches: mechanisms that promote stem cell maintenance throughout life. *Cell* 132**:** 598-611

Mullighan CG, Phillips LA, Su X, Ma J, Miller CB, Shurtleff SA, Downing JR (2008) Genomic analysis of the clonal origins of relapsed acute lymphoblastic leukemia. *Science* 322**:** 1377-1380

Nair AB, Jacob S (2016) A simple practice guide for dose conversion between animals and human. *Journal of basic and clinical pharmacy* 7**:** 27-31

Nair SC, Jacobs JW, Bakker MF, Jahangier ZN, Bijlsma JW, van Laar JM, Lafeber FP, Welsing PM, Utrecht Arthritis Cohort Study G (2016) Determining the Lowest Optimally Effective Methotrexate Dose for Individual RA Patients Using Their Dose Response Relation in a Tight Control Treatment Approach. *PloS one* 11**:** e0148791

Ninomiya M, Abe A, Katsumi A, Xu J, Ito M, Arai F, Suda T, Ito M, Kiyoi H, Kinoshita T, Naoe T (2007) Homing, proliferation and survival sites of human leukemia cells in vivo in immunodeficient mice. *Leukemia* 21**:** 136-142

Nombela-Arrieta C, Pivarnik G, Winkel B, Canty KJ, Harley B, Mahoney JE, Park SY, Lu J, Protopopov A, Silberstein LE (2013) Quantitative imaging of haematopoietic stem and progenitor cell localization and hypoxic status in the bone marrow microenvironment. *Nature cell biology* 15**:** 533-543

Ong V, Liem NL, Schmid MA, Verrills NM, Papa RA, Marshall GM, Mackenzie KL, Kavallaris M, Lock RB (2008) A role for altered microtubule polymer levels in vincristine resistance of childhood acute lymphoblastic leukemia xenografts. *The Journal of pharmacology and experimental therapeutics* 324**:** 434-442

Owellen RJ, Owens AH, Jr., Donigian DW (1972) The binding of vincristine, vinblastine and colchicine to tubulin. *Biochemical and biophysical research communications* 47**:** 685-691

Paiva B, Corchete LA, Vidriales MB, Puig N, Maiso P, Rodriguez I, Alignani D, Burgos L, Sanchez ML, Barcena P, Echeveste MA, Hernandez MT, Garcia-Sanz R, Ocio EM, Oriol A, Gironella M, Palomera L, De Arriba F, Gonzalez Y, Johnson SK et al (2016) Phenotypic and genomic analysis of multiple myeloma minimal residual disease tumor cells: a new model to understand chemoresistance. *Blood* 127**:** 1896-1906

Pal D, Heidenreich O, Vormoor J (2016) Dormancy Stems the Tide of Chemotherapy. *Cancer cell* 30**:** 825-826

Pelayo R, Miyazaki K, Huang J, Garrett KP, Osmond DG, Kincade PW (2006) Cell cycle quiescence of early lymphoid progenitors in adult bone marrow. *Stem cells* 24**:** 2703-2713

Poglio S, Lewandowski D, Calvo J, Caye A, Gros A, Laharanne E, Leblanc T, Landman-Parker J, Baruchel A, Soulier J, Ballerini P, Clappier E, Pflumio F (2016) Speed of leukemia development and genetic diversity in xenograft models of T cell acute lymphoblastic leukemia. *Oncotarget* 7**:** 41599-41611

Portell CA, Advani AS (2014) Novel targeted therapies in acute lymphoblastic leukemia. *Leukemia & lymphoma* 55**:** 737-748

Pui CH, Robison LL, Look AT (2008) Acute lymphoblastic leukaemia. *Lancet* 371**:** 1030-1043

Raitano AB, Halpern JR, Hambuch TM, Sawyers CL (1995) The Bcr-Abl leukemia oncogene activates Jun kinase and requires Jun for transformation. *Proceedings of the National Academy of Sciences of the United States of America* 92**:** 11746-11750

Raychaudhuri S, Stuart JM, Altman RB (2000) Principal components analysis to summarize microarray experiments: application to sporulation time series. *Pacific Symposium on Biocomputing Pacific Symposium on Biocomputing***:** 455-466

Risso D, Ngai J, Speed TP, Dudoit S (2014) Normalization of RNA-seq data using factor analysis of control genes or samples. *Nature biotechnology* 32**:** 896-902

Saito Y, Kitamura H, Hijikata A, Tomizawa-Murasawa M, Tanaka S, Takagi S, Uchida N, Suzuki N, Sone A, Najima Y, Ozawa H, Wake A, Taniguchi S, Shultz LD, Ohara O, Ishikawa F (2010) Identification of therapeutic targets for quiescent, chemotherapy-resistant human leukemia stem cells. *Science translational medicine* 2**:** 17ra19

Samuels AL, Beesley AH, Yadav BD, Papa RA, Sutton R, Anderson D, Marshall GM, Cole CH, Kees UR, Lock RB (2014) A pre-clinical model of resistance to induction therapy in pediatric acute lymphoblastic leukemia. *Blood cancer journal* 4**:** e232

Schepers K, Campbell TB, Passegue E (2015) Normal and leukemic stem cell niches: insights and therapeutic opportunities. *Cell stem cell* 16**:** 254-267

Schepers K, Campbell Timothy B, Passegué E Normal and Leukemic Stem Cell Niches: Insights and Therapeutic Opportunities. *Cell stem cell* 16**:** 254-267

Schluter H, Kaur P (2013) In vivo transplantation assay at limiting dilution to identify the intrinsic tissue reconstitutive capacity of keratinocyte stem cells and their progeny. *Methods in molecular biology* 989**:** 165-182

Schultz KR, Bowman WP, Aledo A, Slayton WB, Sather H, Devidas M, Wang C, Davies SM, Gaynon PS, Trigg M, Rutledge R, Burden L, Jorstad D, Carroll A, Heerema NA, Winick N, Borowitz MJ, Hunger SP, Carroll WL, Camitta B (2009) Improved early event-free survival with imatinib in Philadelphia chromosome-positive acute lymphoblastic leukemia: a children's oncology group study. *Journal of clinical oncology : official journal of the American Society of Clinical Oncology* 27**:** 5175-5181

Shackleton M (2010) Normal stem cells and cancer stem cells: similar and different. *Seminars in cancer biology* 20**:** 85-92

Sharma V, McNeill JH (2009) To scale or not to scale: the principles of dose extrapolation. *British journal of pharmacology* 157**:** 907-921

Shultz LD, Lyons BL, Burzenski LM, Gott B, Chen X, Chaleff S, Kotb M, Gillies SD, King M, Mangada J, Greiner DL, Handgretinger R (2005) Human lymphoid and myeloid cell development in NOD/LtSz-scid IL2R gamma null mice engrafted with mobilized human hemopoietic stem cells. *Journal of immunology* 174**:** 6477-6489

Stow P, Key L, Chen X, Pan Q, Neale GA, Coustan-Smith E, Mullighan CG, Zhou Y, Pui CH, Campana D (2010) Clinical significance of low levels of minimal residual disease at the end of remission induction therapy in childhood acute lymphoblastic leukemia. *Blood* 115**:** 4657-4663

Subramanian A, Tamayo P, Mootha VK, Mukherjee S, Ebert BL, Gillette MA, Paulovich A, Pomeroy SL, Golub TR, Lander ES, Mesirov JP (2005) Gene set enrichment analysis: a knowledge-based approach for interpreting genome-wide expression profiles. *Proceedings of the National Academy of Sciences of the United States of America* 102**:** 15545-15550

Sugiyama T, Kohara H, Noda M, Nagasawa T (2006) Maintenance of the hematopoietic stem cell pool by CXCL12-CXCR4 chemokine signaling in bone marrow stromal cell niches. *Immunity* 25**:** 977-988

Takeishi S, Matsumoto A, Onoyama I, Naka K, Hirao A, Nakayama KI (2013) Ablation of Fbxw7 eliminates leukemia-initiating cells by preventing quiescence. *Cancer cell* 23**:** 347-361

Terziyska N, Castro Alves C, Groiss V, Schneider K, Farkasova K, Ogris M, Wagner E, Ehrhardt H, Brentjens RJ, zur Stadt U, Horstmann M, Quintanilla-Martinez L, Jeremias I (2012) In vivo imaging enables high resolution preclinical trials on patients' leukemia cells growing in mice. *PloS one* 7**:** e52798

Townsend EC, Murakami MA, Christodoulou A, Christie AL, Koster J, DeSouza TA, Morgan EA, Kallgren SP, Liu H, Wu SC, Plana O, Montero J, Stevenson KE, Rao P, Vadhi R, Andreeff M, Armand P, Ballen KK, Barzaghi-Rinaudo P, Cahill S et al (2016) The Public Repository of Xenografts Enables Discovery and Randomized Phase II-like Trials in Mice. *Cancer cell* 29**:** 574-586

van 't Veer LJ, Dai H, van de Vijver MJ, He YD, Hart AA, Mao M, Peterse HL, van der Kooy K, Marton MJ, Witteveen AT, Schreiber GJ, Kerkhoven RM, Roberts C, Linsley PS, Bernards R, Friend SH (2002) Gene expression profiling predicts clinical outcome of breast cancer. *Nature* 415**:** 530-536

van Dongen JJ, van der Velden VH, Bruggemann M, Orfao A (2015) Minimal residual disease diagnostics in acute lymphoblastic leukemia: need for sensitive, fast, and standardized technologies. *Blood* 125**:** 3996-4009

Vick B, Rothenberg M, Sandhofer N, Carlet M, Finkenzeller C, Krupka C, Grunert M, Trumpp A, Corbacioglu S, Ebinger M, Andre MC, Hiddemann W, Schneider S, Subklewe M, Metzeler KH, Spiekermann K, Jeremias I (2015) An advanced preclinical mouse model for acute myeloid leukemia using patients' cells of various genetic subgroups and in vivo bioluminescence imaging. *PloS one* 10**:** e0120925

Vora A, Goulden N, Wade R, Mitchell C, Hancock J, Hough R, Rowntree C, Richards S (2013) Treatment reduction for children and young adults with low-risk acute lymphoblastic leukaemia defined by minimal residual disease (UKALL 2003): a randomised controlled trial. *The Lancet Oncology* 14**:** 199-209

Vormoor HJ (2009) Malignant stem cells in childhood acute lymphoblastic leukemia: the stem cell concept revisited. *Cell cycle* 8**:** 996-999

Wang C, Gong B, Bushel PR, Thierry-Mieg J, Thierry-Mieg D, Xu J, Fang H, Hong H, Shen J, Su Z, Meehan J, Li X, Yang L, Li H, Labaj PP, Kreil DP, Megherbi D, Gaj S, Caiment F, van Delft J et al (2014) The concordance between RNA-seq and microarray data depends on chemical treatment and transcript abundance. *Nat Biotech* 32**:** 926-932

Wang Y, Probin V, Zhou D (2006) Cancer therapy-induced residual bone marrow injury-Mechanisms of induction and implication for therapy. *Current cancer therapy reviews* 2**:** 271-279

Weston SA, Parish CR (1990) New fluorescent dyes for lymphocyte migration studies. Analysis by flow cytometry and fluorescence microscopy. *Journal of immunological methods* 133**:** 87-97

Whitfield ML, George LK, Grant GD, Perou CM (2006) Common markers of proliferation. *Nature reviews Cancer* 6**:** 99-106

Willfuhr KU, Westermann J, Pabst R (1989) Immunohistological localization and characterization of FITC-labelled lymphocytes. A rapid and inexpensive method for studying migration. *Journal of immunological methods* 120**:** 29-36

Wilson A, Laurenti E, Oser G, van der Wath RC, Blanco-Bose W, Jaworski M, Offner S, Dunant CF, Eshkind L, Bockamp E, Lio P, Macdonald HR, Trumpp A (2008) Hematopoietic stem cells reversibly switch from dormancy to self-renewal during homeostasis and repair. *Cell* 135**:** 1118-1129

Wong NC, Bhadri VA, Maksimovic J, Parkinson-Bates M, Ng J, Craig JM, Saffery R, Lock RB (2014) Stability of gene expression and epigenetic profiles highlights the utility of patient-derived paediatric acute lymphoblastic leukaemia xenografts for investigating molecular mechanisms of drug resistance. *BMC genomics* 15**:** 416

Xie Y, Yin T, Wiegraebe W, He XC, Miller D, Stark D, Perko K, Alexander R, Schwartz J, Grindley JC, Park J, Haug JS, Wunderlich JP, Li H, Zhang S, Johnson T, Feldman RA, Li L (2009) Detection of functional haematopoietic stem cell niche using real-time imaging. *Nature* 457**:** 97-101

Yanada M, Takeuchi J, Sugiura I, Akiyama H, Usui N, Yagasaki F, Kobayashi T, Ueda Y, Takeuchi M, Miyawaki S, Maruta A, Emi N, Miyazaki Y, Ohtake S, Jinnai I, Matsuo K, Naoe T, Ohno R, Japan Adult Leukemia Study G (2006) High complete remission rate and promising outcome by combination of imatinib and chemotherapy for newly diagnosed BCR-ABL-positive acute lymphoblastic leukemia: a phase II study by the Japan Adult Leukemia Study Group. *Journal of clinical oncology : official journal of the American Society of Clinical Oncology* 24**:** 460-466

Zeller KI, Jegga AG, Aronow BJ, O'Donnell KA, Dang CV (2003) An integrated database of genes responsive to the Myc oncogenic transcription factor: identification of direct genomic targets. *Genome biology* 4**:** R69

Zhang J, Niu C, Ye L, Huang H, He X, Tong W-G, Ross J, Haug J, Johnson T, Feng JQ, Harris S, Wiedemann LM, Mishina Y, Li L (2003) Identification of the haematopoietic stem cell niche and control of the niche size. *Nature* 425**:** 836-841

Zhao S, Fung-Leung WP, Bittner A, Ngo K, Liu X (2014) Comparison of RNA-Seq and microarray in transcriptome profiling of activated T cells. *PloS one* 9**:** e78644

Zhou BB, Zhang H, Damelin M, Geles KG, Grindley JC, Dirks PB (2009) Tumour-initiating cells: challenges and opportunities for anticancer drug discovery. *Nature reviews Drug discovery* 8**:** 806-823

Zuber J, Radtke I, Pardee TS, Zhao Z, Rappaport AR, Luo W, McCurrach ME, Yang MM, Dolan ME, Kogan SC, Downing JR, Lowe SW (2009) Mouse models of human AML accurately predict chemotherapy response. *Genes & development* 23**:** 877-889

10 Acknowledgement

I would like to thank…

PD Dr. Irmela Jeremias and PD Dr. Aloys Schepers for giving me the opportunity to carry out my PhD thesis in their labs. Thank you for all your support and constructive criticism through the years.

Prof. Wolfgang Enard for the cooperation and discussion of the RNA-seq data.

Prof. Olivier Gires and Dr. Lothar Strobl for taking part in my thesis committee and for the mentoring.

Prof. Panzer-Grümayer and her colleagues for providing and sorting primary ALL MRD samples.

Christoph Ziegenhain for performing RNA-seq and supporting me in the RNA-seq analysis.

all the Postdocs, PhD students and former colleagues in the institute for all the help and pleasant working atmosphere.

especially Dr. Binje Vick, Dr. Andrea Liebl and Dr. Wen-Hsin Liu for all the discussion supporting my PhD thesis.

especially Sarah Ebinger for the perfect cooperation in our projects.

all the TAs in the lab for handling the mice work and organizing a well-functioning lab. Without their help it would not be possible to run so many *in vivo* experiments. Thank you!

all the animal caretakers in the mouse facility.

finally my family, especially my parents, for the endless support during all the stages of my education.